Technische Universität München

Department Chemie, Lehrstuhl für Technische Chemie II

Oxidative chlorination of methane over LaCl₃-based catalysts

Elvira Theresia Peringer

Vollständiger Abdruck der von der Fakultät für Chemie

der Technischen Universität München zur Erlangung des akademischen Grades eines

Doktors der Naturwissenschaften (Dr. rer. nat.)

genehmigten Dissertation.

Vorsitzender: Univ.-Prof. Dr. K.-O. Hinrichsen

Prüfer der Dissertation: 1. Univ.-Prof. Dr. J. A. Lercher

2. Univ.-Prof. Dr. U. K. Heiz

Die Dissertation wurde am 06.05.2008 bei der Technischen Universität München eingereicht und durch die Fakultät für Chemie am 23.06.2008 angenommen.

„Man merkt nie, was schon getan wurde...

Man sieht immer nur, was noch zu tun bleibt...“

Marie Curie

Acknowledgment

Now that my time as a PhD student comes to an end, it is time to look back on the probably most challenging period of my life and to express my gratitude to all those who accompanied and helped me during the last four years.

First, I would like to thank Johannes (Prof. J.A. Lercher) for giving me the chance to work in his international team and an exciting project. Thank you for all your guidance, patience, helpful and critical discussions. This period has been an important part of my life and I have enjoyed it very much. Thank you for giving me also the opportunities to join several national and international conferences as well as to spend a research visit at the University of Utrecht.

I would also like to express my great gratitude to Angeliki (Prof. A. Lemonidou) who spent many hours on reading, discussing and correcting my thesis, even though I'm not one of her students.

It would not have been possible or would have been very difficult to finish these four years without the help of Xaver. He taught me how to operate my reactor system, the GC and especially how to solve the numerous problems. With your help I learned to keep cool about pressure drops, gas leaks, missing compounds in my GC analysis... I also enjoyed our trips with the canoe and gourmet trips to the French restaurant.

I would like to express my gratitude also to my diploma students who contributed to this work, e.g. Chirag Tejuja. Sorry that I trouble you by providing you a bicycle during your stay in Garching. Thank you very much for being our guide in Bombay. Markus Hutt, for your very creative interpretations. Sometimes a bit too abstract ;)

Of course I would also like to thank my project partners at The DOW Chemical Company in Midland and in particular Simon Podkolzin for the stimulating telephone discussions and the work on two joint publications.

Table of Contents

Chapter 1

General Introduction

Abstract

This chapter introduces to natural gas and the most important processes for direct or indirect methane activation. Especially the functionalization of methane as methyl chloride via oxyhydrochlorination is highlighted and furthermore the characteristics of the studied catalytic system, LaOCl and LaCl$_3$ are presented.

1 General Introduction

1.1 Motivation

Crude oil is one of the most important primary energy sources covering 38% of the global energy demand. However, the world crude oil reserves are limited and non reversible. According to the latest statistics released by BP at the end of 2007, the world proven oil reserves, which can be recovered in future under existing economic and geological conditions, are 1208.2 billion barrels (Figure 1.1). One barrel is equal to around 159 liters. At the current production level this reserves will last for around 41 years. The world distribution of the reserves is shown in Figure 1.1 [1].
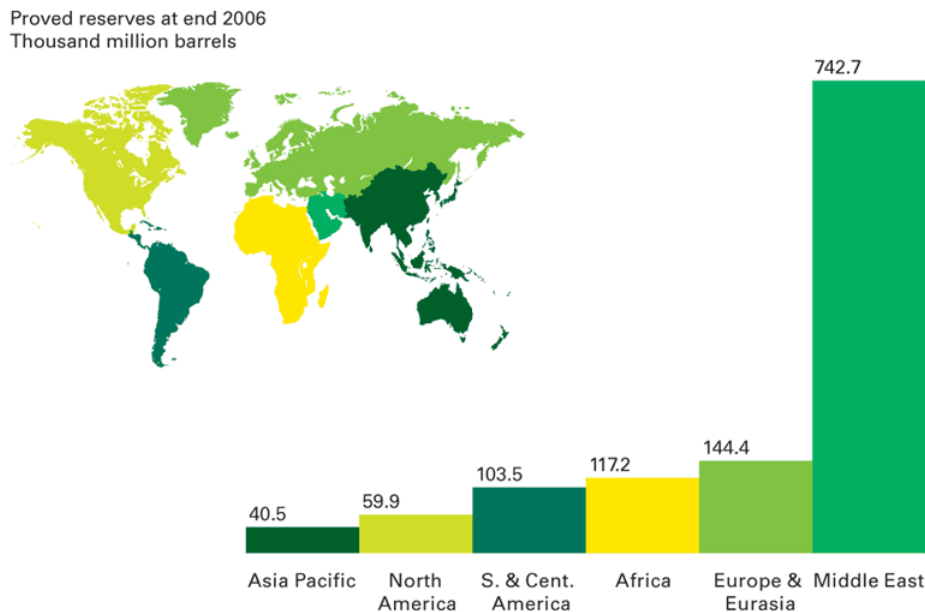
Figure 1.1: World distribution of the proven oil reserves [1]

While 75 % of the oil is used for transportation and heating purposes, only 6% of the oil produced is used in the manufacture of petrochemicals. Nevertheless, many important branches like the pharmaceutical or the chemical industry are depending on hydrocarbon feedstocks. It is therefore mandatory for the future to find a suitable substitute for oil.

On the other hand, natural gas is a strongly underutilized resource for chemicals and liquid fuels. Natural gas is a combustible mixture of hydrocarbon gases. Methane is the major component of natural gas, an inexpensive and accessible source of energy. The typical

composition of natural gas before processing can vary widely (see Table 1.1). Besides its major use as energy source, methane is an important raw material for the chemical industry.

Table 1.1: Typical composition of natural gas [2]

Methane	CH_4	70-90 %
Ethane	C_2H_6	2-8%
Propane	C_3H_8	0-2%
Butane	C_4H_{10}	0-0.8%
Carbon dioxide	CO_2	0-8%
Oxygen	O_2	0-0.2%
Nitrogen	N_2	0-5%
Hydrogen sulphide	H_2S	0-5%
Rare gases	Ar, He, Ne, Xe	traces

The known natural gas reserves are enormous and rival those of crude oil. Moreover, the proved reserves are increasing more rapidly than those of liquid petroleum, and it is anticipated that this trend will continue in the 21st century [3]. It is the most abundant energy sources on the planet, but more than one-third of the global natural reserves are classified as stranded (natural) gas [4], meaning gas reservoirs which are too small, geographically harsh to develop or in remote areas and cannot be used locally or efficiently transported to market due to a lack of infrastructure. The proven natural gas reserves, which can be recovered in the future from known reservoirs under existing economic and operating conditions, are 181.5 trillion m³ or 6405.5 trillion cubic feet. To draw a direct comparison with oil, 6040 cubic feet of gas have the same energy equivalent as one barrel oil. The energy equivalent of the natural gas reserves is 1061 billion bbl oil. The geographical distribution of these reserves is given in Figure 1.2. When stranded natural gas is produced in the crude oil production it is usually burned or vented. In recent years, approximately 150 billion m³ of natural gas have been flared or vented worldwide annually, which is equivalent to about 5% of the global annual natural gas consumption or about 25% of the consumption in the United States [5, 6].

Proved reserves at end 2006
Trillion cubic metres
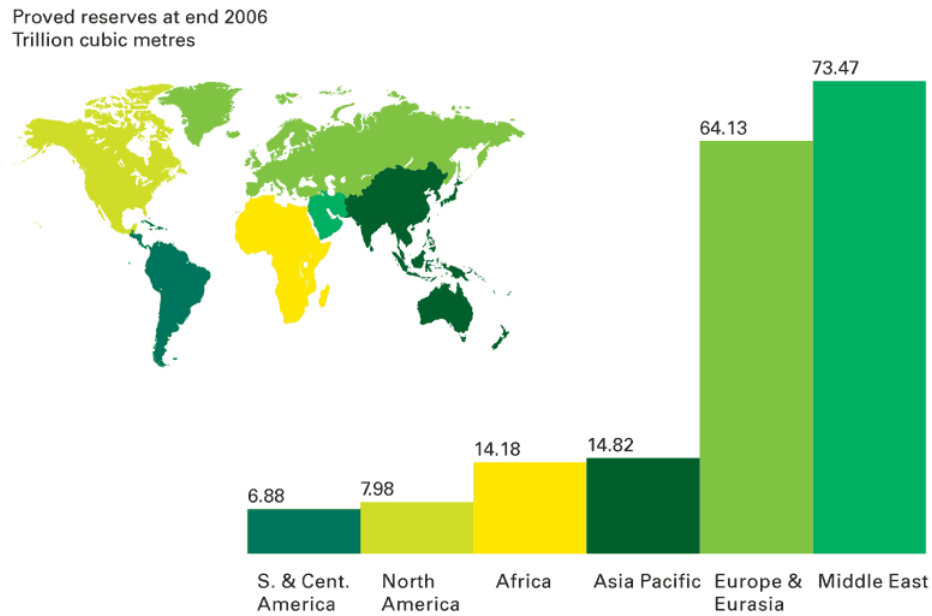
Figure 1.2: World distribution of the proven gas reserves [1]

This fact is economically and environmentally harmful since methane has a high global warming potential (GWP) of 23 [7]. GWP is based on a number of factors, including the radiative efficiency (heat-absorbing ability) of each gas relative to that of carbon dioxide, as well as the decay rate of each gas (the amount removed from the atmosphere over a given number of years) relative to that of carbon dioxide. This means, that 1g CH_4 warms the earth 23 times as much as 1g of CO_2. The development of viable technologies for methane utilization at remote locations or of natural gas fields of marginal size is therefore an important step for the future.

The dominant technology used for the exploitation of natural gas reserves is the synthesis gas production, a mixture of carbon monoxide and hydrogen. Syngas can then be further converted into synthetic crude oil using the Fischer-Tropsch technology. Syncrude can be upgraded to transportation fuels with the standard methods of refinery. Alternatively, syngas can be converted into liquid oxygenates, such as alcohols, which in turn can be transformed to conventional transportation fuels over zeolite catalysts. These indirect utilizations are disadvantageously costly, if only small amounts of natural gas are available, as it is the case for stranded natural gas.

The direct utilization is challenging due to the low reactivity of methane. A potential alternative for the liquefaction of methane is the oxidative halogenation, where in the first step

methyl chloride is formed. In a second reaction step the gaseous methyl chloride can be converted into liquid commodity chemicals such as methanol, dimethyl ether, light olefins, and higher hydrocarbons, including gasoline. While converting the methyl halide into higher hydrocarbons, the produced hydrogen halide can be separated from the hydrocarbon product and recycled back to the halogenation process.

In the following sections more details will be given for the direct activation of methane, especially the functionalization of methane as methyl chloride via oxyhydrochlorination. Furthermore the characteristics of the studied catalytic system, LaOCl and $LaCl_3$, are presented.

1.2   Fundamentals of C-H bond activation

The activation of methane and higher alkanes is in general very challenging due to their low reactivity. The low reactivity of alkanes is attributed to the unavailability of lone electron pairs and empty orbitals. This is a consequence of the fact that for carbon and hydrogen the number of valence electrons is equal to the number of valence orbitals. The strong bond between C and H (dissociation energy 375-460 kJ/mol) means that the HOMOs are energetically low σ-bonding orbitals and the LUMOs are at energetically high anti-bonding σ*-levels, none of them is easily accessible to an attacking reagent. Furthermore due to the low polarity of the C-H bond, the reactivity of alkanes is extremely low.

As illustrated in Figure 1.3 the interaction of a reagent molecule with a C-H of methane is sterically hindered by the tetrahedral structure of methane.
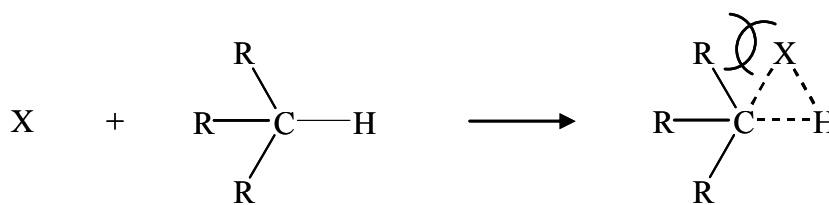
Figure 1.3: Steric hindrance in the transition state [8].

An incoming reagent has the choice of (i) donating electron density to the σ*-H orbital, (ii) of abstracting C-H σ-bonding electrons, or (iii) of doing both at once. Strategy (i) seems to be the least successful approach because nucleophiles do not react with alkanes. Strategy (ii) is adopted by a variety of electrophilic reagents such as Lewis acids. Strategy (iii) seems to be the most successful. It appears to be the one adopted by radicals, by carbenes, by metal surfaces and by low-valent metal complexes. It is likely that for metal complexes electron withdrawal from the σ-orbital is at least as important as donation into the σ*-orbital. The second strategy is typified by electrophilic attack on the C-H bond. This occurs when strong acids such as $AlCl_3$ [9], H_2SO_4, HF, super acids in general [10, 11] and acidic sites of certain aluminosilicates and related metal oxides are applied.

A further problem related to the reactivity of methane, is the thermochemistry of the reactions. The primary selective oxidation products of methane, such as alcohol, are much

more susceptible to further oxidation than saturated hydrocarbons. As an example, the C-H bond in methanol is 46 kJ/mol weaker than the C-H bond in methane and therefore more easily broken. Consequently, the total oxidation to CO_2 and H_2O is more favorable than the formation of primary oxidation products such as methanol or methyl chloride, as can be seen directly from the reaction enthalpies:

$$CH_4 + 2O_2 \rightarrow CO_2 + 2H_2O \qquad \Delta H^0 = \text{-803 kJ/mol} \qquad (1.1)$$

$$CH_4 + 0.5O_2 \rightarrow CH_3OH \qquad \Delta H^0 = \text{-126 kJ/mol} \qquad (1.2)$$

An organic molecule can react with oxygen along many possible consecutive and parallel reaction pathways, giving a number of different products. The role of a catalyst is to accelerate only one of them. Very often the desired product is not the thermodynamically most favorable one. The selectivity is the most important and characteristic feature of a catalyst. A highly selective catalyst, which accelerates a particular reaction, can lead to the formation of products that would have never been formed in the absence of it due to other faster competitive reaction routes.

Often a slight modification of the composition of the catalyst or variation in the method of its preparation can alter its catalytic properties to such an extent, that the direction of the reaction is changed with the formation of a new product.

1.3   Catalytic processes for the C-H bond activation

Exploitation of remote natural gas is impeded by the high costs of both gas transportation and current methods for converting hydrocarbon gas into more readily transportable liquids. Methane, as discussed above, is a very stable molecule and starts to decompose into carbon and hydrogen at 785°C. At higher temperatures (1250°C) acetylene is formed which does not decompose into its constituting elements if the gas mixture is rapidly quenched. The resulting acetylene can be oligomerized to aromatic compounds. At 1000-1100°C methane and steam react to acetylene, ethylene and ethane, but these processes have been proven as too energy intensive for general application. Therefore, the available conversion methods are indirect involving the production of synthesis gas (carbon monoxide and hydrogen), and its subsequent conversion to the desired product [12].

1.3.1   Methane oxidation to synthesis gas

The production of CO and H_2 in the appropriate ratios is achieved through three principal processes or combinations thereof [3]:

$$CH_4 + H_2O \rightleftharpoons CO + 3H_2 \qquad \Delta H^0 = 206 \text{ kJ/mol} \qquad \text{Steam reforming} \qquad (1.3)$$

$$CH_4 + CO_2 \rightleftharpoons 2CO + 2H_2 \qquad \Delta H^0 = 247 \text{ kJ/mol} \qquad CO_2 \text{ reforming} \qquad (1.4)$$

$$CH_4 + 0.5O_2 \rightleftharpoons CO + 2H_2 \qquad \Delta H^0 = -35 \text{ kJ/mol} \qquad \text{Partial oxidation} \qquad (1.5)$$
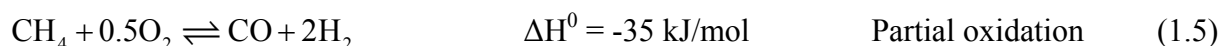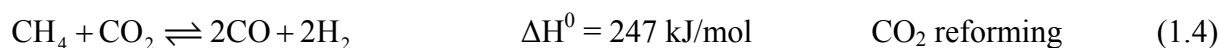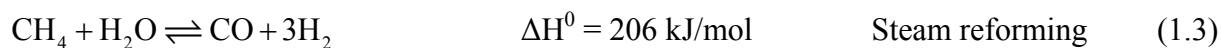
The first two processes are highly endothermic and thus requiring the transfer of large heat amount to the reactor. The third process, in contrast, is slightly exothermic. The combination of steam reforming with partial oxidation in which the endothermic and exothermic reaction are coupled is often referred to as autothermal reforming [13]. The final H_2 to CO ratio under reaction conditions is adjusted via the water gas shift reaction:

$$CO + H_2O \rightleftharpoons CO_2 + H_2 \qquad \Delta H^0 = -41 \text{ kJ/mol} \qquad \text{water gas shift} \qquad (1.6)$$
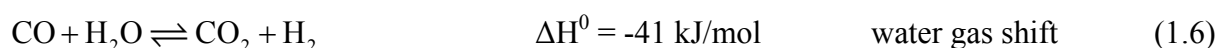
Steam reforming is the most widely used process to generate synthesis gas for the methanol production. This process takes place over nickel based catalysts at high temperatures and a

high steam to methane ratio to shift the equilibrium towards H_2 and CO. One of the disadvantages of Ni catalysts is the formation of carbonaceous species which deposit on the catalytic particles leading to deactivation. The catalytic partial oxidation which has not been applied commercially proceeds with high rates over noble metals and nickel catalysts [14]. The main drawback for its realization is the high cost of using pure oxygen and the safety limits.

Syngas is mainly used in the synthesis of methanol and the synthesis of hydrocarbons *via* the Fischer-Tropsch synthesis. For the methanol production the most widely used catalyst is a mixture of copper, zinc oxide, and alumina first used by ICI in 1966 [15]. CuO-ZnO-Al_2O_3 catalyze at 5–10 MPa and 250 °C, the production of methanol from carbon monoxide and hydrogen with high selectivity (equ. 1.7).

$$CO + 2H_2 \ \rightarrow \ CH_3OH \tag{1.7}$$

However, the synthesis gas from methane produces 3 moles of hydrogen for every mole of carbon monoxide, while the methanol synthesis consumes only 2 moles of hydrogen for every mole of carbon monoxide. Therefore carbon dioxide is injected into the methanol synthesis reactor, where it forms methanol according to the chemical equation:

$$CO_2 + 3H_2 \ \rightarrow \ CH_3OH + H_2O \tag{1.8}$$

The Fischer-Tropsch synthesis is a catalytic process which converts synthesis gas to hydrocarbons. In 1926 Franz Fischer and Hans Tropsch reported that linear alkenes and alkanes (as well as some oxygenates) are formed from syngas at 200–300°C and pressures of 2.5-2.7 MPa over Co or Fe catalysts [16, 17]:

$$nCO + 2nH_2 \rightarrow C_nH_{2n} + nH_2O \tag{1.9}$$

$$mCO + (2m+1)H_2 \rightarrow C_mH_{2m+2} + nH_2O \tag{1.10}$$

$$pCO + 2pH_2 \ \rightarrow \ C_{p-1}H_{2p-1}CH_2OH + (p-1)H_2O \tag{1.11}$$
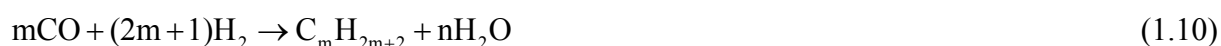
Under the conditions normally used industrially and in many studies for CO hydrogenation, iron catalysts favor the formation of mainly linear alkenes and oxygenates, while cobalt gives mostly linear alkanes. Ruthenium, one of the most active catalysts but of limited industrial

interest due to its high costs, yields mainly high molecular weight hydrocarbons. Rhodium catalysts produce significant amounts of oxygenates in addition to hydrocarbons, while nickel yields mainly methane. The primary products of the Fischer-Tropsch Synthesis are 1-alkenes. Consecutive reactions as isomerization to 2- and 3-alkenes and hydrogenation to alkanes cause a reduction of the 1-alkene-selectivity.

1.4 Direct activation of methane

The direct oxidative conversion of methane to higher hydrocarbons or to monosubstituted derivatives such as methyl halide or methyl alcohol avoid the expensive step of syngas formation [18, 19]. Some of these direct methods are described below.

1.4.1 Oxidative coupling of methane (OCM)

A promising route for the activation of methane is the oxidative coupling to higher olefinic hydrocarbons. However, the dehydrogenation-dimerization of methane has a large positive change in reaction enthalpy as shown in the following equation:

$$2CH_4 \rightarrow C_2H_6 + H_2 \qquad\qquad \Delta H^0 = 65 \text{ kJ/mol} \qquad\qquad (1.12)$$

The thermodynamic disadvantage can be overcome by introducing an oxidant, for example oxygen or nitrous oxide [20]:

$$2CH_4 + 0.5O_2 \rightarrow C_2H_6 + H_2O \qquad\qquad \Delta H^0 = -177 \text{ kJ/mol} \qquad\qquad (1.13)$$

The oxidative coupling of methane in the temperature range of 650°C to 800°C involves a series of complex heterogeneous and homogeneous free radical reactions. It is initiated by H-abstraction from CH_4 by surface active-oxygen species forming $CH_3^{\cdot}$ radicals, which after desorption couple in the gas phase to give C_2H_6 as the primary product together with H_2O. Ethylene appears to be a secondary product formed via oxidative dehydrogenation of ethane at the catalyst surface, and via free radical hydrogen-transfer reaction in the gas phase, and

probably in minor amount by thermal dehydrogenation at the high temperature of OCM. All of the hydrocarbons may undergo deep oxidation to CO_2 and CO at the catalyst surface, or in the gas phase in the presence of O_2. The high temperatures and low product yields have been the main obstacles for the commercial application of the process [3, 21].

The OCM catalysts may be divided into four groups:
- Highly basic pure oxides, of the early members of the lanthanide oxide series (excluding CeO_2) [22]
- Alkaline and alkaline earth ions supported on basic oxides, e.g. Li/MgO, Ba/MgO and Sr/La_2O_3 [23]
- A few transition metal oxides that contain alkaline ions [24, 25]
- Any of the above materials promoted with chloride ions [26].

One of the most promising catalysts studied are SrO/La_2O_3 [23] and $Mn/Na_2WO_4/SiO_2$, which can achieved at 800°C a CH_4 conversion of 20% and show a selectivity to C_2 hydrocarbons of about 80% [25]. However in order to reach the minimum yield as proposed by the industry the catalyst should reach 90% selectivity at 40% methane conversion.

The nature of the active centers for oxidative coupling is not elucidated yet. Reactive oxygen ions are apparently required for the activation of CH_4. Some authors report O^- or O^{2-} responsible for catalytic activity [21]. The addition of chloride ions to an oxidative coupling catalyst has a marked effect on the C_2H_4/C_2H_6 product ratio. The chlorine may be introduced either as constituent of the catalyst or through HCl or organic chlorine compounds that are added to the reagents. C_2H_4/C_2H_6 ratio between 3 and 5 are obtained, as chlorine is known to dehydrogenate C_2H_6 in the gas phase. The presence of Cl^- ions at a certain amount modifies the catalyst so that it no longer acts as a strongly basic oxide. In particular the catalyst is not poisoned by CO_2. However, the reported lifetimes of the chloride-containing catalysts are relatively short [27, 28].

1.4.2 Direct chlorination of methane

The direct chlorination is known since the year 1840, when Dumas discovered the direct chlorination of paraffins [29]. The direct chlorination of methane to methyl chloride and HCl can proceed via thermal, catalytic or photochemical route:

$$CH_4 + Cl_2 \rightarrow CH_3Cl + HCl \tag{1.14}$$

The first step of this radical substitution is the homolytic cleavage (Initiation) of a chlorine molecule. In the second step, the chlorine radical attacks the methane molecule, breaks the C-H bond and creates a methyl-radical. Then the methyl radical abstracts a Cl atom out of a chlorine-molecule resulting in methyl chloride and chlorine radical (Propagation). The radical starts the reaction again, leading to a chain reaction. Methyl chloride undergoes further chlorination forming methylene chloride via polychlorination [30]:

$$Cl_2 \xrightarrow{\ h\nu\ } 2Cl^{\cdot} \qquad \text{Initiation} \tag{1.15}$$

$$CH_4 + Cl^{\cdot} \rightarrow CH_3^{\cdot} + HCl$$
$$\qquad\qquad\qquad\qquad\qquad \text{Propagation} \tag{1.16}$$
$$CH_3^{\cdot} + Cl_2 \rightarrow CH_3Cl + Cl^{\cdot}$$

$$CH_3^{\cdot} + Cl^{\cdot} \rightarrow CH_3Cl \qquad \text{Inhibition} \tag{1.17}$$

$$CH_3Cl + Cl^{\cdot} \rightarrow CH_2Cl^{\cdot} + HCl$$
$$\qquad\qquad\qquad\qquad\qquad \text{Polychlorination} \tag{1.18}$$
$$CH_2Cl^{\cdot} + Cl_2 \rightarrow CH_2Cl_2 + Cl^{\cdot}$$
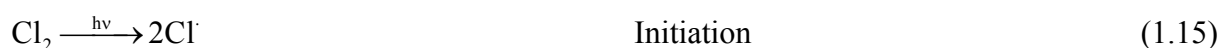
The rate of hydrogen abstraction from hydrocarbons increases with decreasing C-H bond strength. For n-alkanes, the ratio of the relative rates (per H) for primary, secondary, and tertiary bonds at 27°C is 1.0:3.3:3.9. For unchlorinated molecules, these rates are essentially independent of the specific molecule. One disadvantage of this radical process is thus the low selectivity to methyl chloride, which is caused by the higher reactivity of the methyl halide in comparison to methane:

$$CH_4 \ < \ CH_3Cl \ < \ CH_2Cl_2 \ < \ CHCl_3 \tag{1.19}$$

This leads to undesired higher substituted products and eventually a mixture of all four chloromethanes are obtained:

$$CH_4 \xrightarrow{\ Cl_2\ } CH_3Cl \xrightarrow{\ Cl_2\ } CH_2Cl_2 \xrightarrow{\ Cl_2\ } CHCl_3 \xrightarrow{\ Cl_2\ } CCl_4 \tag{1.20}$$
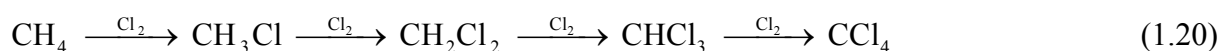
The formation of higher chlorinated products can be controlled by two approaches. On the one hand a 10-fold methane excess would suppress the further chlorination of methyl chloride. However, the disadvantage of using high methane ratios is the separation and

recycling of large quantities of unreacted methane from the product which results in higher production costs. On the other hand higher chlorination can be overcome by electrophilic chlorination with supported solid acids as catalysts which favors the monochlorination since incorporation of Cl atoms to methane makes the carbon progressively electropositive. In consequence, a further electrophilic reaction with $Cl^{\delta+}$ is progressively less favorable. Olah *et al.* reported for the electrophilic chlorination over FeO_xCl_y/Al_2O_3, $TaOF_3/Al_2O_3$, $NbOF_3/Al_2O_3$, $ZrOF_3/Al_2O_3$, $SbOF_3/Al_2O_3$, $SbF_5/graphite$ and $Nafion/TaF_5$ at 270°C a high selectivity of 96% towards CH_3Cl at a conversion of 34% [31]. The acidic sites of the catalysts polarize chlorine and form a surface-coordinated electrophilic chlorine species, which is inserted into the C-H bond by forming a five-coordinated carbonium ion intermediate which undergoes a decomposition in parallel with halogenolysis of chlorine, producing CH_3Cl and HCl. Same results are obtained with superacidic sulfated zirconia and supported platinum catalysts with electron-deficient metal-coordinated chlorine as active site [32]. Zeolites have also been investigated as selective catalysts for the electrophilic chlorination of methane. However, they lose their activity very fast due to aluminum extraction from the zeolite framework by hydrogen chloride [33].

However, the use of chlorine is undesirable due to the requirement of converting the HCl by-product back to Cl_2 and the corrosion problems. An alternative for the oxidation with chlorine is the oxyhydrochlorination of methane, a reaction of methane with hydrogen chloride and oxygen.

1.4.3 Methane conversion to methyl chloride via Oxyhydrochlorination (OHC)

An alternative to the problematic use of chlorine gas is the use of hydrogen chloride as a chlorine source. By introducing oxygen to the reaction feed the reaction becomes exothermal. This reaction, the conversion of a hydrocarbon, hydrogen chloride and oxygen to a chlorinated hydrocarbon and water is also known as oxyhydrochlorination (OHC). The oxyhydrochlorination was first applied for the production of 1,2-dichloroethane (EDC) from ethylene (equ. 1.21). Ethylene oxyhydrochlorination is a fundamental step in the PVC production.

$$C_2H_4 + 2HCl + 0.5O_2 \rightarrow C_2H_4Cl_2 + H_2O \qquad \Delta H^0 = \text{-240 kJ/mol} \qquad (1.21)$$

Catalysts for this reaction are based on a reducible metal, usually copper chloride, which is generally deposited on oxidic supports such as alumina or silica. Also supported iron and ruthenium compounds have been reported as active catalysts [34, 35]. The same catalysts are also active in oxyhydrochlorination of methane to methyl chloride:

$$CH_4 + HCl + 0.5O_2 \rightarrow CH_3Cl + H_2O \qquad \Delta H^0 = \text{-157 kJ/mol} \qquad (1.22)$$

However, ethylene oxyhydrochlorination is performed in the temperature range between 200°C and 300°C and methane oxyhydrochlorination is carried out in the temperature range between 350 and 450°C. The state of the active species and the mechanisms involved are believed to be different for methane and ethylene. Under methane OHC conditions $CuCl_2$-CuCl are expected to be in the state of a melt dispersed on the surface whereas the catalyst is in a solid state under ethylene OHC conditions (lower temperature).

Leofanti *et. al.* characterized the structure of the copper species on alumina supports at low and high copper loadings under ethylene OHC conditions. They observed at low Cu content (< 0.95 wt% Cu/100 m^2 of support) the formation of stable surface copper (II) aluminate species which are unreactive towards ethylene and do not change either after aging or heating. At concentrations higher than 0.95 wt.% Cu/100 m^2 an amorphous $CuCl_2 \cdot 2H_2O$ phase is formed, which covers the surface aluminate species. It undergoes a slow hydrolysis reaction giving the insoluble $Cu_2(OH)_3Cl$ (paratacamite) and HCl. The liberated HCl partially chlorinates the alumina surface. Upon heating, the initially formed paratacamite can react with the chlorinated aluminum species with nearly total restoration of $CuCl_2$, which is consequently the main species present and the active phase on the catalyst during the oxyhydrochlorination reaction [36-39].

Pieters e*t al.* reported a non-aqueous impregnation procedure for SiO_2-supported Cu-K-La chloride catalysts, which are active in methane oxyhydrochlorination below 200°C. Under these reaction conditions the catalyst is not molten and the Deacon reaction is not involved. In that case, the promoter and the support stabilize the active phase, which is proposed to be Cu^{1+} [40-42]. The catalyst is activated by treatment in hydrogen flow between 200°C and 280°C for 10 minutes or HCl flow between 280°C and 320°C. In order to keep the catalyst in its active form it is vital, that CH_4 introduction precedes the introduction of oxygen. Oxygen, without CH_4, may poison the catalyst.

The key step in the mechanism in the ethylene OHC reaction is the reduction of $CuCl_2$ to CuCl by ethylene. This reaction (equ. 1.23) is fast and highly endothermic (ΔH = -120

kJ/mol). It is followed by the rate–determining step of reoxidation of CuCl by oxygen to an oxychloride and the restoration of $CuCl_2$ with HCl. This reaction is first order in oxygen partial pressure and second order in $[Cu^+]$ or in a chloride complex of the cuprous ion [43]. The last step is very fast and therefore the reaction order in HCl is zero [43].

$$2CuCl_2 + C_2H_4 \rightleftharpoons C_2H_4Cl_2 + 2CuCl \qquad \text{fast} \qquad\qquad (1.23)$$

$$2CuCl + 0.5O_2 \rightarrow Cu_2OCl_2 \qquad \text{rds} \qquad\qquad (1.24)$$

$$Cu_2OCl_2 + 2HCl \rightarrow 2CuCl_2 + H_2O \qquad \text{very fast} \qquad\qquad (1.25)$$
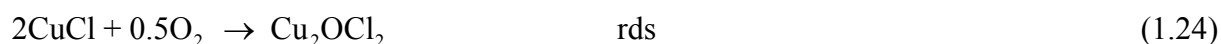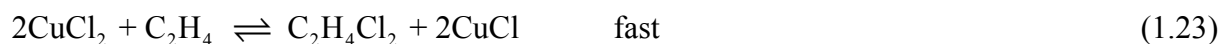
In contrast, the mechanism, originally suggested by Deacon, for the oxyhydrochlorination of methane involves a Cu^{+1}/Cu^{2+} redox cycle. The overall reaction is the oxidation of hydrogen chloride to chlorine and water, the so called Deacon reaction [44]:

$$2Cu^{2+} + 2Cl^- \rightleftharpoons 2Cu^+ + Cl_2 \qquad \text{fast} \qquad\qquad (1.26)$$

$$2Cu^+ + 0.5O_2 \rightleftharpoons 2Cu^{2+} + O^{2-} \qquad \text{rds} \qquad\qquad (1.27)$$

$$O^{2-} + 2HCl \rightleftharpoons H_2O + 2Cl^- \qquad \text{fast} \qquad\qquad (1.28)$$

$$\overline{2HCl + 0.5O_2 \rightleftharpoons H_2O + Cl_2} \qquad \text{Deacon reaction} \qquad\qquad (1.29)$$
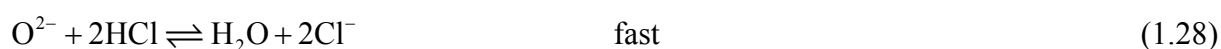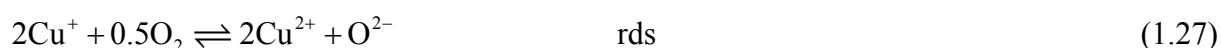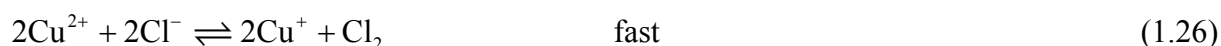
The oxyhydrochlorination of methane involves due to the Deacon reaction a radical gas phase chlorination with the already mentioned disadvantage of low selectivity towards methyl chloride and the formation of higher chlorinated methanes:

$$CH_3Cl + HCl + 0.5O_2 \rightarrow CH_2Cl_2 + H_2O \qquad \Delta H = \text{-153 kJ/mol} \qquad\qquad (1.30)$$

$$CH_2Cl_2 + HCl + 0.5O_2 \rightarrow CHCl_3 + H_2O \qquad \Delta H = \text{-149 kJ/mol} \qquad\qquad (1.31)$$

$$CHCl_3 + HCl + 0.5O_2 \rightarrow CCl_4 + H_2O \qquad \Delta H = \text{-142 kJ/mol} \qquad\qquad (1.32)$$

Aglulin *et al.* studied the mechanism of carbon monoxide formation. Only chloromethanes and not methane contribute to the formation of products of complete oxidation. Carbon monoxide is formed by hydrolysis of chloromethane, followed by the rapid oxidation of the formed alcohols:

$$CH_3Cl + H_2O \rightarrow CH_3OH + HCl \qquad (1.33)$$

$$CH_3OH + 2O_2 \rightarrow CO + 2H_2O \qquad (1.34)$$

$$\overline{CH_3Cl + H_2O + 2O_2 \rightarrow CO + HCl + 2H_2O} \qquad (1.35)$$

Commercially used catalysts are promoted with alkaline chloride and rare-earth chloride, preferably KCl and $LaCl_3$. With no KCl the low valence copper is present in the melt as a mixture of undissociated Cu_2Cl_2 and CuCl which are quite volatile and also difficult to oxidize. A rapid deactivation occurs by the formation of a CuCl film on the surface of the $CuCl_2$ particles. Addition of KCl promotes the formation of cuprous complexes with a structure of $(Cu_2Cl_6)^{4-}$ or $(CuCl_4)^{2-}$ if sufficient Cl^- is present. The chlorine bridge of this complex is easily oxidized (Scheme 1.1).
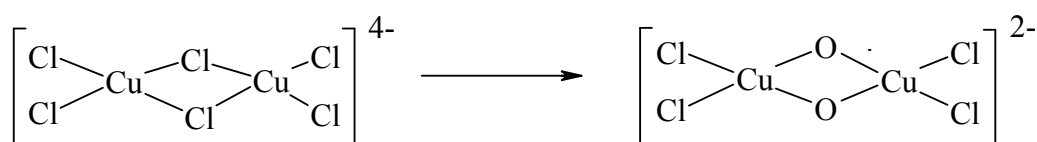
Scheme 1.1: Cuprous complex formed in the presence of potassium promoters[43]

The oxygen bridge is rapidly broken by reaction with HCl, which in contrast to O_2 is easily absorbed in a chloride melt. Furthermore KCl lowers the melting point of the salt mixture. This depression allows the mixture to be even partially molten under ethylene OHC reaction conditions and copper chloride and KCl to be mobile at 225°C in a C_2H_4/N_2 atmosphere.

By the presence of potassium a decrease of combustion and an increase of selectivity to EDC are observed [45]. However, some authors believe that if $CuCl_2$ is supported it is still in the solid state at 300°C [46]. Moreover, the vapor pressure of CuCl is strongly depressed by the presence of the alkali halides. With alkali-containing catalysts practically no vaporization at the reaction temperature of 350 – 365°C occurs. The promotion of KCl only occurs at higher temperatures. This behavior is due to an increase in the apparent activation energy with the addition of KCl. When the temperature falls to the point at which the entire mixture is in the solid state, evolution of chlorine is drastically decreased and the reaction proceeds via a surface mechanism (see equ.1.23-1.35).

Supported $CuCl_2$-KCl catalysts show an irreversible deactivation when heated to 300°C and cooled to room temperature due to segregation of K and Cu. The addition of $LaCl_3$

prevents the dissociation of the K-Cu-Cl double salts and thus inhibits the segregation of copper chloride/potassium chloride at high temperatures, which is the main cause of deactivation. $LaCl_3$ increases the activity with no effect on the apparent activation energy [47].

The segregation of Cu and K is more marked on γ-Al_2O_3 than on the other supports due to the strong affinity of Cu for the support. Thus, surface copper oxychloride species are stabilized and the segregation is consequently enhanced. However, the oxychloride species is also catalytically active and the deactivation is not evident. The salt-support interaction follows the sequence γ-Al_2O_3 > TiO_2 >> SiO_2 [47]. However, Brønsted >Al-OH and Lewis Al^{3+} sites of the support are supposed to play a role in the undesired side reactions and coking processes, responsible for the loss of selectivity and catalyst decay during industrial runs. Furthermore alumina is chemically not resistant to HCl. [38, 44].

Commercially used catalysts have a loading with active material of 25 to 35wt.%. The atomic ratio of alkali metal to copper is between 0.8 and 1.3, and the ratio of rare earth metal to copper is greater than 0.15. Larger amounts of alkali leads to loss of activity while less alkali leads to degradation of the catalyst by sublimation of copper chlorides [43].

1.5   Characterization of the studied catalysts for oxidative chlorination of CH$_4$

1.5.1   Lanthanum oxychloride

According to X-Ray diffraction structural analysis, lanthanum oxychloride crystallizes in a Matlockite-type crystal structure (PbFCl) belonging to the tetragonal space group $D_{4h}^7 \equiv$ P4/nmm (Z = 2). The crystallographic unit cell, which is a primitive unit cell, contains two formula units [48, 49]. Lanthanum is surrounded by four oxygen atoms and four chlorine atoms [50]. Spectroscopic results indicate that the chlorine-terminated (001) plane in the LaOCl crystal is the predominant crystal phase [51]. It has a higher stability compared to the other planes. In the absence of experimental evidence for the structure sensitivity of the methane oxyhydrochlorination reaction, it is reasonable to use it as a surface model. The LaOCl (001) plane is shown Figure 1.4.
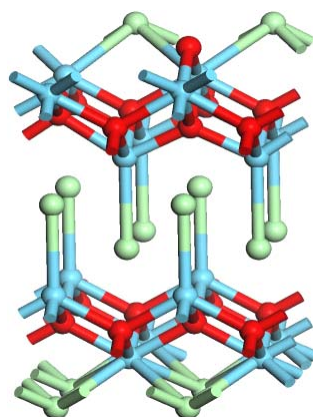
Figure 1.4: LaOCl (001) layered structure [51]. (• La   • Cl   • O)

Since each primitive cell in a LaOCl crystal consists of six monoatomic sites, the structure of the reduced representation of the 15 normal modes of vibration is found to be:

$$\Gamma = 2A_{1g} + 1B_{1g} + 3E_g + 2A_{2u} + 2E_u \tag{1.36}$$

All fundamentals are optically active. The vibrations of the A_{1g}, $B1_g$ and E_g species are active in Raman and those of A_{2u} and E_u species are IR active. The observed wavenumbers are summarized in Table 1.2.

Table 1.2: Raman and IR active fundamentals in lanthanum oxychloride [48]

Raman active		IR active	
Wavenumber [cm^{-1}]	Species	Wavenumber [cm^{-1}]	Species
440	E_g	550-515	La-O bond, E_u
335	B_{1g}	450-378	La-O bond, A_{2u}
188	A_{1g}	250-190	La-Cl bond, E_u
125	A_{1g}	126-108	La-Cl bond, A_{2u}
215	E_g		
67	E_g		

LaOCl is in the presence of HCl in equilibrium with LaCl$_3$ [52]:

$$\text{LaOCl} + 2\text{HCl} \rightleftharpoons \text{LaCl}_3 + \text{H}_2\text{O} \qquad \Delta H° = 118 \text{ kJ/mol} \qquad (1.37)$$

1.5.2   Lanthanum chloride

LaCl$_3$ crystallizes in a hexagonal dipyramidal type and belongs to the space group $C_{6h}{}^2 \equiv$ P63/m [53]. The point of symmetry at the site of a La ion is C_{3h} while the point of symmetry at a chlorine site is C_3, i.e., (E, σ_h) [54]. In LaCl$_3$ the chlorine terminated (100) plane which is shown in Figure 1.5 is the most stable [51].
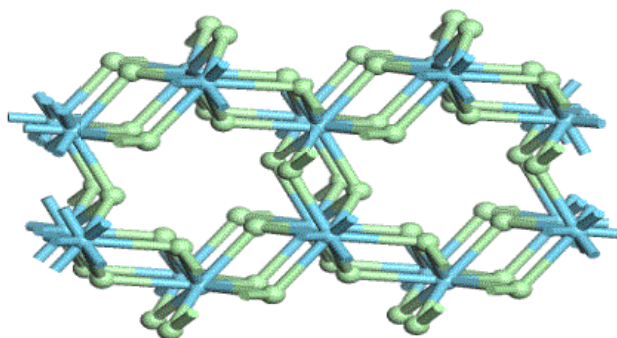
Figure 1.5: LaCl$_3$ (100) layered structure (• La   • Cl) [51]

The structure of the reduced representation can be given as following:

$$\Gamma = 1A_{1u} + 2E_{1u} + 2A_{1g} + 1E_{1g} + 3E_{2g} + 2B_g + 2B_u + 1E_{2u} \qquad (1.38)$$

LaCl$_3$ shows three infrared active (1A$_{1u}$ and 2E$_{1u}$), six Raman-active (2A$_{1g}$, 1E$_{1g}$, and 3E$_{2g}$) and five non active (2B$_g$, 2B$_u$, and 1E$_{2u}$) vibrational modes. The observed Raman and IR active wavenumbers are summarized in Table 1.3.

Table 1.3: Raman and IR active fundamentals in lanthanum chloride [55]

Raman active		IR active	
Wavenumber [cm^{-1}]	Species	Wavenumber [cm^{-1}]	Species
217	E$_{2g}$	210	E$_{1u}$
211	E$_{2g}$	165	A$_u$
186	E$_{1g}$	138	E$_{1u}$
179	A$_{1g}$		
148	A$_{1g}$		
108	E$_{2g}$		

As already mentioned above, LaOCl can be transformed with HCl into LaCl$_3$ (equ. 1.37). By heating hydrated LaCl$_3$ at temperatures near 400°C, the equilibrium is shifted back to LaOCl. Further heating of LaOCl to 800°C yields in the decomposition of LaOCl to La$_2$O$_3$ with the anhydrous LaCl$_3$ volatilizing away [56].

$$3\text{LaOCl} \rightleftharpoons \text{La}_2\text{O}_3 + \text{LaCl}_3 \hspace{4cm} (1.39)$$

The equilibrium between LaOCl and LaCl$_3$ is shown in Figure 1.6. The equilibrium concentration for water and hydrogen chloride are not shown.
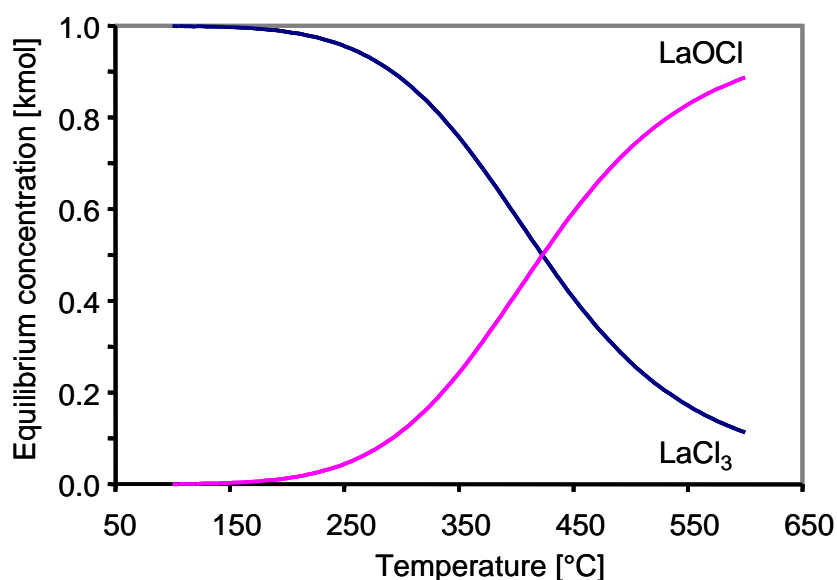
Figure 1.6: Thermodynamic equilibrium between LaCl$_3$ and LaOCl in the presence of water and hydrogen chloride

1.5.3   Acid and base properties of LaOCl and LaCl$_3$

Manoilova *et al.* has extensively characterized the surface acidity and basicity of La$_2$O$_3$, LaOCl, and LaCl$_3$ with probe molecules using infrared spectroscopy, temperature-programmed desorption (TPD), and density-functional theory (DFT) calculations [51]. Lewis acidity is associated with La^{3+} sites. These acid sites can be probed experimentally with CO adsorption at 77K. The magnitude of the CO frequency shift on adsorption compared to the

gas-phase value of 2143 cm⁻¹ can be used as a measure of surface Lewis acidity. The experimental CO frequency values which were collected at low surface coverage show that that the surface acidity increases with the extent of chlorination. A comparison of the CO adsorption results of different acidic materials show that the Lewis acidity of ZrO_2 is similar to that of La_2O_3 and the acidity of $LaCl_3$ is comparable to that of TiO_2. The acidity ranking can be displayed in the following order:

$$ZrO_2 \sim La_2O_3 \quad < \quad LaOCl \quad < \quad LaCl_3 \sim TiO_2 \quad\quad\quad\quad (1.40)$$
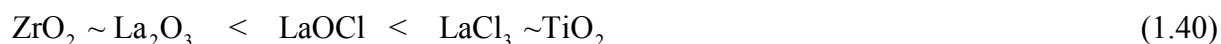
The shift of OH vibrational frequencies to lower wavenumbers at high CO coverage, suggests that the hydrogen-bond strength increases in the same sequence as Lewis acidity. The strength of Brønsted acid sites, studied by adsorption of basic molecules, like pyridine and 2,6-dimethylpyridine (DMP) confirm the acidity ranking.

IR studies of CO_2 adsorption on La_2O_3 indicate that at low coverage monodentate and polydentate carbonates are formed. High coverage spectra are consistent with bulk $La_2(CO_3)_3$. CO_2 adsorption on LaOCl showed the formation of bridged carbonates, sharing a single O adsorption site. CO_2 evolution in TPD experiments can be interpreted in terms of conversion of coupled bridged species into polydentated carbonates and the eventual decomposition of the latter at elevated temperatures. The amount of CO_2 evolved from $LaCl_3$ in TPD experiments was negligibly small due to the absence of lattice O adsorption sites. Therefore the basicity ranking is in the following order:

$$La_2O_3 \quad > \quad LaOCl \quad >> \quad LaCl_3 \quad\quad\quad\quad (1.41)$$

However, proton affinity calculations suggest that lattice O sites may exist on a mixed Cl-O surface of LaOCl which are more basic than those on La_2O_3. The calculations also indicate that Cl^- sites are less basic on $LaCl_3$ than on LaOCl. The decomposition of bulk $La_2(CO_3)_3$ proceeds in 3 steps. Lanthanum carbonate initially converts at around 475°C to lanthanum oxycarbonate $La_2O(CO_3)_2$, which decomposes at 530°C to lanthanum dioxycarbonate $La_2O_2CO_3$. The decomposition is completed around 725°C by the formation of La_2O_3 [57, 58]. Marsal *et al.* presented LaOCl samples as a promising material for CO_2 gas sensors, offering low working temperature and enhanced sensitivity to CO_2 under humid conditions [59, 60]. Okamoto *et al.* reported a Ca^{2+} doped LaOCl as a new type of high Cl^- anion

conducting solid electrolyte. Due to its insolubility in water and high thermal stability it can have a practical application as an HCl or Cl_2 gas monitoring sensor.

1.5.4 Catalytic activity of LaOCl and LaCl₃

Catalytic activity has been reported for La_2O_3, LaOCl, and $LaCl_3$. La_2O_3 and LaOCl were studied for methane coupling [21, 56, 61, 62], for ethane oxidative dehydrogenation [63, 64] and for the destructive adsorption of chlorinated hydrocarbons. $LaCl_3$ is known as a promoter in catalysts for the oxyhydrochlorination and ethane conversion to vinyl chloride [65]. LaOCl doped with Pr^{3+} is known to be catalytically active in methane oxidation under mild conditions (T < 700°C) [56].

1.5.4.1 Catalytic destruction of chlorinated C1 hydrocarbons over LaOCl

Weckhuysen and coworkers reported that lanthanum oxychloride show in the temperature range between 250°C and 450°C a superior activity in destructive adsorption of chlorinated C1 hydrocarbons, which are toxic and environmentally harmful compounds. This process, involves the exchange of chlorine of the CHCs with the lattice oxygen of LaOCl. As a result, LaOCl is partially or completely converted into $LaCl_3$:

$$LaOCl + 0.5CCl_4 \rightarrow LaCl_3 + 0.5CO_2 \tag{1.42}$$

The noncatalytic destructive adsorption can be combined with a concurrent dechlorination of the partially chlorinated solid with steam resulting in the formation of HCl in order to form a heterogeneous catalytic cycle [66]. The dechlorination with steam is very fast compared to other catalysts which results in the high activity of LaOCl.

Van der Heijden *et al.* elucidate the mechanism for the destructive adsorption of chlorinated hydrocarbons over LaOCl. Two initial pathways are proposed for the destructive adsorption of the chlorinated C1 series, i.e. CCl_4, $CHCl_3$, CH_2Cl_2 and CH_3Cl. The first reaction pathway is that two Cl atoms of the reactant are exchanged for a lattice O atom, which leads to the formation of a gas phase intermediate, namely COH_xCl_{2-x}. In the case of CH_3Cl which possesses only one Cl atom, another reaction may occur which resembles this pathway. Two

CH$_3$Cl molecules donate one Cl atom to the Lewis site La^{3+}, which initializes the destructive adsorption. Whereas the basic oxygen stabilizes the remaining fragment and enables the conversion into oxygen containing products [67].

For CH$_3$Cl, CH$_2$Cl$_2$, and CHCl$_3$ a second pathway exists which results after the removal of a H and Cl atom from the reactant by an oxygen site in the formation of an adsorbed CH$_{x-1}$Cl$_{3-x}$ fragment. A hydroxyl group is formed as a result of the removal of the H-atom and the Cl-atom forms a bond with the La-ion. The strength of the basic O ion directly influences the initial step of the reaction pathway. The CH$_{x-1}$Cl$_{3-x}$ fragment is able to migrate across the surface and remove a lattice O atom to form the gas phase intermediate COH$_{x-1}$Cl$_{3-x}$. The two initial pathways result in the formation of two similar intermediate products. The rapid readsorption of the two intermediates, COH$_x$Cl$_{2-x}$ and COH$_{x-1}$Cl$_{3-x}$, results in the formation of hydroxyls, formats, carbonates or methoxy groups. The relative amount of each of these surface intermediates depends on the Cl/H ratio of the reactant. The formed surface species can further interconvert or dissociate into gas phase product, depending on the chlorination degree of the surface and the reaction temperature. In general, higher H-content of the reactant results in more hydrogenated reaction products. The two reaction pathways are summarized in Figure 1.7.
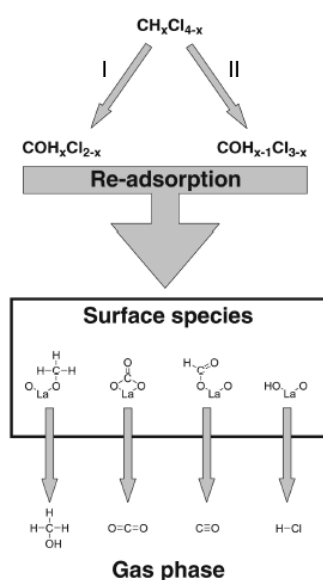

Figure 1.7: Proposed mechanism for the destructive adsorption of CH$_x$Cl$_{4-x}$ [68]

The two reaction pathways for methyl chloride are shown in Figure 1.8. Species 1a and 1a' are related to pathway I. The formation of methoxy groups is accompanied by the formation

of dimethyl ether by the exchange of two Cl atoms from two CH_3Cl molecules for one O atom (Species 1a to 1a'). Species 1b to 6b' are related to pathway II. However, hydrogen abstraction is not favorable in the case of CH_3Cl (Species 1b to 2b).
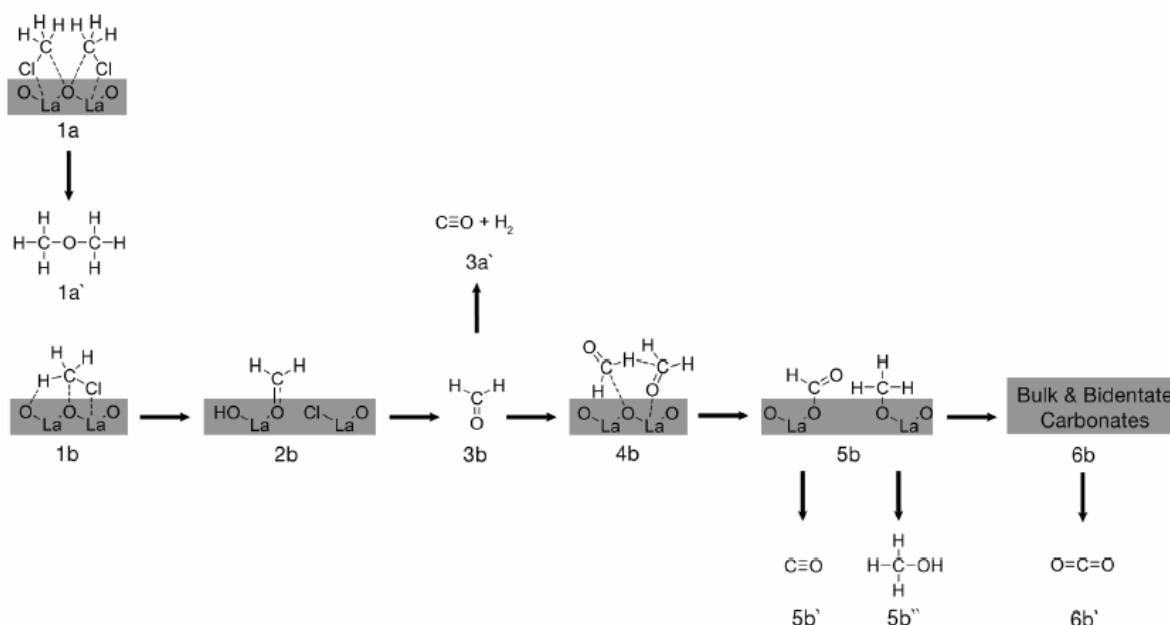
Figure 1.8: Proposed mechanism for the destructive adsorption of CH_3Cl [68]

The reactivity towards catalytic destruction decreases with decreasing Cl-content due to the change in polarization in the bonds of the CH_xCl_{4-x} molecule. Loss of polarization as a result of decreasing chlorine content stabilizes the reactant molecule, and hence reduces the susceptibility to proton or chlorine abstraction, resulting in lower activity [68].

The relative activity of surface sites for the catalytic destruction of chlorinated C1s can be ranked in the following order: $LaOCl > LaCl_3$, with a partially dechlorinated surface > La_2O_3. The higher activity of LaOCl is attributed to the combined effect of high acidity of the La site which allows it to polarize the C-Cl bond more easily and high basicity of the O site which allows it to stabilize the remaining fragment more effectively. Additionally the basic site is in proximity of the acid site, so that the remaining fragment can be stabilized simultaneously with the abstraction of $Cl^{\delta-}$. Thus, LaOCl represents the optimum combination of a strong Lewis acid site with sufficient basic oxygen. $LaCl_3$ is inactive for the catalytic destruction due to the missing basic oxygen site [67]. Intermediate activity of $LaCl_3$ is attributed to higher acidity of La sites but lower basicity of O sites. After a period of high

activity, the rate of conversion decreases and stabilizes at a steady state, where the reaction is controlled by diffusion of oxygen to the surface and chlorine to the bulk. Finally, when the material is fully chlorinated, the material is deactivated and the conversion drops to almost zero [67].

1.6   Methyl chloride an important feedstock for industry

Methyl chloride plays a major role as an intermediate in a number of chemical processes. Currently, methyl chloride is produced commercially by reacting methanol with hydrogen chloride either in liquid phase with a $ZnCl_2$ catalyst or in the gas phase over an alumina catalyst at 350°C [69].

$$CH_3OH + HCl \rightarrow CH_3Cl + H_2O \qquad (1.43)$$

It is an intermediate in the production of silicone materials. The silicone industry utilizes methyl chloride in the Rochow direct process in a reaction with silicon to form $(CH_3)_2SiCl_2$ which is then hydrolyzed to form silicones [14]. Methyl chloride is also used in the production of methyl cellulose and quarterny ammonium salts, which are used as cationic surfactants in shampoos and detergents. Furthermore, methyl chloride can be hydrolyzed to methanol and dimethyl ether which are important raw material feedstocks for the chemical industry.

Methyl chloride can be also converted to light olefins like ethene and propene over ZSM-5 zeolites in the temperature range between 400°C and 500°C (equ. 1.45). In this step HCl is formed as a byproduct which can be recycled and reused for the formation of methyl chloride, e.g. via oxyhydrochlorination. The combination of oxyhydrochlorination with conversion of methyl chloride over ZSM-5 results in an overall reaction which is identical to light olefin production via oxidative coupling (equ. 1.46).

$$nCH_4 + nHCl + n/2O_2 \rightarrow nCH_3Cl + nH_2O \qquad (1.44)$$

$$nCH_3Cl \rightarrow C_nH_{2n} + nHCl \qquad (1.45)$$

$$\overline{nCH_4 + n/2O_2 \rightarrow C_nH_{2n} + nH_2O} \qquad (1.46)$$

This is also an alternative to the Mobil process which uses methanol which is generated via capital intensive syngas production.

Several authors reported that metal exchanged ZSM-5 zeolites exhibit higher activity and longer lifetime [70-72]. Lersch *et al.* published that Mg-exchanged ZSM-5 is the most promising catalyst with high activity (≥99.2 % at 425°C) and an improved selectivity for alkenes and therefore a longer lifetime (≥40h) compared to H-ZSM-5. For Mg-ZSM-5 an alkene yield of 49.4% was reached compared to an alkene yield of 20.7% for H-ZSM-5. However, after a long time-on-stream the metal exchanged zeolites are destroyed by the released hydrochloric acid. The selectivity to olefins increases also for ZSM-5 catalysts with higher Si/Al ratio due to the fact, that the sites are more isolated and hydrogen transfer is reduced. The function of Mg^{2+} is the activation of methyl chloride through the formation of an Mg-Cl bond. While the chlorine atom departs from one side, the framework oxygen atom attacks from the other side. This transition state for the methoxide formation resembles the transition state of a S_N2 like reaction. This surface intermediate decomposes to a carbene and HCl. The formation of a C-C bond occurs via the addition of a carbene intermediate to the surface methoxide group. Ethylene is the initial hydrocarbon product, which oligomerizes and cracks back to the observed distribution of propylene and ethylene [71].

Sun *et al.* reported that selectivity can be enhanced by modification of the Mg-ZSM-5 zeolite with phosphorus. The phosphorus treatment improves the selectivity by reduction of the strong Brønsted acidity of the catalyst by dealumination of the lattice and formation of extra-lattice aluminum and aluminophosphate material. These Brønsted acid groups are responsible for the conversion of light olefins to aromatics and paraffins which cause the deactivation of the catalyst by coking [72].

1.7   Scope of the thesis

Methane is one of the most abundant and low-cost carbon-based feedstock available. Its conversion to chemicals has been one of the main topics in hydrocarbon research for several decades. However, the direct functionalization of methane is very challenging due to the strong C-H bonds (439 kJ mol^{-1}) and its tetrahedral geometry. The main objective of this thesis is the investigation of the reaction mechanism over $LaCl_3$-based materials in oxidative chlorination of methane with hydrogen chloride and oxygen to methyl chloride and water. In order to increase the specific surface area of the catalysts, the influence of different bases used for precipitation in the preparation of the catalyst precursor, LaOCl, is studied. Furthermore the effect of different metal dopants on the catalytic performance of LaOCl was examined.

A general introduction about the catalytic processes of methane activation and the chlorination of methane is given in Chapter 1. Furthermore the characteristics of the used catalysts system $LaOCl/LaOCl_3$ are described. The design of the plug flow reactor system and the gas chromatography analysis unit is presented in Chapter 2.

The general catalytic performance of the catalyst and the reaction network over $LaCl_3$ for oxidative chlorination of methane is investigated in Chapter 3. The role of the different reactants is studied with pulse and Raman measurements. Based on the experimental results and DFT calculations of the intermediate structures a reaction mechanism is proposed.

Chapter 4 focuses on the synthesis of the catalyst precursor LaOCl by precipitation with organic bases like tetraethylammonium hydroxide (TEAOH), tetrapropylammonium hydroxide (TPAOH) and tetrabutylammonium hydroxide (TBAOH). Various physicochemical methods were applied to investigate the influence of the precipitating agent on the morphology and the structural parameters. Moreover the role of lanthanum carbonate during the chlorination of LaOCl to $LaCl_3$ is studied.

The influence of the metal dopants $MgCl_2$, $CoCl_2$, $NiCl_2$ and $CeCl_3$ on $LaCl_3$ are discussed in Chapter 5. The prepared catalysts are characterized and tested for oxidative chlorination at 475°C with variation in the residence time. A temperature programmed reaction is applied in order to study the difference in the catalytic performance of these catalysts. The thermal stability of the catalysts and the ability to adsorb oxygen are explored via thermogravimetry.

Chapter 6 gives a summary of the most important results and conclusions.

1.8 References

1. *BP Statistical Review of World Energy*. 2007, London: Britisch Petroleum Co.

2. http://www.uniongas.com/aboutus/aboutng/composition.asp, **2008**.

3. Lunsford, J.H., Catal. Today, **2000,** 63(2-4), 165-174.

4. Thackeray, F. and Leckie, G., Pet. Econ., **2002,** 69, 10-12.

5. Bank, T.W., *A voluntary standard for global gas flaring and venting reduction*. 2004, Washington, DC, USA.

6. Podkolzin, S.G., Stangland, E.E., Jones, M.E., Peringer, E., and Lercher, J.A., J. Am. Chem. Soc., **2007,** 129, 2569-2576.

7. Hansen, J., Sato, M., Kharecha, P., Russell, G., Lea, D.W., and Siddall, M., Philos. Trans. R. Soc. A-Math. Phys. Eng. Sci., **2007,** 365(1856), 1925-1954.

8. Crabtree, R.H., Chem. Rev, **1985,** 85(4), 245-269.

9. Stetter, H. and Goebel, P., Chem. Ber., **1962,** 95, 1040.

10. Fabre, P.-L., Devynck, J., and Tremillon, B., Chem. Rev., **1982,** 82(17), 591-614.

11. Olah, G.A., Acc. Chem. Res., **1987,** 20(11), 422-428.

12. Crabtree, R.H., Chem. Rev., **1995,** 95(7), 2599-2599.

13. Dissanayake, D., Rosynek, M.P., Kharas, K.C.C., and Lunsford, J.H., J. Catal., **1991,** 132(1), 117-127.

14. Bablin, J.M., Lewis, L.N., Bui, P., and Gardner, M., Ind. Eng. Chem. Res., **2003,** 42(15), 3532-3543.

15. Bao, J., Liu, Z.L., Zhang, Y., and Tsubaki, N., Catal. Commun., **2008,** 9(5), 913-918.

16. Fischer, F. and Tropsch, H., Brennstoff-Chem, **1926,** 7, 97.

17. Fischer, F. and Tropsch, H., Chem. Ber., **1926,** 59, 830.

18. Olah, G.A., US Patents 4373109 and 4467130.

19. Olah, G.A., Doggweiler, H., Felberg, J.D., Frohlich, S., Grdina, M.J., Karpeles, R., Keumi, T., Inaba, S., Ip, W.M., Lammertsma, K., Salem, G., and Tabor, D.C., J. Am. Chem. Soc., **1984,** 106(7), 2143-2149.

20. Amenomiya, Y., Birss, V.I., Goledzinowski, M., Galuszka, J., and Sanger, A.R., Cat. Rev. - Sci. Eng., **1990,** 32(3), 163-227.

21. Lunsford, J.H., Angew. Chem., Int. Ed. Engl., **1995,** 34(9), 970-980.

22. Le Van, T., Che, M., Tatibouet, J.M., and Kermarec, M., J. Catal., **1993,** 142(1), 18-26.

23. Mimoun, H., Robine, A., and Bonnaudet, S., Appl. Catal., **1990,** 58(2), 269-280.

24.   Fang, X., Li, S., Lin, J., Gu, J.L., and Yang, D., J. Mol. Catal., **1992,** 6, 427.

25.   Pak, S., Qiu, P., and Lunsford, J.H., J. Catal., **1998,** 179(1), 222-230.

26.   Lunsford, J.H., Hinson, P.G., Rosynek, M.P., Shi, C.L., Xu, M.T., and Yang, X.M., J. Catal., **1994,** 147(1), 301-310.

27.   Thomas, J.M., Ueda, W., Williams, J., and Harris, K.D.M., Faraday Discussions of the Chemical Society, **1989,** 87 33-45.

28.   Burch, R., Squire, G.D., and Tsang, S.C., Appl. Catal., **1989,** 46(1), 69-87.

29.   Dumas, J.B., Ann. Chim. Phys., **1840,** 73(2), 94.

30.   Chiltz, G., Martens, G., Huybrechts, G., Goldfinger, P., and Verbeke, G., Chem. Rev., **1963,** 63(4), 355-372.

31.   Olah, G.A., Gupta, B., Farina, M., Felberg, J.D., Ip, W.M., Husain, A., Karpeles, R., Lammertsma, K., Melhotra, A.K., and Trivedi, N.J., J. Am. Chem. Soc., **1985,** 107(24), 7097-7105.

32.   Batamack, P., Bucsi, I., Molnar, A., and Olah, G.A., Catal. Lett., **1994,** 25(1-2), 11-19.

33.   Bucsi, I. and Olah, G.A., Catal. Lett., **1992,** 16(1-2), 27-38.

34.   Ohtsuka, Y. and Tamai, Y., J. Catal., **1978,** 51(2), 169-172.

35.   Tret'yakov, V.P. and Osetskii, A.N., Kinet. Catal., **1982,** 23(5), 958-961.

36.   Leofanti, G., Padovan, M., Garilli, M., Carmello, D., Zecchina, A., Spoto, G., Bordiga, S., Palomino, G.T., and Lamberti, C., J. Catal., **2000,** 189(1), 91-104.

37.   Leofanti, G., Padovan, M., Garilli, M., Carmello, D., Mara, G.L., Zecchina, A., Spoto, G., Bordiga, S., and Lamberti, C., J. Catal., **2000,** 189, 105-116.

38.   Leofanti, G., Marsella, A., Cremaschi, B., Garilli, M., Zecchina, A., Spoto, G., Bordiga, S., Fisicaro, P., Berlier, G., Prestipino, C., Casali, G., and Lamberti, C., J. Catal., **2001,** 202(2), 279-295.

39.   Leofanti, G., Marsella, A., Cremaschi, B., Garilli, M., Zecchina, A., Spoto, G., Bordiga, S., Fisicaro, P., Prestipino, C., Villain, F., and Lamberti, C., J. Catal., **2002,** 205(2), 375-381.

40.   Pieters, W.J.M., Conner, J., Wm. C., and Carlson, E.J., Appl. Catal., **1984,** 11(1), 35-48.

41.   Conner, W.C.J., Pieters, W.J.M., Gates, W., and Wilkalis, J.E., Appl. Catal., **1984,** 11(1), 49-58.

42.   Conner, C.J.W., Pieters, W.J.M., and Signorelli, A.J., Appl. Catal., **1984,** 11(1), 59-71.

43.   Villadsen, J. and Livbjerg, H., Cat. Rev. - Sci. Eng., **1978,** 17(2), 203-272.

44.   Wattimena, F. and Sachtler, W.M.H., Stud. Surf. Sci. Catal., **1982,** 7, 816-827.

45. Rouco, A.J., J. Catal., **1995,** 157(2), 380-387.

46. Arcoya, A., Cortes, A., and Seoane, X.L., Can. J. Chem. Eng., **1982,** 60(1), 55-60.

47. Garcia, C.L. and Resasco, D.E., J. Catal., **1990,** 122(1), 151-165.

48. Hase, Y., Dunstan, P.O., and Temperini, M.L.A., Spectrochim. Acta, Part A, **1981,** 37(8), 597-599.

49. Haeuseler, H., J. Raman Spectrosc., **1984,** 15(2), 120-121.

50. Basile, L.J., Ferraro, J.R., and Gronert, D., J. Inorg. Nucl. Chem., **1971,** 33(4), 1047.

51. Manoilova, O.V., Podkolzin, S.G., Tope, B., Lercher, J., Stangland, E.E., Goupil, J.M., and Weckhuysen, B.M., J. Phys. Chem. B, **2004,** 108(40), 15770-15781.

52. Koch, C.W., Broido, A., and Cunningham, B.B., J. Am. Chem. Soc., **1952,** 74(9), 2349-2351.

53. Zachariasen, W.H., Chem. Phys., **1948,** 16, 254.

54. Murphy, J., Buchanan, R.A., and Caspers, H.H., J. Chem. Phys., **1964,** 40(3), 743.

55. Richman, I., Wong, E.Y., and Satten, R.A., J. Chem. Phys., **1963,** 39(7), 1833.

56. Kaddouri, A.H., De Blasio, N., and Del Rosso, R., React. Kinet. Catal. Lett., **2001,** 72(2), 309-320.

57. Klingenberg, B. and Vannice, M.A., Chem. Mater., **1996,** 8(12), 2755-2768.

58. Paama, L., Pitkanen, I., Halttunen, H., and Peramaki, P., Thermochim. Acta, **2003,** 403(2), 197-206.

59. Marsal, A., Dezanneau, G., Cornet, A., and Morante, J.R., Sens. Actuators, B, **2003,** 95, 266-270.

60. Marsal, A., Rossinyol, E., Bimbela, F., Tellez, C., Coronas, J., Cornet, A., and Morante, J.R., Sens. Actuators, B, **2005,** 109, 38-43.

61. Campbell, K.D., Zhang, H., and Lunsford, J.H., J. Phys. Chem., **1988,** 92(3), 750-753.

62. Au, C.T., He, H., Lai, S.Y., and Ng, C.F., Appl. Catal. A, **1997,** 159(1-2), 133-145.

63. Sugiyama, S., Sogabe, K., Miyamoto, T., Hayashi, H., and Moffat, J.B., Catal. Lett., **1996,** 42, 127-133.

64. Ciambelli, P., Lisi, L., Pirone, R., Ruoppolo, G., and Russo, G., Catal. Today, **2000,** 61, 317-323.

65. Schweizer, A.E., Jones, M.E., and Hickman, D.A., WO Patent 6,452,058 A1, **2002**.

66. Van der Avert, P., Podkolzin, S.G., Manoilova, O., De Winne, H., and Weckhuysen, B.M., Chem. Eur. J., **2004,** 10(7), 1637-1646.

67. Podkolzin, S.G., Manoilova, O.V., and Weckhuysen, B.M., J. Phys. Chem. B, **2005,** 109(23), 11634-11642.

68. Van der Heijden, A.W.A.M., Garcia Ramos, M., and Weckhuysen, B.M., Chem. Eur. J., **2007,** 109(1-2), 97-101.

69. Svetlano, E., Flid, R.M., Dzhagats.Rv, and Taber, A.M., Russian Journal Of Physical Chemistry, **1967,** 41(4), 487.

70. Lersch, P. and Bandermann, F., Appl. Catal., **1991,** 75(1), 133-152.

71. Noronha, L.A., Souza-Aguiar, E.F., and Mota, C.J.A., Catal. Today, **2005,** 101(1), 9-13.

72. Sun, Y., Campbell, S.M., Lunsford, J.H., Lewis, G.E., Palke, D., and Tau, L.M., J. Catal., **1993,** 143(1), 32-44.

Chapter 2

Experimental Section

Abstract

This chapter explains in detail the construction of the used kinetic reactor and analysis unit. Furthermore the evaluation of the results is shown.

2 Experimental Section

2.1 Catalytic reactor

Methane oxyhydrochlorination was performed in a conventional fixed bed down stream reactor at atmospheric pressure. The reactor is a quartz glass tube with 4 mm i.d. and approximately 43.5 cm length. This tube is placed in a vertical furnace. The catalyst was placed in the middle of the reactor supported between two plugs of quartz wool. The remaining dead volume of the reactor was filled with glass beads of a size between 0.63 to 0.75 mm to minimize void space. A 4-port valve was used for measuring the feed composition before entering the reactor via the bypass line. The temperature was measured with a thermocouple located above the catalyst bed and controlled by a *Eurotherm 2416*. The glass lining lines were heated at 150°C to avoid the condensation of liquid HCl inside the lines, which could result in corrosion and plugging of the lines. Teflon or Hastelloy tubings and fittings were used to avoid corrosion due to hydrogen chloride. The outlet of the effluent lines was first connected to a water scrubber and then to a scrubber with a 4M NaOH solution in order to neutralize the HCl and other acidic gases coming out of the reactor. The effluent was further purified by passing through activated charcoal. Bronkhorst mass flow controllers (MFC) were used to measure and control the gas flows of helium as inert gas, methane, hydrogen chloride and oxygen as reactants and nitrogen as an internal standard. Liquid feeds can be dosed by a syringe pump. The whole experiment can be controlled by the computer using the hp*vee* program, version *5.0. Advanced EZChrom* is used as analysis program for the GC. A schematic overview of the reactor unit is shown in Figure 2.1.

The exact experimental conditions for each experiment and the used setups for physicochemical characterization are mentioned at the experimental part of each chapter.
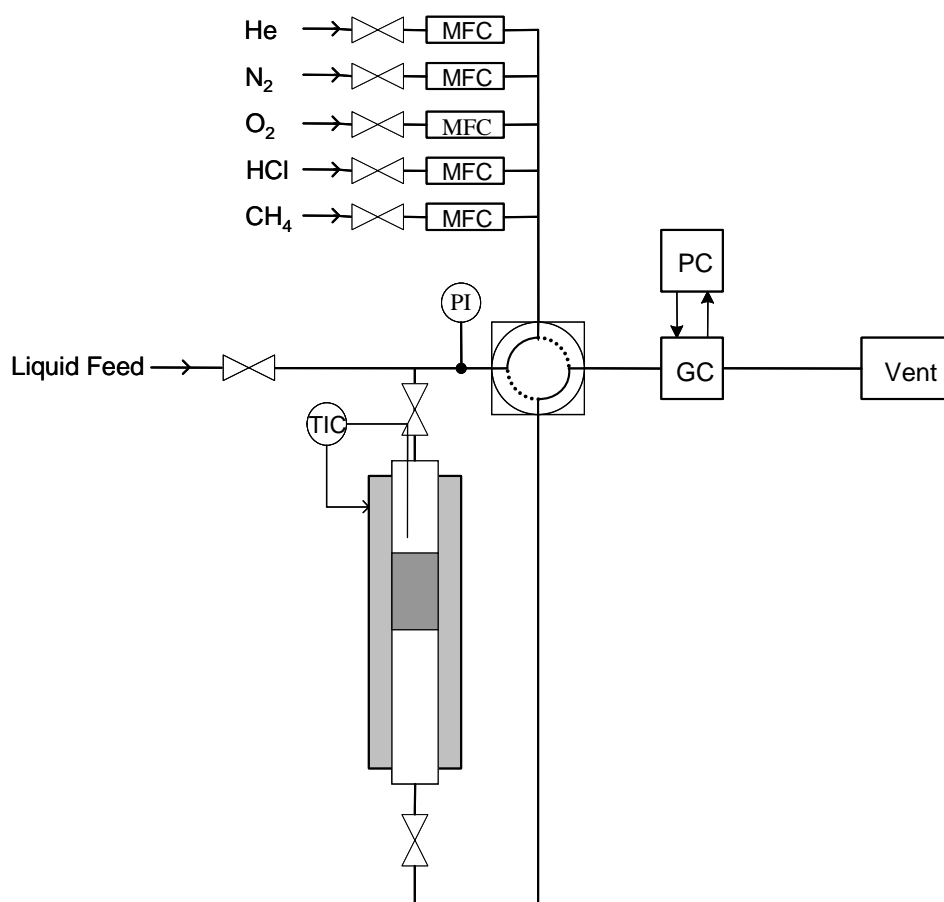
Figure 2.1: Schematic overview of the reactor unit for oxyhydrochlorination of methane (MFC = Mass flow controller, PI = Pressure indicator, PC = Personal computer, GC = Gas chromatograph, TIC = Temperature indicator control)

2.2   Product analysis

The product distribution was analyzed by a Siemens Maxum-Edition II online GC equipped with two ovens heated to 80°C and 130°C and thermal-conductivity detectors (TCD). Six columns were used for separating the product effluent gases. The columns are located in the oven tempered at 130°C. Helium is used as carrier gas. The retention time of the analyzed products is controlled by controlling the carrier gas inlet pressure with electronic pressure controllers (EPC). The design of the SIEMENS MAXUM II gas chromatograph is shown in Figure 2.2.
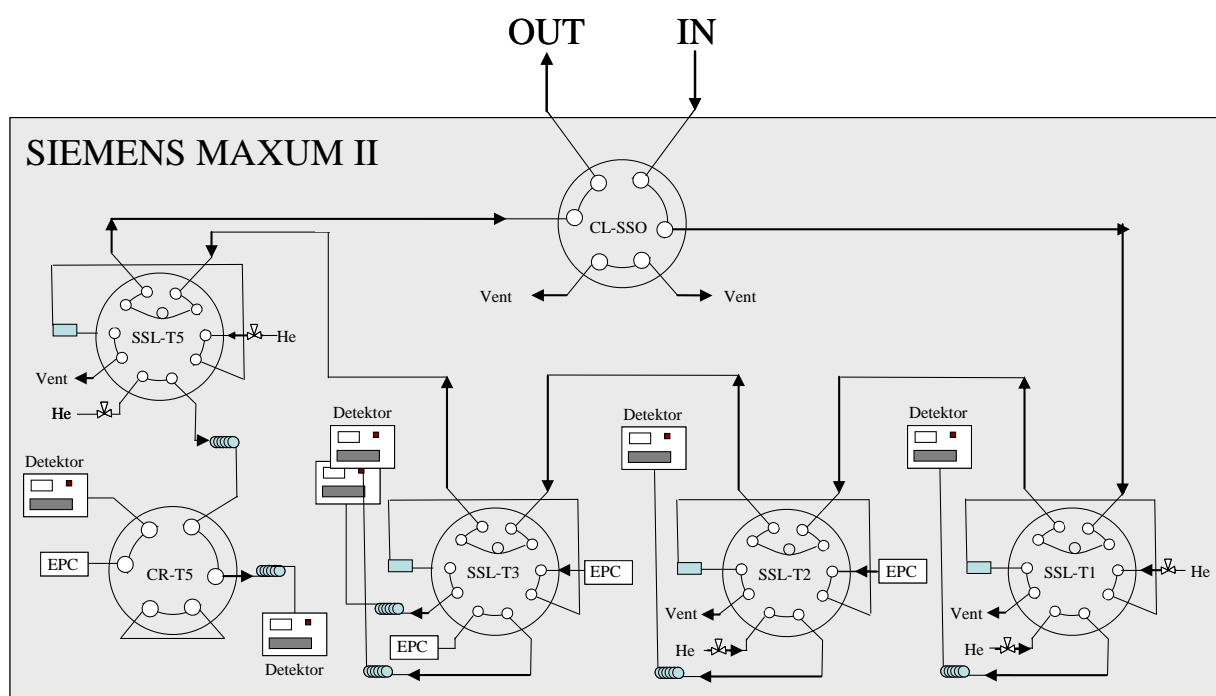
Figure 2.2: Schematic overview of the used gas chromatograph (EPC = Electronic pressure controller)

The parameters and packing material of the used analytical columns are listed in Table 2.1.

Table 2.1: Parameter and packing material of the used analytical columns

Analytical column	Parameter and Packing material
RR1_T1	2m x 1/8" OD, Nickel, Molesieve 5A, 60/80 mesh
RR2_T2	2m x 1/8" OD, Nickel, Hayesep Q, 80/100 mesh
RR3_T3a	4m x 1/8" OD, Nickel, Tenax TA, 60/80 mesh
RL1_T3b	2m x 0.03" ID, 1/16" OD, Nickel, micro-packed Hayesep Q, 80/100 mesh
RL2_T5a	30 m x 0.53mmID, 1.0μ film, MTX-1, metal capillary
RL3_T5b	30 m x 0.53mmID, 1.0μ film, MTX-1, metal capillary

The analytes of each column are listed in Table 2.2. The calibrated compounds are written in bold letters.

Table 2.2: Analytes of the different columns

Analytical Column	Analytes
RR1_T1	**O_2+Ar, N_2, CO, CH_4**
RR2_T2	**CH_4, CO_2, C_2H_4, C_2H_6**
RR3_T3a	**CH_4, CO_2, C_2H_4, C_2H_6, HCl**
RL1_T3b	$H_2$0, **methyl chloride (MeCl)**, vinyl chloride (VCM)
RL2_T5a	methyl chloride + methanol + vinyl chloride (MeCl+MeOH+VCM), H_2O, methyl formate, ethyl chloride (EtCl), formic acid, **methylene cloride (MeCl2)**, trans-1,2 dichloroethylene (12ene_trans), cis-1,2 dichloroethylene (12ene_cis), **chloroform (CCl3)**, 1,2 dichloroethane (EDC)
RL3_T5b	**carbon tetrachloride (tet)**, tetrachloroethylene (perc)

The amount of the products after reaction is calculated via equation. 2.1. The response factors are determined for each compound by using a calibration bottle or by multilevel calibration.

$$[A] = \frac{Area\_A}{RF} \qquad (2.1)$$

with   [A] = concentration of component A (Vol%)

Area_A = area of component A

RF = response factor for A

2.3 Evaluation of kinetic data

The oxyhydrochlorination of methane underlies a change of mole number, therefore the GC concentrations have to be corrected by a normalizing factor. N_2 is used as an internal standard to obtain the normalizing factor N_2F:

$$N_2F = \frac{\text{mol}\%\,\text{nitrogen}}{\text{mol}\%\,\text{nitrogen} \;\; \text{before} \;\; \text{reaction}} \tag{2.2}$$

Catalytic results in this work are presented as conversion and selectivity. The conversion is defined according to the following equation:

$$X_i(\%) = 100 \times \left(\frac{\text{mol}\%\,\text{component}(i_0) \times N_2F - \text{mol}\%\,\text{component}(i)}{\text{mol}\%\,\text{component}(i_0) \times N_2F} \right) \tag{2.3}$$

with $\quad i_0 = $ Bypass-concentration of component i

$\qquad\quad N_2F = $ normalization factor

The selectivity of a given product towards the other compounds is given by following equation:

$$S_i(\%) = 100 \times \left(\frac{\text{mol}\%\,\text{product}(i_0)}{\text{total} \;\; \text{amount} \;\; \text{of} \;\; \text{products}} \right) \tag{2.4}$$

To verify the results of the GC the carbon and chlorine balance are calculated using equation 2.5 and 2.6, respectively.

$$\text{BalanceC} = \frac{\text{mol}\%\,CH_3Cl + \text{mol}\%\,CH_2Cl_2 + \text{mol}\%\,CHCl_3 + \text{mol}\%\,CCl_4 + \text{mol}\%\,CO_x + \text{mol}\%\,CH_4}{\text{mol}\%\,CH_{4,0} \times N_2F}$$

$$\tag{2.5}$$

$$\text{BalanceCl} = \frac{\text{mol}\%\,CH_3Cl + 2 \times \text{mol}\%\,CH_2Cl_2 + 3 \times \text{mol}\%\,CHCl_3 + 4 \times \text{mol}\%\,CCl_4 + \text{mol}\%\,HCl}{\text{mol}\%\,HCl_0 \times N_2F}$$

$$\tag{2.6}$$

Chapter 3

Reaction network of oxidative chlorination of methane over lanthanum-based catalysts

Abstract

LaCl$_3$ is an active, selective and stable catalyst for oxidative chlorination of methane to methyl chloride. Selective conversion to methyl chloride can be achieved by limiting methane conversion, for example, by using an excess of methane in the feed. Methylene chloride and carbon monoxide are the main side products at higher methane conversion levels. Flow and pulse experiments indicate that the presence of hydrogen chloride is not required for activity, and its role appears to be limited to maintaining the extent of catalyst chlorination. In contrast, the present of gas-phase oxygen is essential for catalytic activity. Transient OCl$^-$ anion, formed by oxidation of Cl$^-$ in LaOCl and LaCl$_3$ with molecular oxygen, is proposed to be the active site for the initial step of methane activation.

3 Reaction network of oxidative chlorination of methane over lanthanum-based catalysts

3.1 Introduction

Methane is one of the most abundant and low-cost carbon-based feedstocks available. Its conversion to chemicals has been one of the main topics in hydrocarbon research for several decades. Conversion of methane currently requires the production of synthesis gas, a mixture of carbon monoxide and hydrogen, through steam methane reforming, partial oxidation or a combination. Synthesis gas-based processes currently produce vast quantities of methanol and ammonia from natural gas [1]. Methane conversion through synthesis gas is capital and energy intensive, yet this route remains the only commercially viable technology for converting methane into chemicals. It is expected to remain the dominant technology in the industrial conversion of natural gas to chemical products.

Selective methane activation is difficult because of the symmetry of the molecule, with all four C-H bonds being equally very strong, which results in an overall low reactivity [2]. On the other hand, any products formed after activation of the first C-H bond are inherently more reactive, making reaction selectivity challenging. Moreover, high thermodynamic stability of methane leads to unfavorable reaction equilibria in most cases, unless an oxidative step is involved. A combination of methane activation with an oxidation reaction, however, makes it especially difficult to stop methane functionalization at an initial stage to achieve high selectivities.

Conceptually, use of an electrophilic halogen or a halogen compound for methane activation is intriguing since, in contrast to chalcogenides, the thermodynamic driving force is lower and, thus, the selectivity to monofunctionalized products can be better controlled. Methane functionalization with chlorine to methyl chloride is probably the most promising approach because methyl chloride is used in a variety of applications including its further conversion to higher hydrocarbons [3, 4] and, in addition, all higher chlorine substituted products are large-scale commodity chemicals.

Currently, methyl chloride is produced commercially by reacting methanol with hydrogen chloride either in liquid phase with a $ZnCl_2$ catalyst or in the gas phase over an alumina catalyst at 350°C [5]. Alternatively, methyl chloride can be produced by radical gas-phase reaction with Cl_2. The major disadvantage of the radical reaction is an unfavorable distribution of chloromethanes that are produced due to the higher reactivity of methyl

chloride compared to methane and, similarly, sequentially higher reactivity of more highly substitutes chloromethanes.

Olah *et al.* showed that with supported solid acids, such as FeO_xCl_y/Al_2O_3, $TaOF_3/Al_2O_3$, $NbOF_3/Al_2O_3$, $ZrOF_2/Al_2O_3$, $SbOF_3/Al_2O_3$, SbF_5/graphite and Nafion-H/TaF_5, selectivity to CH_3Cl of 96% at a conversion of 34% at 270°C can be achieved [6, 7]. Olah's proposed chlorination mechanism involves insertion of a surface-coordinated electrophilic chlorine species into the C-H bond, forming a five-coordinated carbonium ion intermediate. The carbonium ion undergoes decomposition in parallel with halogenolysis, producing CH_3Cl and HCl. However, the use of chlorine is undesirable due to the requirement of converting the HCl byproduct to Cl_2. An alternative is oxidative chlorination where methane is reacted with O_2 and HCl. Copper-based catalysts are used in the industrial oxychlorination of ethylene. These catalysts, when operated at higher temperature, have been shown to convert methane to chloromethanes [8]. While ethylene conversion over copper-based catalysts is believed to proceed through a mechanism, which involves a Cu^{+1}-Cu^{+2} redox cycle [9], the mechanism with methane has not been well studied. Since copper-based catalysts are known to be active for the Deacon chemistry [10], the oxidation of HCl to Cl_2, methane activation through liberation of elemental chlorine is one possible mechanism. As methane chlorination proceeds, at least partially, *via* a radical gas-phase mechanism, selectivity to methyl chloride is usually low at significant methane conversion levels [10]. A major drawback is the volatility of copper salts at the usual temperatures required for methane activation, resulting in unstable catalysts, which contaminate and potentially plug downstream equipment. The stability of copper catalysts has been enhanced by different promoters; for example, KCl reportedly lowers the melting point of copper chlorides and promotes the copper redox steps [9, 11, 12]. In order to prevent melt segregation of copper and potassium chlorides at high reaction temperatures, $LaCl_3$ has been used as a stabilizing promoter [13, 14]. Until now, however, $LaCl_3$ by itself was believed to be unreactive in this chemistry because La^{+3} cations, in contrast to Cu, cannot change their oxidation state. It is, therefore, surprising that recently, catalysts based exclusively on LaOCl, which transforms to $LaCl_3$ in the presence of HCl under reaction conditions, were reported to be active and, importantly, stable for oxidative chlorination [15].

In this chapter, we explore the catalytic chemistry of $LaCl_3$ in oxidative chlorination of methane by combining activity measurements with characterization of $LaCl_3$ catalysts and their LaOCl precursors. Furthermore the role of each reactant is studied with pulse and Raman

measurements. Consolidated experimental information and density-functional theory (DFT) calculations are used to propose a mechanism for this intriguing new reaction.

3.2   Experimental

3.2.1   Catalyst preparation

The $LaCl_3$ catalysts were prepared *in situ* in an HCl flow from LaOCl precursors. One LaOCl precursor (Sample 1) was prepared by precipitation at room temperature using ammonium hydroxide (NH_4OH) and a solution of lanthanum (III) chloride heptahydrate (99%, Merck) in ethanol. After drop-wise addition of the base to the solution, the suspension was stirred for 1 h to facilitate complete precipitation. The gel obtained by centrifugation was washed twice with an excess of ethanol to remove the residual base. Finally, the gel was freeze dried and calcined at 550°C using a temperature increment of 5°C min^{-1} under a flow of 200 ml min^{-1} of synthetic air for 8 h. LaOCl was initially activated in He flow (40 ml min^{-1}) at 550°C for 1 h using a temperature increment of 10°C min^{-1}. Subsequently, the material was converted to $LaCl_3$ *in situ* by reacting with HCl (20 vol. % HCl in He, total flow 50 ml min^{-1}) at 400°C for 12 h.

Another LaOCl precursor (Sample 2) was prepared by reacting $LaCl_3 \cdot 7H_2O$ with an aqueous solution of ammonium hydroxide under argon atmosphere. The resulting precipitate was then washed, dried and calcined similarly to LaOCl (Sample 1).

3.2.2   Physicochemical characterization

The crystallographic structure of the LaOCl precursors and resulting $LaCl_3$ catalysts was determined by XRD with a Philips X'Pert Pro System ($CuK_{\alpha 1}$-radiation, 0.154056 nm) at 40 kV / 40 mA. The measurements were performed with a step scan of 0.017°/min from 10° to 60° 2θ. The morphology and particle size of the LaOCl precursor (Sample 1) was examined by scanning electron microscopy using a *JEOL* 500 SEM-microscope (accelerating voltage 25 kV). Before recording the SEM image, the sample was outgassed for two days at room temperature and sputtered with gold before collecting the images. BET surface area and pore volume were determined by nitrogen adsorption at 77 K using a PMI automated BET Sorptometer. Prior to measurement, the LaOCl sample was outgassed in vacuum (10^{-3} Pa) at

250°C for 2 h. To determine the carbonate content in the precursor, gases formed on heating the LaOCl sample in vacuum up to 550°C for 1h (ramp of 10°C min^{-1}) were analyzed with a *Balzers QM 420* mass spectrometer (MS). The MS signal 44 was used to quantify CO_2, using $NaHCO_3$ for quantification.

3.2.3   Catalytic tests

The *in situ* prepared $LaCl_3$ sample was tested in methane oxidative chlorination using a fixed-bed quartz tubular reactor filled initially with 250 mg of LaOCl precursor (0.3 - 0.6 mm size fraction). The temperature of the reactor oven was controlled by a thermocouple placed above the catalyst bed. The gas flows (CH_4, O_2, HCl, N_2, He) were controlled using digital mass flow meters (Bronkhorst). The catalytic tests were performed between 400 and 500°C using 5 ml min^{-1} of the stoichiometric mixture CH_4:HCl:O_2:He:N_2 = 2:2:1:4:1. Helium was used as a diluent, and nitrogen as an internal standard. The reactor outlet was analyzed by an online Siemens Maxum Edition II gas chromatograph (GC). After analysis, the gases were passed through a NaOH scrubber to remove unreacted HCl. Gas lines of the setup were coated with glass lining and heated to 150°C to prevent water condensation and corrosion.

The dependence of the product distribution on methane conversion was evaluated by varying the space velocity (total flow from 5 to 25 ml min^{-1}) using a stoichiometric ratio of reactants (CH_4:HCl:O_2:He:N_2 = 2:2:1:4:1) and by varying reactant ratios at 475°C. The effect of feed components was evaluated using 500 mg of catalyst with the total feed flow of 10 ml min^{-1} at 475°C. The effect of the presence and absence of O_2 and HCl in the feed on the rate of CH_3Cl formation was studied at 400°C.

The dependence of the product distribution on temperature was probed with temperature programmed reaction (TPR) by heating 250 mg of catalyst from 50 to 650°C with a temperature increment of 2°C min^{-1} and feeding reactants at a stoichiometric ratio (CH_4:HCl:O_2:He:N_2 = 2:2:1:4:1) with the total flow rate of 5 ml min^{-1}. Another TPR experiment was carried out in the absence of HCl (CH_4:O_2:He:N_2 = 2:1:6:1; total flow 5 ml min^{-1}). In addition, to investigate the reaction network, yet another TPR experiment was performed where CH_4 was substituted with CH_2Cl_2, which was injected with a syringe pump (CH_2Cl_2:HCl:O_2:He:N_2 = 2:2:1:4:1; total flow 5 ml min^{-1}). To investigate the stability of the catalyst, a reaction test was performed at 475°C (CH_4:HCl:O_2:He:N_2 = 2:2:1:4:1; total flow 5 ml min^{-1}). The apparent activation energy and initial rates were estimated by varying the temperatures between 400 and 500°C in 25°C increments and by adjusting the total flow rate

to maintain the conversion below 10 %, so that a differential reactor model could be used in data analysis. In order to keep the catalyst in its chlorinated form, the catalyst was regenerated after each temperature step for 3h with 30 vol.% HCl in He.

The reaction rates of Cl incorporation into chloromethanes and Cl incorporation into Cl_2 in the absence of CH_4 were compared by varying the O_2 partial pressure at 402 and 477°C using the LaOCl (Sample 2) precursor. In one set of experiments, CH_4 and HCl partial pressures were kept constant at, respectively, 4.8 and 24 kPa by adjusting the feed composition with He. In a complimentary set of experiments, the catalyst was tested under the same conditions but without CH_4 in the feed. In this second set of experiments, HCl and O_2 were converted to Cl_2 and H_2O (Deacon reaction). The order of experiments was randomized, and measurements at each of the reported conditions were collected at least twice. The detection limit for feed and product components in these experiments was 0.01 mol %.

3.2.4   Pulse and Raman measurements

Pulse and spectroscopic Raman measurements were performed with a reactor system that had two feed lines, each equipped with a separate set of mass flow controllers. The two feed lines were connected with a multi-port switch valve, which allowed the feed composition to be changed in a pulse mode. The temperature of the catalyst was initially increased with a temperature increment of 10 °C min^{-1} to 677 °C under He flow and hold at 677 °C for 2 h, lowered to 452 °C, and then maintained at this value for all measurements. The He flow between reaction pulses and exposure to HCl flow was maintained at WHSV of 0.31 h^{-1}. The exposure to HCl in flow mode was performed in 2-min increments at the concentration of 20 mol % in He at total WHSV of 1.35 h^{-1}. In situ Raman spectra were collected with a Kaiser Optical Systems, Inc., Holoprobe 532/633 spectrometer equipped with a frequency-doubled Nd/YAG 532 nm laser, grating, and EEV CCD detector chip with 278x1024 pixels. The exposure time and number of accumulations were optimized for an 80% CCD detector pixel fill. The laser power output was about 35 mW.

3.2.5   DFT calculations

The DMol^3 code in Materials Studio 2.1 software by Accelrys was used to perform gradient-corrected spin-polarized periodic DFT calculations with the same model and settings as those utilized in the study of LaOCl surface acidity and basicity [18]. An infinite

LaOCl (001) stoichiometric model was constructed using a 2x2 unit cell with 12 layers (48 atoms total); only half of the layers are shown in Figure 3.15 for clarity.

3.3 Results

3.3.1 Physicochemical characterization

3.3.1.1 LaOCl precursor

XRD patterns showed that LaOCl was the only crystalline phase. Based on the width and intensity of the X-ray diffraction peaks, Sample 1 had rather small crystals. This contrasts unexpectedly with a relatively low BET surface area (20 m^2 g^{-1}). Thus, the material most likely contained very small LaOCl crystals, which were bound into larger agglomerates. The carbonate content of the precursor was 0.9 wt. %. Sample 2 had the BET surface area of 38.5 $m^2 g^{-1}$, and it was carbonate-free due to the anaerobic synthesis.

The typical morphology of the LaOCl precursor, as recorded by SEM, is shown in Figure 3.1a. Particles with irregular shape and diameters between 1 and 30 μm were observed. These particles were characterized by a fragmented surface and were composed of agglomerated nano-particles.
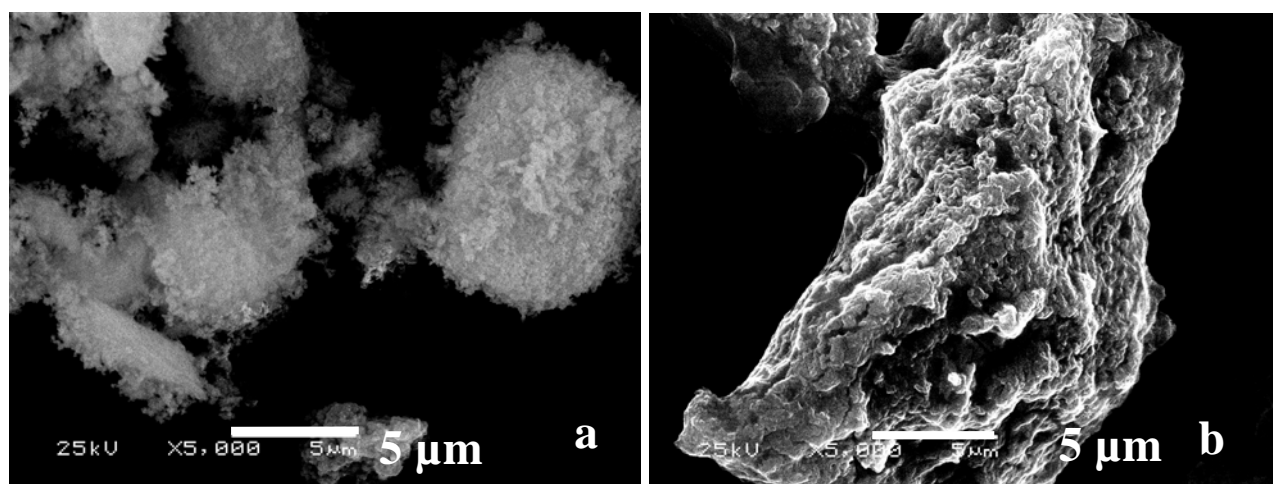

Figure 3.1: SEM photographs of a) precursor and b) chlorinated sample

3.3.1.2 Lanthanum chloride

After 10 h of exposure of LaOCl to an HCl flow at 400°C, all LaOCl diffraction peaks disappeared, and new diffraction peaks were consistent with the presence of $LaCl_3$ and $LaCl_3 \cdot 3H_2O$ (not shown here). As $LaCl_3$ was not generated *in situ* in the diffractometer, it is speculated that the active catalyst phase is largely $LaCl_3$, and the presence of $LaCl_3 \cdot 3H_2O$ was due to sample transfer and handling because of the high hygroscopicity of $LaCl_3$. The overall crystallinity of $LaCl_3$ was significantly higher than that of LaOCl. The specific surface area decreased to 8 $m^2 g^{-1}$, indicating significantly larger primary particles compared to those of LaOCl. The size of secondary particles did not change significantly after the transformation based on SEM graphs. After chlorination, all samples were significantly less fragmented; the particle size increased and the fine agglomeration of nano-particles was completely absent for $LaCl_3$ (Figure 3.1b).

3.3.2 Catalytic conversion of methane

3.3.2.1 Activity and selectivity

The main reaction in oxidative chlorination is the conversion of methane, hydrogen chloride and oxygen to methyl chloride and water (equ. 3.1):

$$CH_4 + HCl + 0.5\ O_2 \rightarrow CH_3Cl + H_2O \qquad \Delta G° = -141\ \text{kJ/mol} \qquad (3.1)$$

A hypothetical reaction without an oxidation step where a hydrogen atom in methane is substituted for a chlorine atom from hydrogen chloride would be highly endothermic and would not be feasible in the studied temperature range (equ. 3.2):

$$CH_4 + HCl \rightarrow CH_3Cl + H_2 \qquad \Delta G° = +88\ \text{kJ/mol} \qquad (3.2)$$
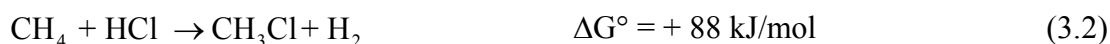
The dependence of the product distribution on temperature at 400-500°C for the reaction of CH_4, HCl and O_2 over $LaCl_3$ is shown in Figure 3.2 as initial product formation rates (left axis) and as conversion of the feed components (right axis). At 400-425°C, when CH_4 conversion was low, CH_3Cl and H_2O were the only products (equ. 3.1). The rate of

CH_3Cl formation, as expected, increased exponentially with temperature. Above 425°C, CO and CH_2Cl_2 were detected as products. In addition, small amounts of CO_2 were also observed. It should be noted that at these higher temperatures, oxygen conversion was always higher than that of methane, indicating that methane or formed chloromethanes were oxidized. The predominant hydrocarbon oxidation to CO rather than CO_2 under the evaluated conditions suggests that the water-gas shift reaction was not catalyzed to a significant extent.

The apparent activation energy of the overall reaction was estimated to be 86 kJ·mol^{-1} based on the initial rate of methane disappearance presented in Figure 3.2.
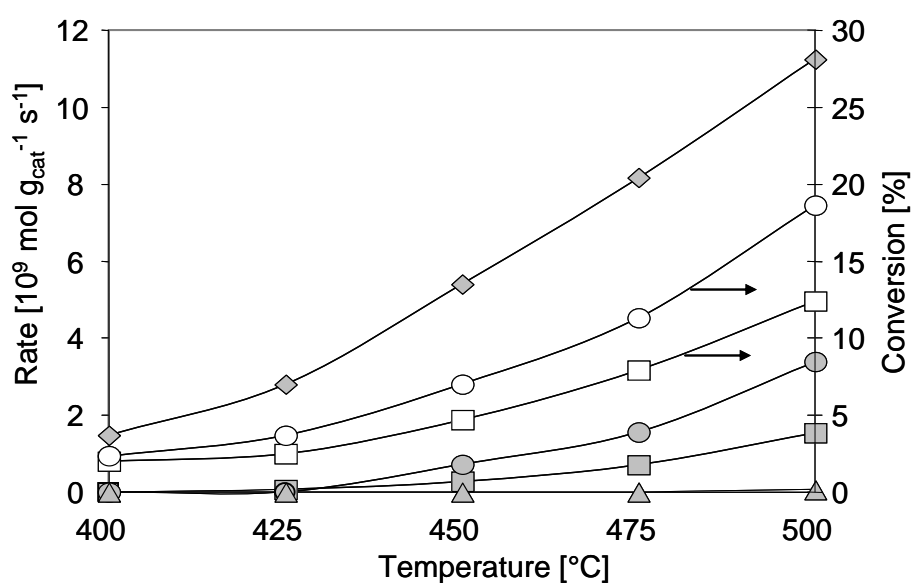

Figure 3.2: Initial rates and conversion vs. temperature with stoichiometric flow CH_4:HCl:O_2:He:N_2 = 2:2:1:4:1 (□ CH_4, ○ O_2, ◇ CH_3Cl, ▣ CH_2Cl_2, ◉ CO, △ CO_2)

With time on stream (Figure 3.3), the activity decreased, reaching a steady state after approximately 7 h, indicating that the catalyst could dynamically change under reaction conditions and that its steady state was determined not only by the temperature but also by the partial pressures of reactants and products. As described above, the activity then remained constant up to 50 h.
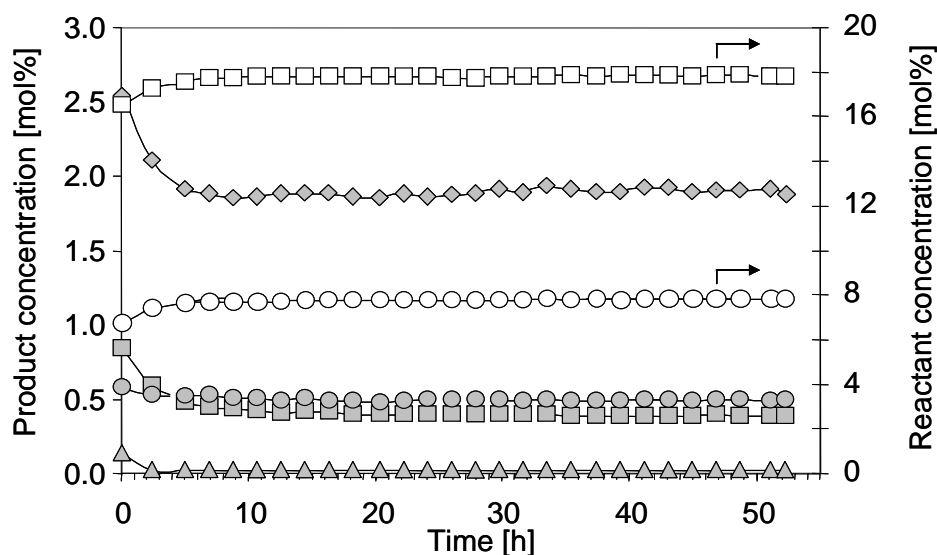
Figure 3.3: Time on stream at 475°C with stoichiometric flow $CH_4:HCl:O_2:He:N_2 = 2:2:1:4:1$
(□ CH_4, ○ O_2, ◇ CH_3Cl, ■ CH_2Cl_2, ◉ CO, △ CO_2)

Figure 3.4a and Figure 3.4b show the results of a TPR experiment for the reaction of CH_4, HCl and O_2 where the temperature was increased linearly. While such an experiment cannot account for deactivation or transient modifications of the catalyst, it probes the general reaction sequences and, thus, should be useful in the evaluation of the reaction mechanism.

Methyl chloride was detected as the only product at about 300°C. As temperature increased to about 360°C, CH_2Cl_2, CO and CO_2 appeared as products. Up to about 470°C, the concentration of all products was increasing. Then, the concentrations of CH_3Cl and CH_2Cl_2 began decreasing at 470 and 540°C, respectively, while the concentrations of CO and CO_2 continuously increased with temperature. The product distribution of the TPR experiment is shown in Figure 3.4b. The O_2 conversion approached 100% around 550°C. During the whole experiment, only trace amounts, less than 0.5 mol %, of $CHCl_3$ and CCl_4 were detected. The consumption of HCl reversed at 490°C, and its outlet concentration was higher than the inlet one up to 615°C. At even higher temperatures, HCl was consumed again.

Based on the chlorine mass balance, we can exclude that this HCl evolution is the result of excess HCl initially adsorbed on the sample. It is likely that the effect is associated with a transformation of $LaCl_3$ to LaOCl due to a higher thermal stability of the latter; one of the LaOCl preparation methods, for example, is based on heating an equimolar mixture of La_2O_3 and $LaCl_3$ [16]. Hydrogen for the HCl formation can come from water, similarly to hydrolysis of $LaCl_3$ to LaOCl [17] or directly from methane decomposition during oxidation to CO.
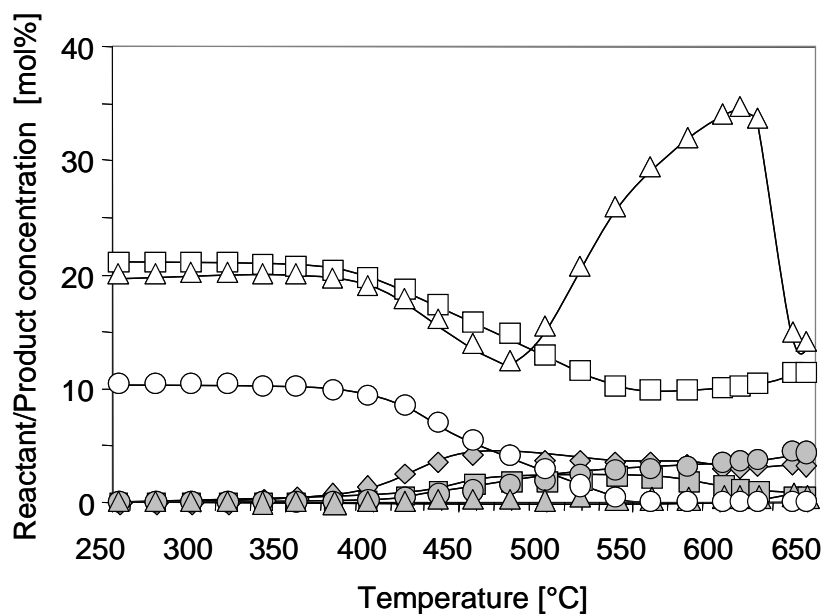
Figure 3.4a: Temperature programmed reaction (2°C min^{-1}) with stoichiometric flow $CH_4:HCl:O_2:He:N_2 = 2:2:1:4:1$ (□ CH_4, △ HCl, ○ O_2, ◇ CH_3Cl, ▣ CH_2Cl_2, ◍ CO, △ CO_2)
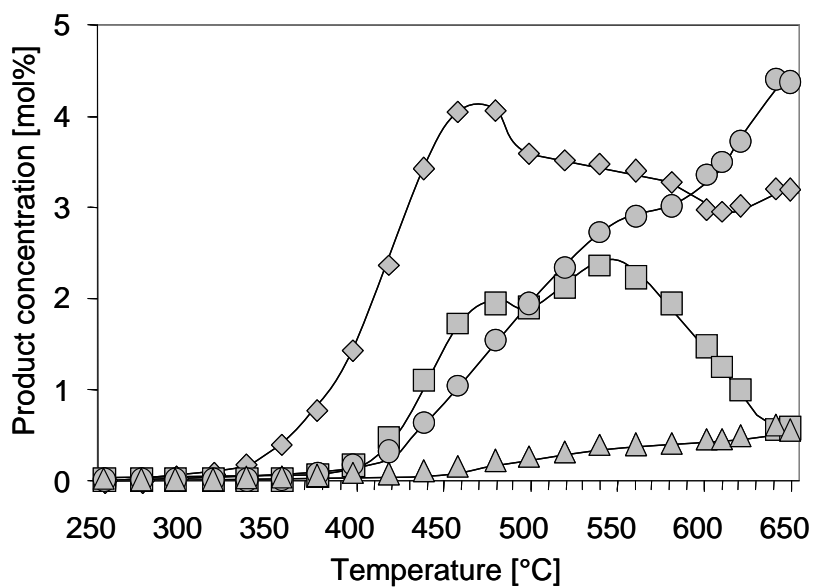
Figure 3.4b: Temperature programmed reaction (2°C min^{-1}) with stoichiometric flow $CH_4:HCl:O_2:He:N_2 = 2:2:1:4:1$ product distribution (◇ CH_3Cl, ▣ CH_2Cl_2, ◍ CO, △ CO_2)

3.3.2.2 Primary and secondary products

The dependence of product selectivities on methane conversion at 475°C is provided in Figure 3.5. As the methane conversion increased, the selectivity to CH_3Cl decreased, while the selectivity to CH_2Cl_2, on the contrary, increased. Such dependence suggests that CH_2Cl_2 was formed from CH_3Cl as a secondary product. The selectivity to CO increased slightly with conversion. In contrast, CO_2 is only hardly detected even at higher conversions.
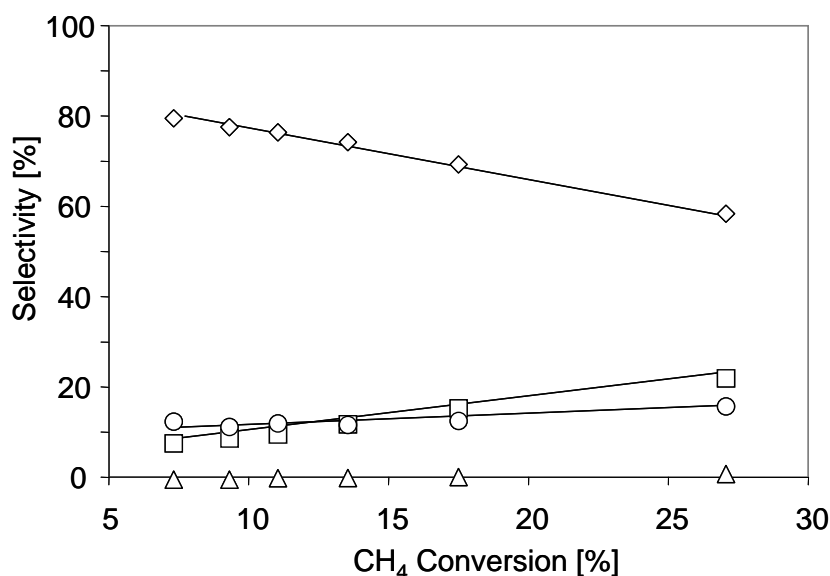

Figure 3.5: Conversion vs. selectivity at 475°C with stoichiometric flow $CH_4:HCl:O_2:He:N_2 = 2:2:1:4:1$ and total flow from 5 ml min^{-1} to 25 ml min^{-1} ($\diamond$ CH_3Cl, $\square$ CH_2Cl_2, $\circ$ CO, $\triangle$ CO_2)

The hypothesis that the (unwanted) formation of CH_2Cl_2 proceeds *via* a consecutive reaction of CH_3Cl was tested by varying the feed composition in an experiment at 475°C. Specifically, the methane ratio was increased from 2:2:1 ($CH_4:HCl:O_2$) to 4:2:1 and finally to 6:2:1, and the results are shown in Figure 3.6. Tripling the methane concentration increased the selectivity to CH_3Cl from 65 to 73 %, while the selectivity to CH_2Cl_2 decreased from 25 to 18 %. A linear extrapolation of the results suggests that a 10-fold methane excess is needed to suppress the formation of CH_2Cl_2. The selectivities to CO and especially to CO_2 side products were hardly affected: CO selectivity decreased from 9 to 7 %, while that of CO_2 increased from 1% to 2%.
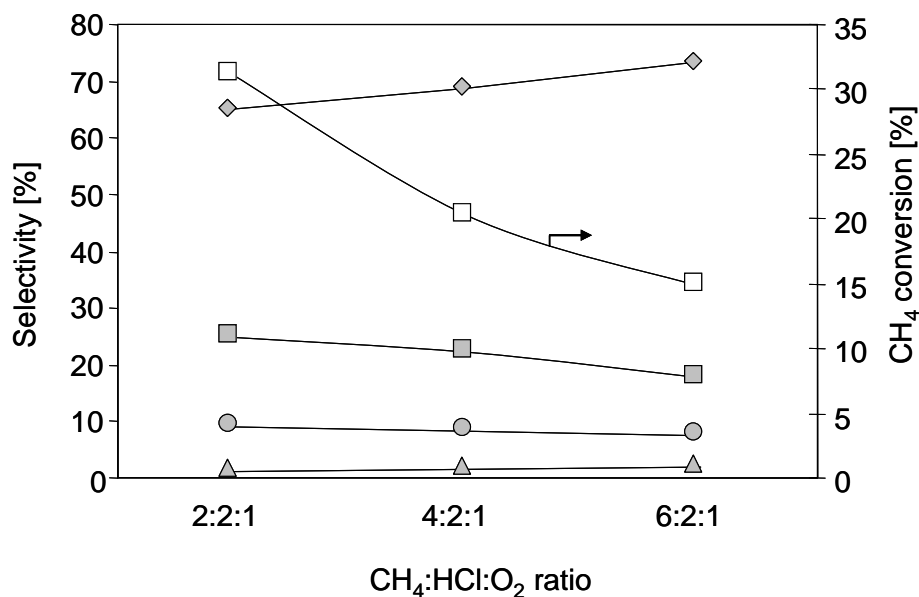
Figure 3.6: Dependence of selectivity and conversion on feed composition at 475°C (□ CH$_4$, ◇ CH$_3$Cl, ▣ CH$_2$Cl$_2$, ◉ CO, △ CO$_2$)

In order to explore to what extent higher chloromethanes could be formed under the employed reaction conditions, CH$_2$Cl$_2$ was fed instead of CH$_4$ in an additional TPR experiment with HCl and O$_2$, and the results are shown in Figure 3.7.
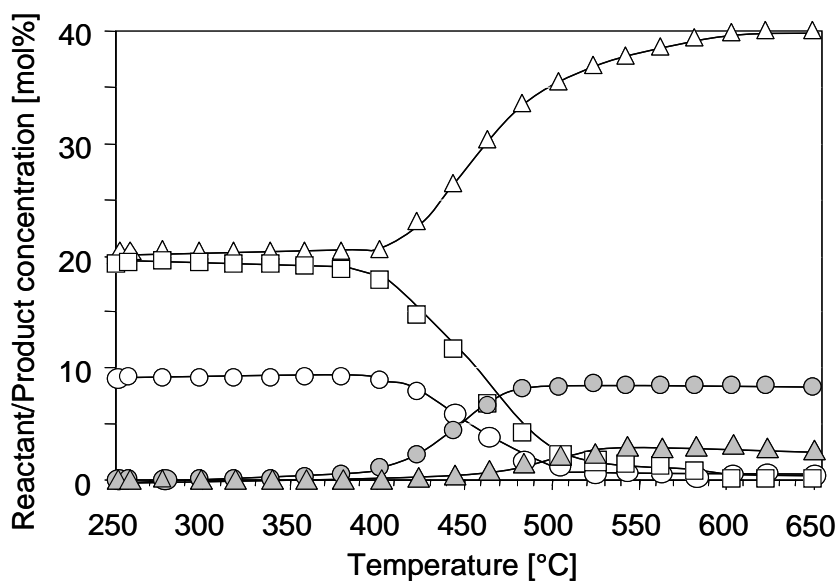

Figure 3.7: Temperature programmed reaction (2°C min^{-1}) with stoichiometric flow CH$_2$Cl$_2$:HCl:O$_2$:He:N$_2$ = 2:2:1:4:1 (□ CH$_2$Cl$_2$, ◦ O$_2$, △ HCl, ◉ CO, △ CO$_2$)

CH_2Cl_2 began reacting with the formation of CO, CO_2 and HCl at about 360°C, which is the same temperature, at which carbon oxide products were detected in the TPR experiment with methane (Figure 3.4b). Similarly to the experiments with methane, higher chloromethanes, $CHCl_3$ and CCl_4, were detected only in trace amounts. Above 500°C, the concentration of CO remained constant at 8.3 mol % , while that of CO_2 stabilized at 3.0 mol % at a slightly higher temperature of 550°C. HCl was not consumed during the experiment; on the contrary, HCl evolution from the catalyst began at 405°C and approached a steady concentration of 40 mol % at 650°C.

3.3.2.3 Impact of the presence of HCl and O_2 in the feed

The effect of HCl and O_2 presence in the feed was evaluated in order to explore the reaction mechanism. Conceptually, the catalyst under reaction conditions is nearly free of oxygen, but it has an abundance of chloride anions. These chloride ions in $LaCl_3$ are strongly nucleophilic and, hence, are hardly capable of methane activation. For this activation to occur, either electrophilic oxygen is needed directly (Pathway 1) or as an intermediate reactant to convert the nucleophilic chloride (Cl^-) anion into an electrophilic hypochlorite, OCl^-, (Pathway 2). Alternatively, molecular oxygen could oxidize Cl^- to Cl_2, which in turn would activate methane *via* gas-phase radical chlorination (Pathway 3). While these pathways are discussed below, it is important to note that for all of them, the expected response of the catalytic system to a transient variation in the HCl concentration should be much slower than that for an O_2 variation.

To test the hypothesis whether the catalytic surface can supply Cl for the reaction with methane, a TPR experiment was performed in the absence of HCl in the feed. Indeed, as shown in Figure 3.8, CH_3Cl started to form at 330°C and reached a maximum at 510°C. In addition, CO started to evolve above 400°C and reached a maximum at 560°C. Even CH_2Cl_2 was observed above 470°C, reaching a maximum concentration around 570°C. At this high temperature, the CO_2 concentration began increasing rapidly, reaching a constant level around 600°C; this marked difference in chemistry can be attributed to the onset of direct methane combustion. Although HCl was not fed in this experiment, it was observed as a product above 460°C, and its concentration reached a maximum at 560°C and then dropped rapidly. This decrease in the rate of HCl formation coincided with the onset of methane combustion. Above 615°C, no formation of CH_3Cl, CH_2Cl_2 or CO was detected, and CO_2 remained as the only detectable product (water was not monitored).
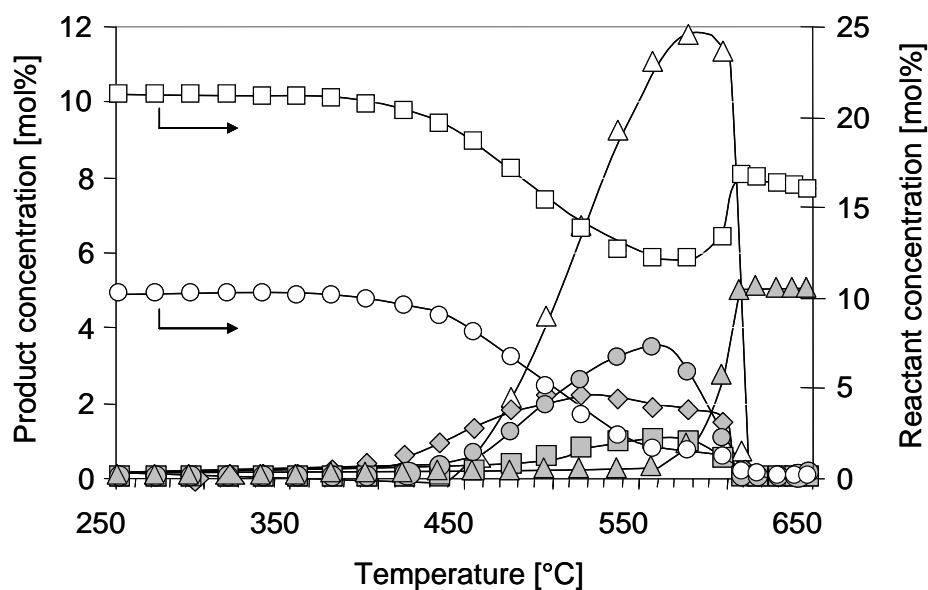
Figure 3.8: Temperature programmed reaction ($2°C$ min^{-1}) with stoichiometric flow $CH_4:O_2:He:N_2 = 2:1:6:1$ (□ CH_4, ○ O_2, △ HCl, ◇ CH_3Cl, ■ CH_2Cl_2, ◉ CO, △ CO_2)

The effect of HCl and O_2 presence was evaluated by rapidly eliminating one of these components from the feed and compensating for this elimination with He, so that the space velocity remained constant, i.e., by performing pressure step-up and step-down transients (Figure 3.9). Under the selected reaction conditions with the full feed, CH_3Cl was formed at a constant rate of about $1.7 \cdot 10^{-9}$ mol CH_3Cl g_{cat}^{-1} s^{-1} (Segment I). In the absence of gas-phase O_2 (Segment II), the rate of CH_3Cl formation dropped immediately to zero, but then it came back to its original value when O_2 flow was restored (Segment III). In contrast, when HCl was eliminated from the feed (Segment IV), the reaction rate decreased slowly and stabilized at about $0.7 \cdot 10^{-9}$ mol CH_3Cl g_{cat}^{-1} s^{-1} or 41% of the original value. When HCl was added again, the original rate of CH_3Cl formation was almost instantaneously restored (Segment V). These observations confirm that the presence of O_2 is essential for the chemistry, which is consistent with the thermodynamic infeasibility of the hypothetical Equation 3.2. Furthermore, the abrupt decline in the reaction rate on O_2 elimination (Segment II) suggests that oxygen-derived surface species are transient and their concentration is minimal. Chloride ions on the $LaCl_3$ surface, on the contrary, can sustain methane chlorination even without HCl in the gas phase.
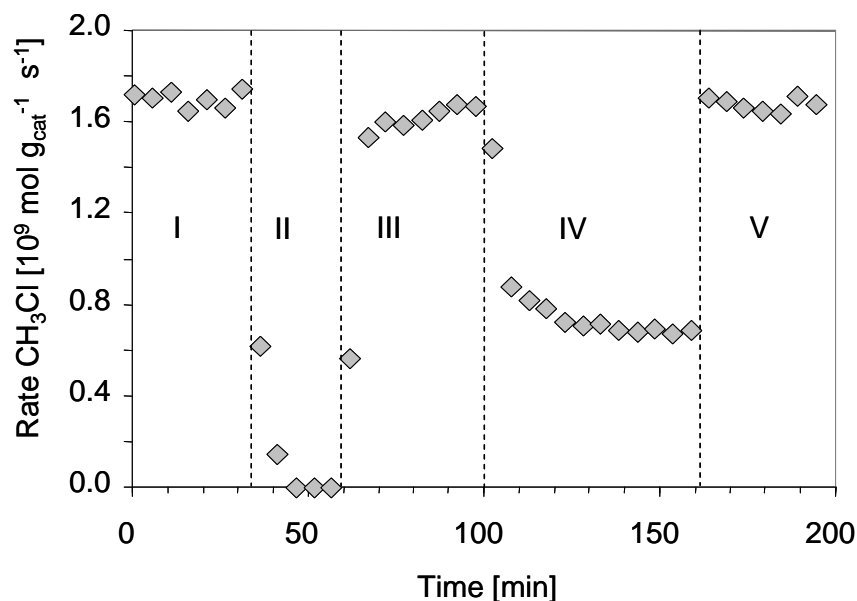
Figure 3.9: Effect of the feed components on the rate of CH₃Cl formation at 400°C. Segment
I, III and V = all gases, II = O₂ off, IV = HCl off

The duration of the chlorination treatment of the LaOCl precursor has no remarkable
influence on the catalytic activity. No difference between the methane conversion and the
methyl chloride selectivity is observed between the catalysts with 1h chlorination treatment
and 20h chlorination treatment as shown in Figure 3.10.

Figure 3.10: Influence of chlorination treatment on methyl chloride selectivity and methane
conversion at 475°C (□ 1h, ◇ 4h, ○ 8h, △ 10h, ▲ 14h, ◆ 20h)

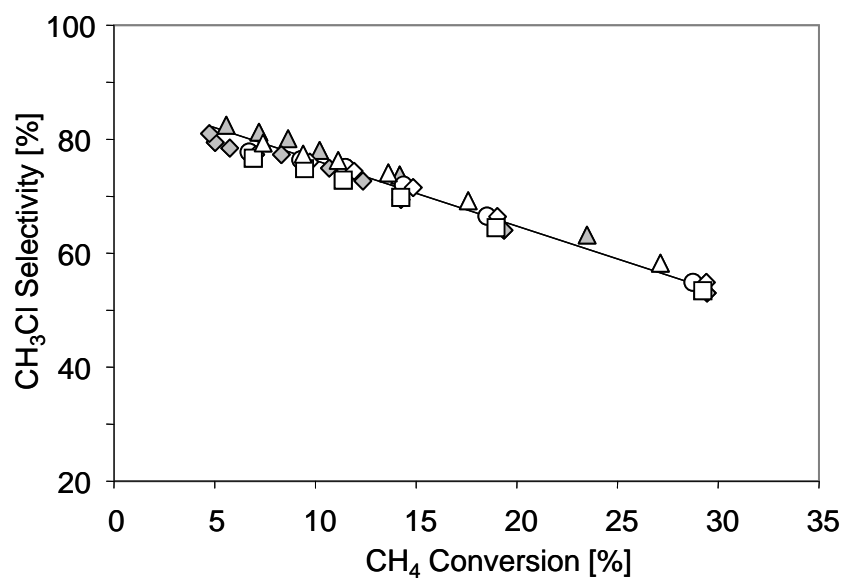As already mentioned the catalyst could dynamically change under reaction conditions and is therefore stabilized for some time prior catalytic measurements. The stabilization is also not influenced by the duration of the chlorination treatment. The decrease in methane conversion is similar for all samples independently of the duration of the chlorination (Figure 3.11).
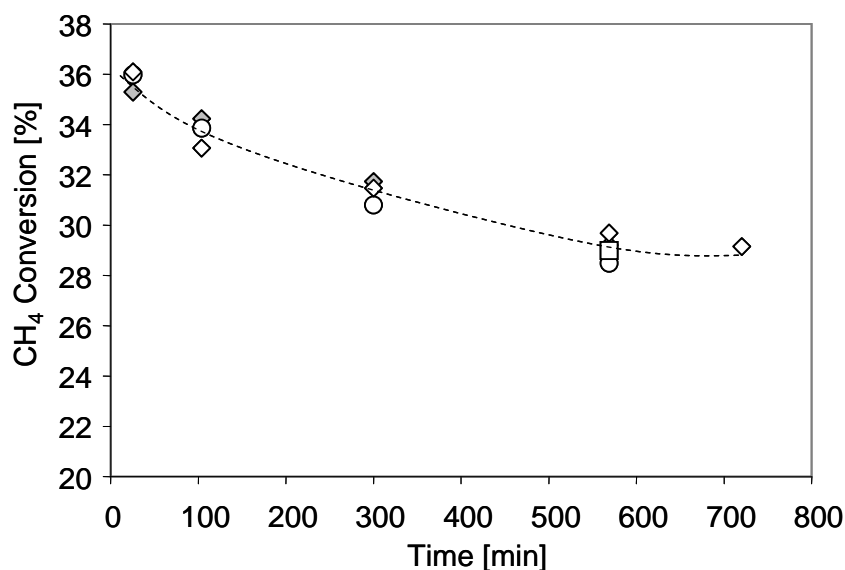

Figure 3.11: Stabilization at 475°C for catalysts with different chlorination treatment (□ 1h, ◇ 4h, ○ 8h, △ 10h, ▲ 14h, ◆ 20h)

The significance of Pathway 3 where O_2 is assumed to produce gas-phase Cl_2, which in turn reacts with gas-phase CH_4, was evaluated by comparing Cl incorporation rates into chloromethanes and into Cl_2. Figure 3.12 shows that the rates of Cl incorporation into chloromethanes (feed CH_4, HCl, O_2, He) were significantly higher than those of Cl evolution as Cl_2 when CH_4 was not present in the feed (Deacon reaction) at 477°C. The main product in the experiments with CH_4 was CH_3Cl with a small amount of CH_2Cl_2; furthermore, CO and CO_2 were not produced due to low CH_4 conversion levels and a large (5:1) HCl to CH_4 ratio. Cl_2 evolution was not detected at all when CH_4 was present in the feed. In the experiments without CH_4 in the feed, attempts were made to measure Cl_2 evolution in the same range of O_2 partial pressures as was done in the experiments with CH_4. However, since Cl_2 formation rates were lower than those of CH_3Cl, the former could not be reliably measured below 4 kPa of O_2 at 402°C (not shown here) and below 2 kPa O_2 at 477 K.
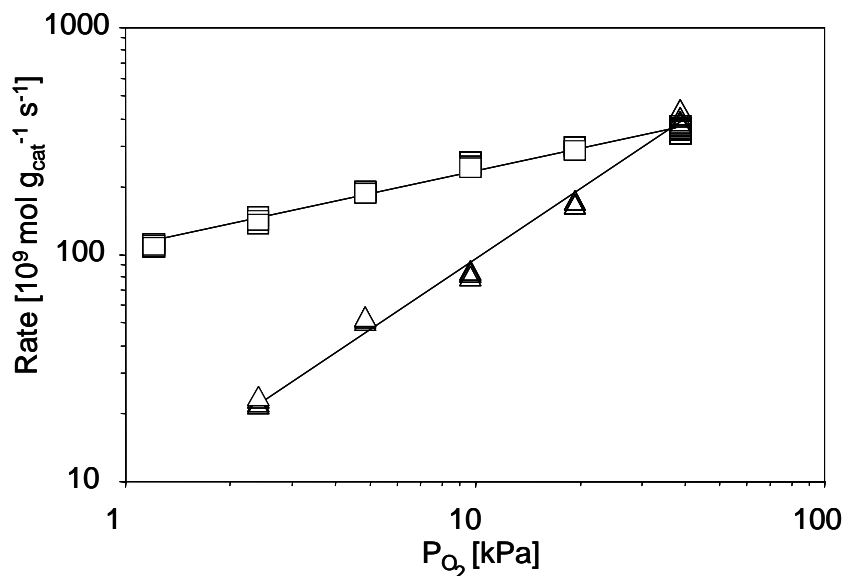
Figure 3.12: Comparison of reaction rates of Sample 2 for Cl incorporation into methane (□ chlorinated C_1's) and for Cl evolution as Cl_2 without methane in the feed (△ Cl_2 evolution) at 477°C

Importantly, the trends for Cl incorporation into chloromethanes and into Cl_2, which are illustrated in Figure 3.12, were substantially different. This difference suggests that the formation of chloromethanes is not likely to proceed through a reaction with gas-phase Cl_2, and, therefore, Pathway 3 is not likely to play a major role in the overall reaction scheme.

3.3.3   Raman spectroscopy and reaction pulse measurements

The nature of the catalytic phase and details of catalyst transformation from LaOCl to $LaCl_3$ were examined with in situ Raman measurements and reaction pulses (Sample 2). Results of a typical run at 452 °C are illustrated in Figure 3.13 and Figure 3.14, respectively. In this run, a Raman spectrum of LaOCl sample was first collected under He flow. This experimental spectrum (Figure 3.13b) is compared to the theoretical vibrational frequencies (Figure 3.13a), which were obtained with Density-functional Theory (DFT) calculations using the LaOCl model in Figure 3.15. The calculated frequencies are shown in Figure 3.13a as lines of arbitrary height because the DFT calculations allowed us to estimate the frequencies but not the intensities of the vibrational modes. The experimental bands in Figure 3.13b are in agreement with the theoretical frequencies in Figure 3.13a and previously reported experimental results for LaOCl [18, 19]. The calculated frequency at 126 cm^{-1} in Figure

3.13a, previously reported based on experimental results was outside of our current experimental data collection range [18, 19].
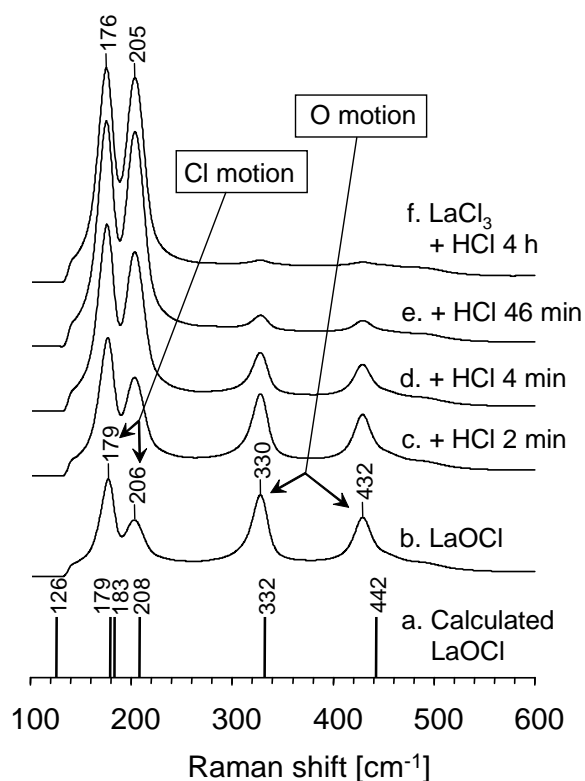

Figure 3.13: In situ Raman spectra of LaOCl (sample 2) as a function of exposure to HCl flow at 452 °C: (a) calculated vibrational frequencies of LaOCl; (b) LaOCl spectrum prior to exposure to HCl flow; (c) after exposure to HCl flow for 2 min; (d) 4 min; (e) 46 min; (f) 4 h. The spectrum (f) is essentially that of LaCl$_3$. DFT calculations suggest that the bands at 179 and 206 cm^{-1} are associated with motion of Cl atoms, and the bands at 330 and 432 cm^{-1} with motion of O atoms

The DFT calculations suggest that the experimental bands at 179 and 206 cm^{-1} are associated with motion of Cl atoms in LaOCl, and the bands at 330 and 432 cm^{-1} with motion of O atoms. After collection of the initial spectrum, the catalyst was probed with a short pulse of CH$_4$ and O$_2$ (15.0 and 7.5 mol %, respectively, in He) to minimize changes caused by any reactions to the surface composition. The total amount of CH$_4$ in the pulse was equivalent to 0.02 mol per mol of catalyst. The mass spectrometer traces for H$_2$O and CH$_3$Cl collected during the pulse interrogation are presented in Figure 3.14a.
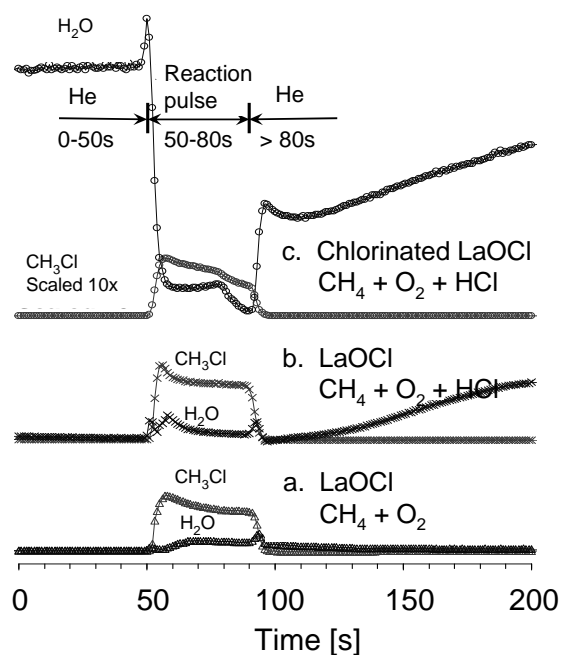
Figure 3.14: Mass spectrometer traces for mass 50 (CH_3Cl) and mass 18 (H_2O) collected with 30 s reaction pulses: (a) CH_4+O_2 pulse over LaOCl injected after collection of the spectrum in Figure 3.13b; (b) CH_4+O_2+HCl pulse over LaOCl injected after completion of the first pulse; (c) CH_4+O_2+HCl pulse injected after collection of the spectrum in Figure 3.13c collected over LaOCl exposed to HCl flow for 2 min. The relative scale of CH_3Cl is increased 10 times for clarity

The concentration of these products was negligible prior to the injection of reactants (0 to 50 s). Then, during the reaction pulse, between 50 and 80 s, CH_3Cl and H_2O (Figure 3.14a) were formed. This result suggests that Cl species on the surface of LaOCl can react with CH_4 in the presence of gas-phase O_2. This reaction, proceeding through surface Cl species, is similar to the one observed with CH_4 and O_2 flow over $LaCl_3$ (segment IV in Figure 3.9). After the first pulse, the catalyst was probed with a pulse of CH_4, O_2 and HCl (15.0, 7.5 and 15.0 mol %, respectively, in He) in the stoichiometric ratios based on Reaction 3.1, which again produced CH_3Cl and H_2O (Figure 3.14b). The total amount of CH_4 introduced in the second pulse was the same as in the first one. Similarly to the first pulse, the conversion of CH_4 and O_2 was low (below 5 mol %), and the amounts of CH_3Cl produced, based on the trace curve areas, was comparable in the two pulses. The difference in the second pulse was the complete consumption of HCl, which resulted in a different H_2O evolution trace: water was slowly evolving long after the completion of the reaction pulse. This behavior can be

attributed to catalyst chlorination (equ. 3.3). After the second pulse in Figure 3.14b, the catalyst was exposed to a flow of HCl for 2 min, which was equivalent to 0.2 mol of HCl per mol of catalyst, and then the Raman spectrum in Figure 3.13c was collected. This spectrum shows that that the intensity of the bands associated with Cl motion increased and those associated with O motion decreased, confirming a higher extent of catalyst chlorination after the reaction with HCl. Following the spectrum acquisition, the catalyst was again probed with another pulse of CH_4, O_2 and HCl (Figure 3.14c). The sequence of exposing the catalyst to HCl flow for 2 min, then acquiring a spectrum and interrogating with a reaction pulse was repeated multiple times. Selected spectra from this sequence, acquired after 4 min, 46 min and 4 h of cumulative exposure to HCl flow, are presented in Figure 3.13d-f. These spectra show a trend of gradual catalyst chlorination. The last shown spectrum collected after 4 h of HCl exposure (Figure 3.13f) with two dominant bands at 176 and 205 cm^{-1} is consistent with those reported for $LaCl_3$ [18, 19]. The experimental spectral series in Figure 3.13, thus, represent a gradual transformation of LaOCl to $LaCl_3$. The results of subsequent pulse measurements in the series were all similar to the traces shown in Figure 3.14c. CH_3Cl formation was detected during the reaction pulse in quantities comparable to those for the initial LaOCl, and H_2O formation was dominated by the catalyst chlorination. Significant amounts of H_2O were evolving from the catalyst even after the HCl flow was stopped and the catalyst was kept under He flow during spectra acquisition and prior to the reaction pulse introduction, as can be seen in the segment from 0 to 50 s in Figure 3.14c. During the pulse, the concentration of H_2O in the outlet actually decreased, which can be attributed to suppression of the continuous and relatively slow catalyst chlorination and subsequent dehydration by methane activation. After the completion of the reaction pulse, the segment after 80 s in Figure 3.14c, the H_2O evolution from the catalyst resumed. The delay and relatively slow rate of H_2O evolution from the catalyst after exposure to HCl flow is similar to the trailing of the H_2O trace after the completion of the very first pulse with HCl in Figure 3.14b.

3.3.4 DFT calculations

A possible reaction mechanism based on the formation of hypochlorite, OCl$^-$, surface species (Pathway 2) was evaluated with DFT calculations, and the results are summarized in Figure 3.15. The presented results were obtained with a chlorine-terminated LaOCl, not $LaCl_3$, slab as a model catalyst surface based on experimental evidence for the catalytic activity of LaOCl catalyst precursors in pulse feed experiments (not shown in this study).
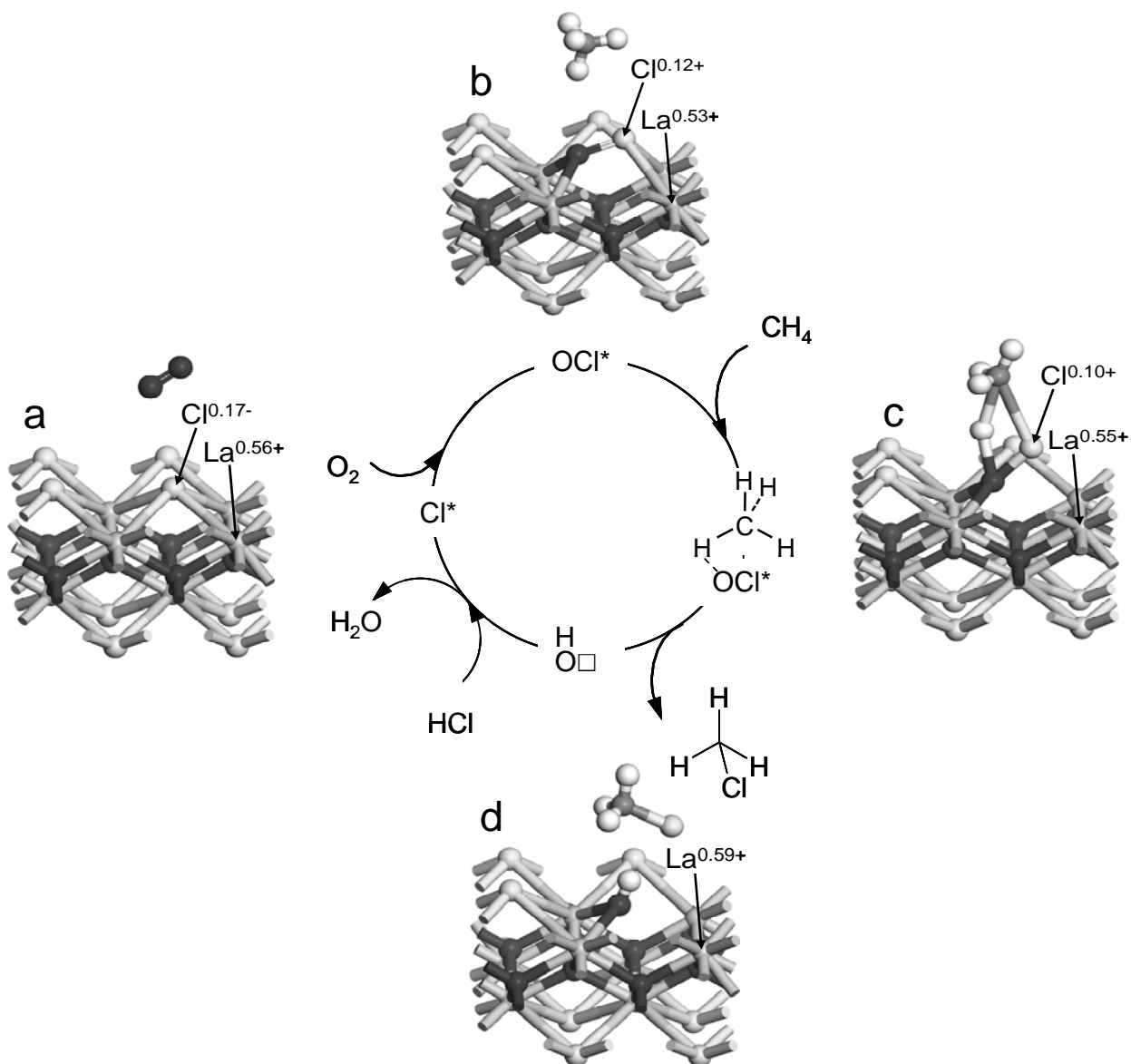
Figure 3.15: Proposed reaction mechanism for oxidative hydrochlorination of methane over LaOCl catalyst based on DFT calculations: a) gas-phase oxygen above LaOCl catalyst; b) dissociative oxygen adsorption with the formation of OCl surface species; c) reaction of gas-phase methane with surface OCl species; d) surface OH and gas-phase CH₃Cl. Numbers next to element symbols show partial atom charges calculated with the Hirshfeld method

Initial computational results with a model LaCl₃ surface (model described in [16]) indicate that they are substantially similar to those shown in this chapter The calculations suggest that

OCl surface species can be formed by dissociative adsorption of O_2 (Figure 3.15b). In this adsorption step, gas-phase O_2 formally oxidizes surface Cl from -1 to +1. This is reflected in the change of the partial atomic charge on reactive Cl from 0.17- to 0.12+, as calculated with the Hirshfeld method (Figure 3.15a and b). As expected, La does not change its formal +3 oxidation state, and the Hirshfeld charges on La are practically invariable for the different surface structures in Figure 3.15. The transformation of CH_4 into CH_3Cl was approximated as a linear geometric interpolation of structures in Figure 3.15b and d, and an approximate midpoint shown in Figure 3.15c was evaluated as a potential intermediate structure with constrained optimization. In this approximated intermediate structure, which has not been confirmed as a transition state, CH_4 reacts with surface OCl species by exchanging a proton for the activated surface Cl, i.e., exchanging H^+ for Cl^+. The product configuration (Figure 3.15d) is a surface OH and gas-phase CH_3Cl. Surface hydroxyls can react with HCl to form gas-phase H_2O and surface Cl, regenerating the catalytic site. The proposed catalytic cycle, thus, involves oxidation of surface chlorine without any changes in the oxidation state of the underlying metal

3.4   Discussion

LaCl$_3$, prepared *in situ* from LaOCl precursor, is an active, selective and highly stable catalyst for oxidative chlorination of methane. This catalytic system represents an important improvement with respect to known copper-based catalysts, which deactivate quickly due to the volatility of copper salts [10]. It is remarkable that LaCl$_3$ shows such significant catalytic activity because it has been previously proposed in the literature that only metal cations that can change their oxidation state can catalyze this chemistry.

Our experimental measurements and theoretical calculations suggest a reaction mechanism for methane activation and chlorination that proceeds without changes in the oxidation state of the metal cation. The proposed pathway, instead, includes a change in the oxidation state of surface chlorine anions: oxidation of Cl^- on the surface of either LaOCl or LaCl$_3$ with molecular oxygen. Oxygen can potentially adsorb on the surface, forming transient $O^{\delta-}Cl^{\delta+}$ species, in which Cl has a formal oxidation state of +1. These OCl$^-$ species can serve as an active site for methane activation, as illustrated in Figure 3.15: while one of methane hydrogen atoms can be activated by nucleophilic oxygen in OCl$^-$, the carbon atom can start bonding with the slightly positively charged chlorine atom, becoming five-

coordinated and forming a transition state, which can be formally described as a carbonium ion. This high-energy state can be expected to decompose quickly, producing a hydroxy group and methyl chloride. The catalytic cycle can then be closed by substituting the OH⁻ group with Cl⁻ from HCl and producing water.

Similarities of the proposed mechanism to the hydrogen-deuterium (H/D) exchange for methane *via* the formation of a carbonium type transition state, in which bonds are formed and broken in a concerted fashion, are striking. Elementary steps in oxidative chlorination of methane closely resemble substitution and exchange steps in H/D exchange over zeolites. Similarly to the H/D exchange catalyzed by Brønsted acid sites, the carbonium ion is formed by addition of a positively charged atom, in this case chlorine. In addition, the absolute positive charge on the proton of the bridging hydroxyl group in zeolites and on the active chlorine in $LaCl_3$ is not very high. On the other hand, the apparent activation energy for oxidative chlorination (86 kJ mol^{-1}) is significantly lower that that for the H/D exchange in zeolites (approximately 130 kJ mol^{-1}) [20]. This difference can be attributed to potentially higher reactivity of oxygen in OCl⁻ species.

The function of $LaCl_3$ is to supply chlorine anions by maintaining a surface, which can be described as a chloride sheet. The Raman spectra in Figure 3.13 and the results of pulse measurements in Figure 3.14 suggest that $LaOCl$, $LaCl_3$ and La phases with an intermediate extent of chlorination are all catalytically active and that the only essential element for methane activation is the presence of chlorine surface species that can be activated by gas-phase oxygen. These chlorine anions can be activated with the formation of transient OCl⁻ species. The role of the oxygen is twofold: (1) to oxidize Cl⁻ to Cl⁺, enabling the substitution reaction with methane's hydrogen and in addition, (2) to oxidize hydrogen, providing the necessary energy to make the overall reaction thermodynamically favorable at reasonable reaction temperatures. It should be noted that elevated temperatures are required to facilitate evolution of water formed on regeneration of surface chlorine anions in the reaction between surface OH with gas-phase HCl. However, the catalyst chlorination is relatively slow and suppressed when CH_4 is present (Figure 3.14).

Let us now analyze products in oxidative chlorination of methane. There are four main products: CH_3Cl, CH_2Cl_2, CO and CO_2 (Figure 3.2). CH_3Cl is by far the most abundant product, followed by CO, CH_2Cl_2, and finally CO_2. Methyl chloride is the primary kinetic product. When methane conversion is extrapolated to zero, the selectivity to CH_2Cl_2 becomes negligible (Figure 3.5), indicating that it is a secondary product. Thus, we conclude that its formation requires CH_3Cl to desorb from the catalyst and then to re-adsorb. Significant CO_2

quantities are formed only under conditions that suggest a direct methane combustion (Figure 3.8). Thus, its formation is of minor importance for understanding the mechanism of oxidative chlorination. The situation is more complex with respect to CO. CO is the dominant carbon oxide under most conditions reported here. This makes it unlikely that CO is formed directly from methane because at the evaluated reaction temperatures, the thermodynamic equilibrium should be nearly quantitatively shifted towards CO_2. The observed high selectivity to CO suggests that reactions that could equilibrate CO and CO_2, such as water-gas shift, do not proceed on $LaCl_3$ or $LaOCl$. Furthermore, the high selectivity to CO requires that its formation proceeds through a specific pathway that prevents CO_2 production. TPR experiments show that CO is generated more readily from CH_2Cl_2 than from CH_4 or CH_3Cl (Figure 3.4 and Figure 3.7). Literature suggests that its formation from $CHCl_3$ is even more facile [21]. It, therefore, can be concluded that CO is produced by decomposition of multiply substituted chloromethanes. This explanation is consistent with the observation that even higher substituted chloromethane, $CHCl_3$, is observed only in trace amounts, because it is too unstable at the reaction conditions. The mechanism of decomposition of chloromethanes in oxidative chlorination can be expected to be similar to the elementary steps proposed for CCl_4 decomposition over the La_2O_3-$LaOCl$-$LaCl_3$ system where the chloromethane adsorbs strongly on a terminal lattice oxygen site [16]. Oxygen sites on $LaCl_3$ can be produced by partial dechlorination of the surface by water (equ. 3.3 below) or molecular oxygen; for example, even bulk $LaCl_3$ can be converted to $LaOCl$ by calcination for an appropriate amount of time.

Since chlorination is a sequential reaction, the selectivity to the primary product, CH_3Cl, can be enhanced at low methane conversions, when the probability of further reacting CH_3Cl is minimized. This can be achieved by increasing the space velocity or increasing the CH_4 ratio in the feed mixture. It is estimated that that a 10-fold excess of CH_4 compared to HCl and O_2 would be sufficient to suppress CH_2Cl_2 formation. Conceptually, this has also the advantage that HCl can be converted nearly quantitatively, so that a costly separation of H_2O and HCl can be avoided in a potential application. The disadvantage of using high methane ratios is that large quantities of unreacted methane would have to be separated from the products and recycled.

The last point to be addressed relates to the state of the catalytic surface under reaction conditions. All catalysts exhibited an initial decrease in activity, while they could be operated at an almost constant activity thereafter. This does not suggests that the catalysts undergo deactivation in the initial period of being on stream, but rather that they achieve a steady state

with respect to their surface composition, reaction temperature and gas-phase composition. We attribute this to a partial transformation of the surface from the $LaCl_3$ to $LaOCl$ stoichiometry according to equation 3.3

$$LaCl_3 + H_2O \rightleftharpoons LaOCl + 2HCl \qquad\qquad (3.3)$$

The activity of the catalyst and the initial decrease of activity are not influenced by the duration of the chlorination treatment of the $LaOCl$ precursor. Thus, only the chlorination degree of the catalyst surface determines the catalytic activity.

The partial transformation of the surface is also supported by the results of the TPR study in Figure 3.4. Below 490°C, the mass balance in HCl was closed. However, above 490°C, the concentration of HCl at the reactor outlet rapidly increased, indicating that HCl was produced in a reaction with $LaCl_3$, which was converting to $LaOCl$ (equ. 3.3). The HCl evolution stopped when the equilibrium between $LaOCl$ and $LaCl_3$ on the catalyst surface under reaction conditions was reached, with $LaOCl$ being thermodynamically favored at high temperatures. It is remarkable that this process also took place when HCl was not present in the feed, as shown in Figure 3.8, suggesting that HCl evolution is faster than the oxidative chlorination. It is important to note that the reaction stopped when the total amount of chlorine released from the catalyst and incorporated in HCl, CH_3Cl and CH_2Cl_2 reached a level that corresponded to about 90% bulk transformation of $LaCl_3$ into $LaOCl$. Above 600°C, when the HCl formation from the catalyst bulk stopped, methane was oxidized to CO_2.

3.5 Conclusion

$LaCl_3$ generated from $LaOCl$ has been shown to be a promising catalyst for oxidative chlorination of methane, exhibiting catalytic activity, selectivity and high stability. The reaction is proposed to proceed without a change in the formal oxidation state of the metal cation *via* transient surface OCl^- species, formed on oxygen adsorption. Depending on the gas-phase composition and the reaction temperature, the catalytic surface can dynamically transform by changing its stoichiometry from $LaCl_3$ to $LaOCl$. At high temperatures, catalytic surface spontaneously dechlorines, and the bulk can be converted to $LaOCl$.

Flow and pulse experiments using CH_4 and O_2 as feed show that CH_3Cl can be formed using chlorine from the catalyst surface. The presence of HCl, thus, is not required for activity, and its role appears to be limited to maintaining the extent of catalyst chlorination. In contrast, the presence of gas-phase O_2 is essential for catalytic activity. Based on this evidence, methane chlorination is proposed to proceed through the surface chlorine species that can be activated by oxygen.

DFT calculations suggest that O_2 can activate surface Cl^- species by dissociatively adsorbing and forming OCl^- species, with the formal oxidation state of Cl changing from -1 to +1. In the postulated rate-determining step, a hydrogen atom in methane is proposed to be substituted by Cl^+ of OCl^- *via* a carbonium ion transition state, resembling the H/D exchange of methane in acidic zeolites. The OH formed is regenerated with HCl to water and chloride ion. Methyl chloride is the primary product formed. Methyl chloride can be further chlorinated to CH_2Cl_2 in a sequential step. CO is proposed to form as a side product from CH_2Cl_2 and $CHCl_3$ over partially dechlorinated surface sites.

Oxidative chlorination of methane over $LaCl_3$ provides an interesting alternative for activating and functionalizing methane. As a generic route it might, however, be limited to substitution of atoms into methane that can assume a positive oxidation state.

3.6   Acknowledgement

3.7   References

1.   Freni, S., Calogero, G., and Cavallaro, S., J. Power Sources, **2000,** 87(1-2), 28-38.

2.   Zhidomirov, G.M., Avdeev, V.I., Zhanpeisov, N.U., Zakharov, I., and Yudanov, I.V., Catal. Today, **1995,** 24(3), 383-387.

3.   Sun, Y., Campbell, S.M., Lunsford, J.H., Lewis, G.E., Palke, D., and Tau, L.M., J. Catal., **1993,** 143(1), 32-44.

4.   Periana, R.A., Mironov, O., Taube, D., Bhalla, G., and Jones, C.J., Science, **2003,** 301(5634), 814-818.

5.   Svetlano, E., Flid, R.M., Dzhagats.Rv, and Taber, A.M., Russian Journal Of Physical Chemistry, **1967,** 41(4), 487.

6.   Olah, G.A., Gupta, B., Farina, M., Felberg, J.D., Ip, W.M., Husain, A., Karpeles, R., Lammertsma, K., Melhotra, A.K., and Trivedi, N.J., J. Am. Chem. Soc., **1985,** 107(24), 7097-7105.

7.   Olah, G.A., Acc. Chem. Res., **1987,** 20(11), 422-428.

8.   Crum, B.R., Jarvis, R.F.J., Naasz, B.M., and Toupadakis, A.I., in *EP 0720975 A1*. 1996.

9.   Rouco, A.J., J. Catal., **1995,** 157(2), 380-387.

10.   Wattimena, F. and Sachtler, W.M.H., Stud. Surf. Sci. Catal., **1982,** 7, 816-827.

11.   Kenney, C.N., Cat. Rev. - Sci. Eng., **1975,** 11(2), 197-224.

12.   Garcia, C.L. and Resasco, D.E., Appl. Catal., **1989,** 46(2), 251-267.

13.   Garcia, C.L. and Resasco, D.E., J. Catal., **1990,** 122(1), 151-165.

14.   Pieters, W.J.M., Conner, J., Wm. C., and Carlson, E.J., Appl. Catal., **1984,** 11(1), 35-48.

15.   Schweizer, A.E., Jones, M.E., and Hickman, D.A., *Oxidative halogenation of C1 hydrocarbons to halogenated C1 hydrocarbons and integrated processes related thereto*, in *US 6452058 B1*. 2002, Dow Global Technologies Inc. (Midland, MI).

16.   Podkolzin, S.G., Manoilova, O.V., and Weckhuysen, B.M., J. Phys. Chem. B, **2005,** 109(23), 11634-11642.

17.   Manoilova, O.V., Podkolzin, S.G., Tope, B., Lercher, J., Stangland, E.E., Goupil, J.M., and Weckhuysen, B.M., J. Phys. Chem. B, **2004,** 108(40), 15770-15781.

18.   Weckhuysen, B.M., Rosynek, M.P., and Lunsford, J.H., Phys. Chem. Chem. Phys., **1999,** 1(13), 3157-3162.

19.   Peringer, E., Podkolzin, S.G., Jones, M.E., Olindo, R., and Lercher, J.A., Top. Catal., **2006,** 38(1-3), 211-220.

20.   Schoofs, B., Martens, J.A., Jacobs, P.A., and Schoonheydt, R.A., J. Catal., **1999,** 183(2), 355-367.

21.   Van der Avert, P., Podkolzin, S.G., Manoilova, O., De Winne, H., and Weckhuysen, B.M., Chem. Eur. J., **2004,** 10(7), 1637-1646.

Chapter 4

Synthesis of LaCl₃ catalysts from LaOCl as advanced materials in oxidative chlorination of methane

Abstract

LaCl₃ is an active and selective catalyst for oxidative chlorination of methane to methyl chloride, generated in situ by chlorination from LaOCl. The latter is prepared by precipitation of La(OH)₂Cl and subsequent calcination. The synthesis route was modified by using different bases in order to synthesize high surface area LaOCl catalyst precursors. Ammonium hydroxide and the organic bases tetraethylammonium hydroxide, tetrapropylammonium hydroxide, and tetrabutylammonium hydroxide are used as precipitating agents. The marked increase of the specific surface area by using organic bases indicates also that they may act as templating agents. After chlorination the specific surface areas of pure LaOCl samples decrease drastically, lanthanum carbonate, however, acts as structural promoter stabilizing the specific surface area during chlorination.

4 Synthesis of LaCl₃ catalysts from LaOCl as advanced materials in oxidative chlorination of methane

4.1 Introduction

LaCl$_3$ has been shown to be a highly stable and selective catalyst for oxidative chlorination of methane with hydrogen chloride and oxygen to methyl chloride and water (equ. 4.1) [1-3].

$$CH_4 + HCl + 0.5O_2 \rightarrow CH_3Cl + H_2O \qquad\qquad (4.1)$$
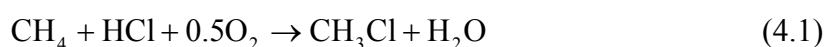
The oxidative chlorination of methane with LaCl$_3$ has been concluded to be a surface catalyzed reaction with a transient hypochlorite species as the active site on the surface [2]. This hypochlorite species is formed by dissociative adsorption of oxygen on the surface. Methane reacts with the hypochlorite and forms a carbonium ion, followed by an exchange of hydrogen with the positively charged chlorine atom, creating a hydroxy group and a chloride vacancy. Hydrogen chloride is regenerating the surface via addition of Cl⁻ and the formation of water. This mechanism (see Figure 4.1) is in line with the results of exploring the corresponding intermediates by DFT calculations.
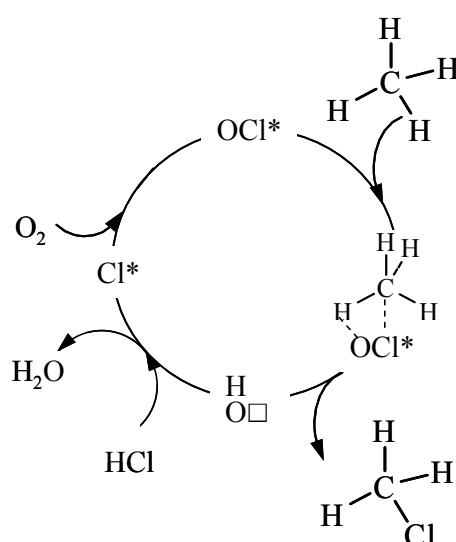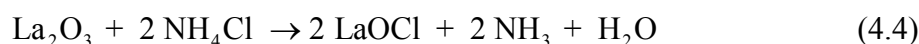

Figure 4.1: Proposed reaction mechanism for oxidative chlorination of methane over LaCl$_3$-based catalysts [2]

The catalyst and the reaction route are advantageous compared to the well-known copper based catalysts which catalyze the Deacon reaction, the oxidation of hydrogen chloride and oxygen to chlorine gas. Methane is, thus, chlorinated via a gas-phase radical reaction with low selectivity towards methyl chloride over copper catalysts. Unlike the radical gas-phase chemistry of the copper catalyst, the surface catalyzed reaction over $LaCl_3$ provides the possibility to change activity and selectivity by modification of the catalyst, e.g., by changing the synthesis route.

$LaCl_3$ is a highly hygroscopic material and has to be prepared in situ. Dehydrated $LaCl_3$ can be generated by thermal transformation of lanthanum chloride heptahydrate in inert gas or hydrogen chloride. However, the dehydration has to proceed very slowly in order to avoid the transformation to $LaOCl$. Such commercially available $LaCl_3$ material possesses low specific surface areas.

A conceptually better route to materials with a high specific surface area is therefore the in situ chlorination of lanthanum oxychloride at 400°C with hydrogen chloride. Lanthanum oxychloride is not hygroscopic and is stable when exposed to air.

Several synthesis routes to prepare $LaOCl$ are known based on various ways to introduce the chlorine atom in the structure. The synthesis routes include the solid state reaction of lanthanum oxide with ammonium chloride at 1000°C (equ. 4.2 – 4.4) [4, 5]. The reaction proceeds over a lanthanum chloride ammonia adduct and the overall reaction is presented in equation 4.4.

$$La_2O_3 + 6\,NH_4Cl \rightarrow 2\,LaCl_3 \cdot 3\,NH_3 + 3\,H_2O \qquad (4.2)$$

$$LaCl_3 \cdot 3\,NH_3 + La_2O_3 \rightarrow 3\,LaOCl + 3\,NH_3 \qquad (4.3)$$

$$La_2O_3 + 2\,NH_4Cl \rightarrow 2\,LaOCl + 2\,NH_3 + H_2O \qquad (4.4)$$

$LaOCl$ can also be synthesized from lanthanum oxide and lanthanum chloride at room temperature via a mechano-chemical synthesis (equ. 4.5), but the upper limits of the specific surface area reachable is rather low for such approaches (1 m^2/g) [6, 7].

$$La_2O_3 + LaCl_3 \rightarrow 3LaOCl \qquad (4.5)$$

Marsal *et al.* used a sol-gel route with acrylamide as macroscopic template. Acrylamide is forming a 3D network in which a solution of La and Cl ions is soaked [8, 9]. The gel is first dried in a microwave, followed by thermal treatment at 600°C to obtain the final LaOCl powder. This method yields a homogenous distribution of faceted stick-shaped particles. The disadvantage of the solid state reactions is the required high temperature treatment leading to very low BET surface areas.

A further possibility for the catalyst preparation is the precipitation of lanthanum dihydroxychloride from a lanthanum chloride solution (equ. 4.6). The precipitated lanthanum hydroxychloride is calcined at 550°C to yield the catalyst precursor lanthanum oxychloride (equ. 4.7) [10]:

$$LaCl_{3,aq} + base \rightarrow La(OH)_2Cl \qquad (4.6)$$

$$La(OH)_2Cl \xrightarrow{550°C, 8h} LaOCl + H_2O \qquad (4.7)$$
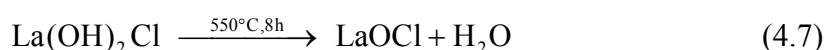
We have taken this approach using different organic bases for precipitation in order to prepare high surface area samples. The influence of the used base on the morphology and composition of the sample before and after chlorination is investigated. Furthermore, the catalytic performance of the prepared samples in oxyhydrochlorination is evaluated.

4.2 Experimental

4.2.1 Catalyst preparation

LaCl$_3$ catalysts were prepared *in situ* in an HCl flow from LaOCl precursors. The LaOCl precursors were prepared by precipitation at room temperature using ammonium hydroxide (NH$_4$OH), tetraethylammonium hydroxide (TEAOH, Merck, 20% aq. sol.), tetrapropylammonium hydroxide (TPAOH, Merck, 40% aq. sol.) or tetrabutylammonium hydroxide (TBAOH, Aldrich 99.9%, 20% aq. sol.) as base and a solution of lanthanum(III) chloride heptahydrate (99%, Merck) in ethanol (1M). After drop-wise addition of the base to the solution, the suspension was stirred for 1 h to facilitate complete precipitation. The gel obtained after centrifugation was washed twice with excess of ethanol to remove the base. Finally, the gel was freeze dried and calcined at 550°C using a temperature increment of 5°C

min^{-1} in a flow of synthetic air (200 ml min^{-1}) for 8 h. LaOCl was initially activated in He flow (40 ml min^{-1}) at 550°C for 1 h. Subsequently, the material was converted to LaCl$_3$ *in situ* by reacting with HCl (20 vol. % HCl in He, total flow 50 ml min^{-1}) at 400°C for 10 h. The samples are denominated as LaOCl S1 to LaOCl S4 with the base used for precipitation in brackets.

4.2.2 Physicochemical characterization

The crystallographic structure of the LaOCl precursors and resulting LaCl$_3$ catalysts was determined by XRD with a Philips X'Pert Pro System (CuK$_{\alpha 1}$-radiation, 0.154056 nm) at 40 kV / 40 mA. The measurements were performed with a step scan of 0.017° min^{-1} from 10° to 60° 2θ and a time per step of 29.84 sec.

The morphology and particle size of the LaOCl precursors and the chemical analysis by Energy dispersive X-ray spectroscopy (EDX) were examined by scanning electron microscopy using a *JEOL* 500 SEM-microscope (accelerating voltage 20 kV). Before recording the SEM image, the sample was outgassed for two days at room temperature and sputtered with gold before collecting the images.

BET surface area and pore volume were determined by nitrogen adsorption at 77.4 K using a PMI automated BET Sorptometer. The mesopore size distribution was obtained from the desorption branch of the isotherm using the Barret–Joyner–Halenda (BJH) method, the micropore volume was obtained from the desorption branch of the isotherm using the Horvath–Kawazoe (HK) method [11]. Prior to measurement, the LaOCl samples were outgassed in vacuum (10^{-3} Pa) at 250°C for 2 h.

4.2.3 Catalytic tests

The *in situ* prepared LaCl$_3$ sample was tested in methane oxidative chlorination using a fixed-bed quartz tubular reactor charged with 250 mg of LaOCl precursor (0.63 - 1 mm size fraction). The temperature of the reactor oven was controlled by a thermocouple placed above the catalyst bed. The gas flows (CH$_4$, O$_2$, HCl, N$_2$, He) were controlled using digital mass flow meters (Bronkorst). The catalytic tests were performed in the temperature range 450 to 550°C using 5 ml min^{-1} of the stoichiometric mixture CH$_4$:HCl:O$_2$:He:N$_2$ = 2:2:1:4:1. Helium was used as a diluent, and nitrogen as an internal standard. The reactor outlet was analyzed by an online Siemens Maxum Edition II gas chromatograph (GC). After analysis, the gases were

passed through water and NaOH scrubbers to remove unreacted HCl. Gas lines of the setup were coated with glass lining and heated to 150°C to prevent water condensation and corrosion.

The ability of the catalyst to accept chlorine was studied with temperature programmed chlorination experiments. A mixture of He:HCl (4:1; 50 ml min^{-1}) was passed over 250 mg of the sample while increasing the temperature from room temperature to 650°C with 2°C min^{-1}. The HCl uptake was monitored by GC analysis.

4.3   Results

4.3.1   Physicochemical characterization

The N_2 physisorption results of the freshly prepared and chlorinated samples are summarized in Table 4.1. The samples precipitated with organic bases exhibit a higher BET surface area compared to the sample precipitated with ammonium hydroxide. The highest specific surface area was obtained with TEAOH as precipitating base. However, with increasing chain length of the alkyl group the specific BET area decreased.

Table 4.1: N_2 physisorption on catalyst precursors and the chlorinated material

Sample	BET area $[m^2\,g^{-1}]$	Pore volume $[cm^3\,g^{-1}]$	BET area $[m^2\,g^{-1}]$	Pore volume $[cm^3\,g^{-1}]$
	precursor		chlorinated	
S1 (NH_4OH)	21	0.063	< 1	-
S2 (TEAOH)	125	0.377	6	0.028
S3 (TPAOH)	118	0.435	11	0.143
S4 (TBAOH)	78	0.360	3	0.036

The adsorption/desorption isotherms of all samples correspond to a type IV isotherm characterized by a hysteresis loop, generated by capillary condensation of the adsorbate in the mesopores. The hysteresis loop corresponds to the type H3 loop, which is observed with aggregates of plate-like particles giving rise to slit-shaped pores [12]. This is also confirmed

by TEM measurements of LaOCl S2 (TEAOH) which showed agglomeration of plate-like primary particles with a median length of 200 nm and 45 nm thickness (see Figure 4.2).
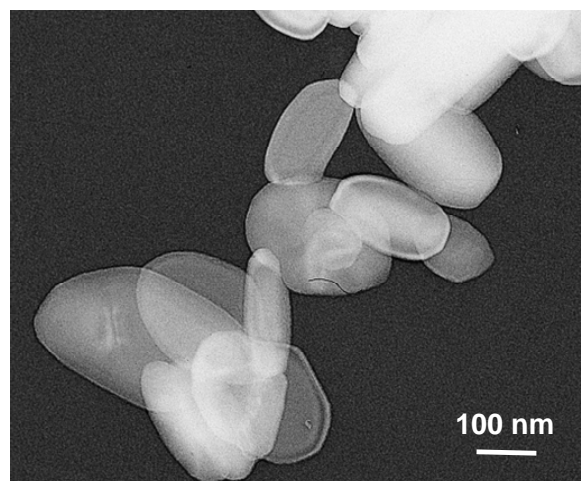

Figure 4.2: TEM photograph of the LaOCl S2 (TEAOH)

The different bases also influenced the pore size distribution as shown by the comparison of the BJH-plot for S1 (NH$_4$OH) and S4 (TBAOH) in Figure 4.3.
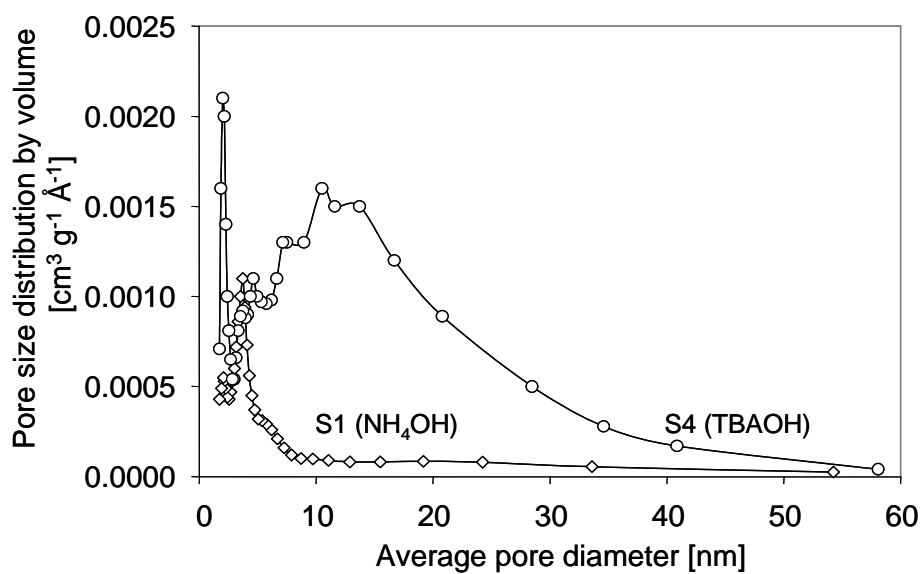

Figure 4.3: Pore size distributions (BJH-plot) of LaOCl S1 (NH$_4$OH) (◇) and LaOCl S4 (TBAOH) (○)

LaOCl S1 (NH$_4$OH) showed a pore size distribution with a main pore diameter of around 3.8 nm. Whereas, larger pores with a pore diameter around 10 nm were obtained by precipitation with organic bases. For LaOCl S4 (TBAOH), the pore size distribution reached a maximum of around 12.5 nm.

The XRD pattern of the synthesized samples showed that LaOCl is the only crystalline phase presents (results not shown). SEM photographs show also the agglomeration of the primary particles to much larger particles with an irregular shape and diameters between 3.5 and 25 μm in case of LaOCl S1 (NH$_4$OH). While, the morphology was similar for all samples, the particle size reached up to 100 μm for the samples precipitated with organic bases. As example, the SEM photograph for the fresh LaOCl S2 (TEAOH) is shown in Figure 4.4a.
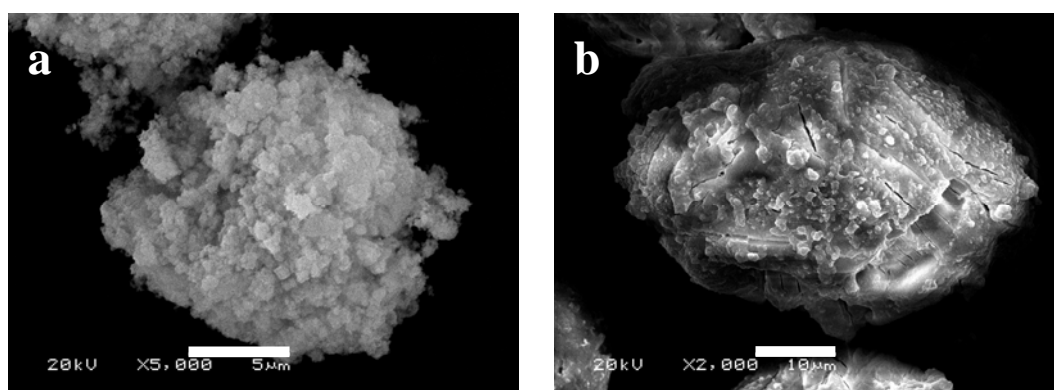

Figure 4.4a+b: SEM photographs of a) LaOCl S2 (TEAOH) precursor and b) chlorinated at 400°C for 10h

In order to prepare LaCl$_3$, typically the most active form of the catalyst, the samples are activated and chlorinated with HCl for 10 h at 400°C prior to the catalysis. After this procedure the BET surface area of all samples decreased. For example, the specific surface area of S2 (TEAOH) decreased from 125 m^2 g^{-1} for the catalyst precursor to 6 m^2 g^{-1} after 10h of chlorination (see Table 4.1). This corresponds to about 5% of the original BET surface area. Figure 4.5 shows that the chlorinated sample adsorbed a much lower amount of N$_2$ compared to the LaOCl precursor. The ratio between the area of hysteresis and the area below the adsorption line increased by a factor of 2.5 for the chlorinated form. This indicates that chlorination reduces the concentration of accessible micropores to a higher extent than for the

mesopores. This effect was even more pronounced with S3 (TPAOH). After chlorination, 36% of the original mesopore volume and only 10% of the original micropore volume was retained. The reduction in BET surface area was observed for all samples. The highest BET surface area after chlorination was observed for S3 (TPAOH). Around 9% of the BET surface area of the precursor were preserved indicating some stabilization during chlorination (see Table 4.1). The SEM photograph (Figure 4.4b) clearly shows the further agglomeration of particles after chlorination leading to particles ranging from 5µm to 210µm.
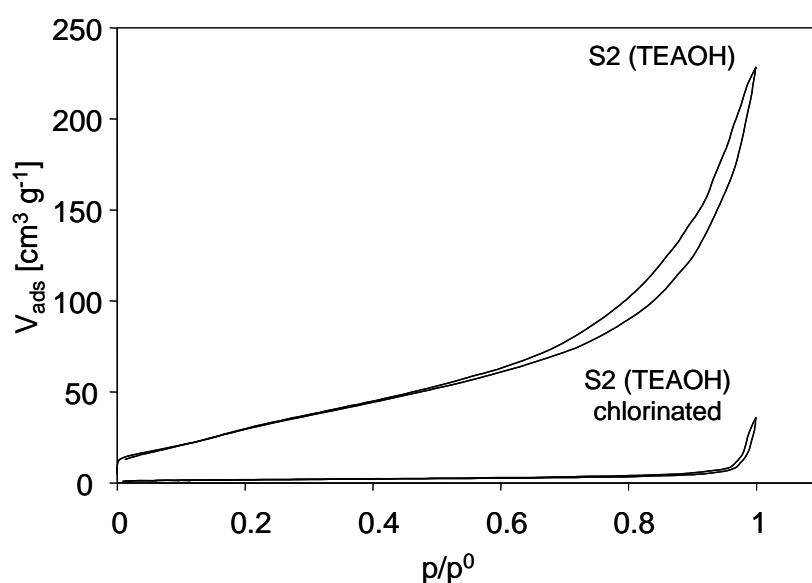

Figure 4.5: N_2 adsorption/desorption isotherm of LaOCl S2 (TEAOH) precursor and chlorinated material

The elemental composition of the synthesized LaOCl precursors was determined by EDX and is summarized in Table 4.2. It should be noted that the concentration of lanthanum and chlorine do not correspond to pure stoichiometric LaOCl. Only the S1 sample precipitated with the inorganic base NH_4OH showed a La/Cl ratio of 1. The La/Cl ratio of the samples precipitated with organic bases ranged between 2 and 3. Together with the presence of carbon in these samples this deviation indicates that $La_2(CO_3)_3$ is present either on the surface or as bulk carbonate. To quantify this observation, the carbon content was determined by CHN analysis and is summarized in Table 4.2. The carbonate content decreases in the following sequence:

$$S3 \ (TPAOH) \ > \ S2 \ (TEAOH) \ > \ S4 \ (TBAOH) \ > \ S1 \ (NH_4OH) \qquad (4.8)$$

The highest carbonate content was found in S3 (TPAOH), followed by S2 (TEAOH) which had a similar carbonate content like S4 (TBAOH). The lowest carbon content was found in S1 (NH$_4$OH).

Table 4.2: Elemental composition of the LaOCl precursor determined by EDX analysis

Sample	La [mol%]	Cl [mol%]	La/Cl ratio	C content [wt.%]
S1 (NH$_4$OH)	26.7	24.2	1.1	0.02
S2 (TEAOH)	26.7	16.1	1.7	0.89
S3 (TPAOH)	15.6	5.2	3.0	1.53
S4 (TBAOH)	30.6	15.1	2.0	0.78

*determined by CHN analysis

4.3.2 Chlorination of the precursor

Full chlorination is essential for a highly active and selective catalyst, as lattice oxygen atoms on the surface are active for the catalytic destruction of chlorinated hydrocarbons. In order to understand the kinetics of this process and to assure the completeness, the ability for HCl uptake was tested in temperature programmed chlorination. The results are compiled in Figure 4.6. The total HCl uptake and the maximum temperature for HCl uptake varied between the different samples. The S3 (TPAOH) sample showed the highest HCl uptake of 0.0112 mol HCl g^{-1} with a maximum uptake at 287°C, followed by S2 (TEAOH) with 0.0088 mol HCl g^{-1} uptake and a maximum at 231°C. The most easily chlorinated catalyst was S4 (TBAOH) with a maximum uptake at 200°C. The total uptake for this sample was 0.0076 mol HCl g^{-1}. The sample synthesized with NH$_4$OH possessed with 0.0064 mol HCl g^{-1} the lowest HCl uptake and also the highest maximum uptake temperature at 325°C. However, it should be noted that the uptake does not correspond to a total chlorination, as exposure of the materials at the optimum chlorination temperature was too short. The HCl uptake of the different samples varies in the following sequence:

$$S3 \text{ (TPAOH)} > S2 \text{ (TEAOH)} > S4 \text{ (TBAOH)} > S1 \text{ (NH}_4\text{OH)} \quad (4.9)$$

$$0.0112 \text{ mol/g} > 0.0088 \text{ mol/g} > 0.0076 \text{ mol/g} > 0.0064 \text{ mol/g} \quad (4.10)$$

As all samples contain a certain amount of lanthanum carbonate, a temperature programmed chlorination with pure lanthanum carbonate hydrate was performed. Activated in the same manner as LaOCl, it showed an optimum temperature for HCl uptake at around 440°C (result not shown).
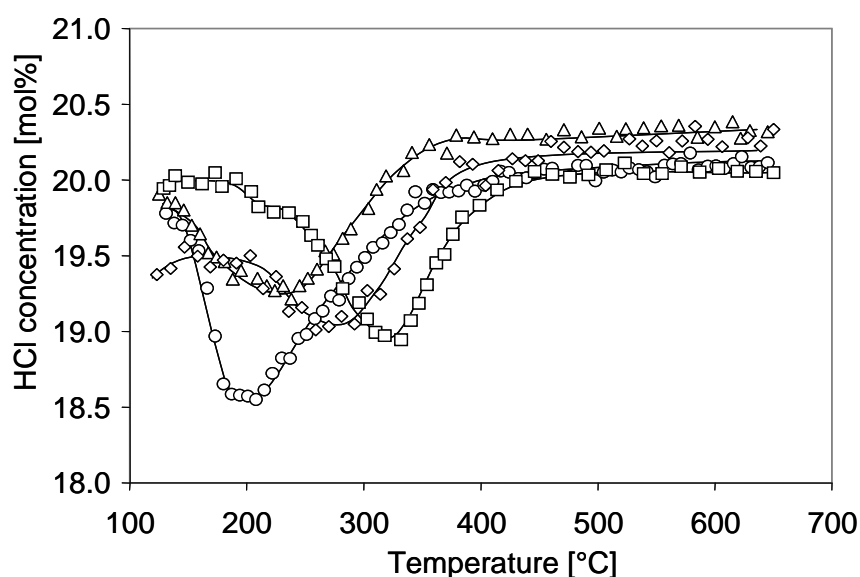

Figure 4.6: Temperature programmed chlorination with 20 vol.% HCl and a temperature increment of 2 °C min^{-1}; □ S1 (NH$_4$OH), △ S2 (TEAOH), ◇ S3 (TPAOH), ○ S4 (TBAOH)

4.3.3 Catalytic conversion of methane

The reactant conversion in the temperature range from 450°C to 550°C over LaOCl S1 (NH$_4$OH) is shown in Figure 4.7a. By increasing the temperature the methane conversion increased from 4.5% to 19.5%. At 450°C the oxygen and hydrogen chloride conversion was equal to the methane conversion. However, the oxygen conversion showed a stronger increase with temperature than the methane conversion and reached at 551°C 38%. The HCl conversion was slightly lower than the methane conversion and the increase parallels with the methane conversion in the whole temperature range. The distribution of the product yields in

the same temperature range is shown in Figure 4.7b. Methyl chloride was the main product formed in the whole temperature range and the yield increased with temperature from 3.6% to 11.5%.
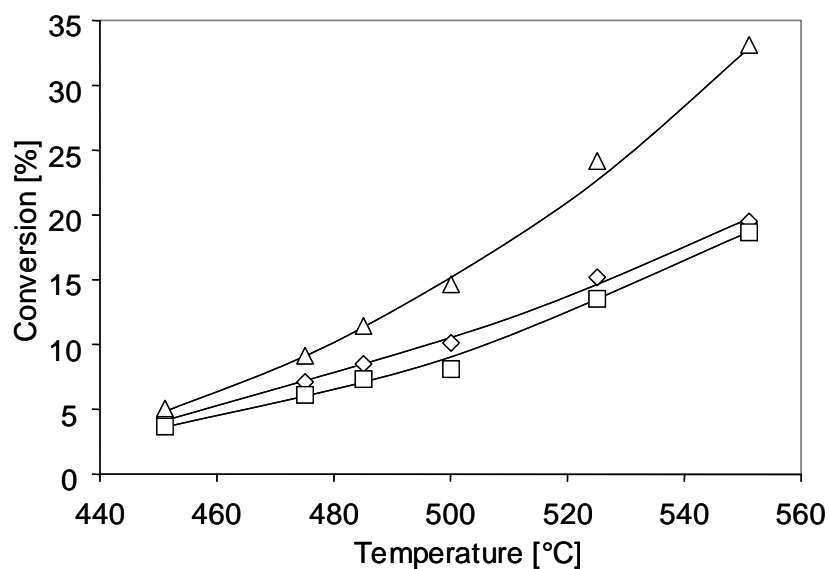

Figure 4.7a: Reactant conversion over LaOCl S1 (NH$_4$OH) in the temperature range between 450°C and 550°C at constant space velocity with stoichiometric flow CH$_4$:HCl:O$_2$:He:N$_2$ = 2:2:1:4:1 ($\diamond$ CH$_4$, $\square$ HCl, $\triangle$ O$_2$)
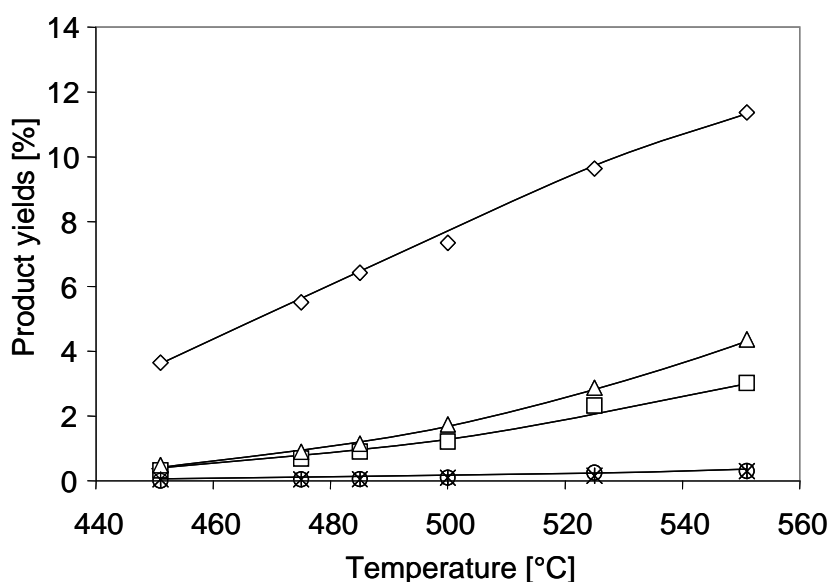

Figure 4.7b: Product yields over LaOCl S1 (NH$_4$OH) in the temperature range between 450°C and 550°C at constant space velocity with stoichiometric flow CH$_4$:HCl:O$_2$:He:N$_2$ = 2:2:1:4:1 ($\diamond$ CH$_3$Cl, $\square$ CH$_2$Cl$_2$, $\bigcirc$ CHCl$_3$, $\triangle$ CO, $\ast$CO$_2$)

As by-products also carbon monoxide and methylene chloride were formed. The yield of carbon monoxide and methylene chloride increased with temperature, with the increase being more pronounced at higher temperatures. Chloroform and tetrachloromethane were formed only in negligible amounts. CO_2 was hardly detected.

The reactant conversion and product yields on methane conversion in the same temperature range over S3 (TPAOH), as example for an organic precipitated catalyst, are shown in Figures 4.8a and 4.8b.
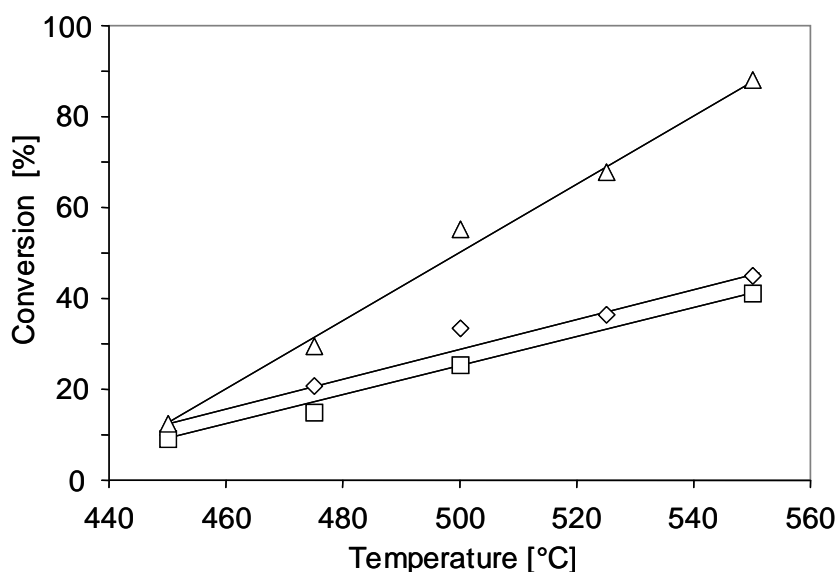

Figure 4.8a: Reactant conversion over LaOCl S3 (TPAOH) in the temperature range between 450°C and 550°C at constant space velocity with stoichiometric flow $CH_4:HCl:O_2:He:N_2 = 2:2:1:4:1$ ($\diamond$ CH_4, $\square$ HCl, $\triangle$ O_2)

LaOCl S3 (TPAOH) showed higher reactivity. At 450°C, similar to LaOCl S1 (NH_4OH), the oxygen and hydrogen chloride conversion were equal to the methane conversion. AT higher temperatures, the HCl conversion was always slightly lower than the methane conversion and the oxygen conversion showed a strong increase with temperature up to 88% at 555°C. Over S3 (TPAOH) methyl chloride was also the main product and reached a maximum yield of 17.1% at 500°C. Carbon monoxide and methylene chloride yield strongly increased with temperature.
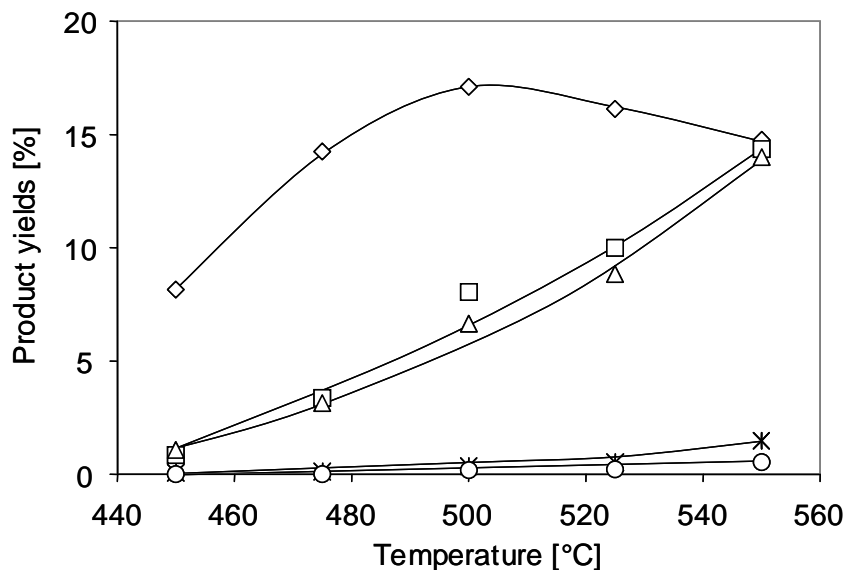
Figure 4.8b: Product yields over LaOCl S3 (TPAOH) in the temperature range between 450°C and 550°C at constant space velocity with stoichiometric flow $CH_4:HCl:O_2:He:N_2 = 2:2:1:4:1$ (◇ CH_3Cl, □ CH_2Cl_2, ✳ $CHCl_3$, ○ CO, △ CO_2)

The catalysts precipitated with organic bases showed in general a higher activity for methane conversion with a slightly higher yield towards CH_3Cl compared to the catalyst precipitated with NH_4OH. The highest rate for methane conversion at 527°C was reached with S3 (TPAOH). This catalyst converted $1.1 \cdot 10^{-6}$ mol CH_4 g_{cat}^{-1} s^{-1}, whereas S1 (NH_4OH) converted at 527°C only $6.8 \cdot 10^{-7} \cdot$ mol CH_4 g_{cat}^{-1} s^{-1}. The selectivity to methyl chloride of all studied catalysts was at the same methane conversion almost equal. The dependence of methyl chloride yield, the desired product, on methane conversion of all studied catalysts is provided in Figure 4.9. The dashed line indicates the yield for 100% selectivity. At low methane conversion the yield towards methyl chloride increased with methane conversion. At higher methane conversion the increase of the methyl chloride yield slowed down or even decreased. It is important to note, that the data were collected at different reaction temperatures, thus we cannot speculate about the mechanism. However, the same trend of the methyl chloride yield with methane conversion indicates that the same active sites are present in all studied catalysts. The dependence of methylene chloride yield is shown in Figure 4.10. The methylene chloride yield was for all samples in the same range and increased with increasing methane conversion.

Figure 4.9: Dependence of CH_3Cl yield on CH_4 conversion in the temperature range between 450°C and 550°C at a constant space velocity (CH_4:HCl:O_2:He:N_2 = 2:2:1:1:4:1); □ S1 (NH_4OH), △ S2 (TEAOH), ◇ S3 (TPAOH), ○ S4 (TBAOH), ⎯ 100% selectivity line
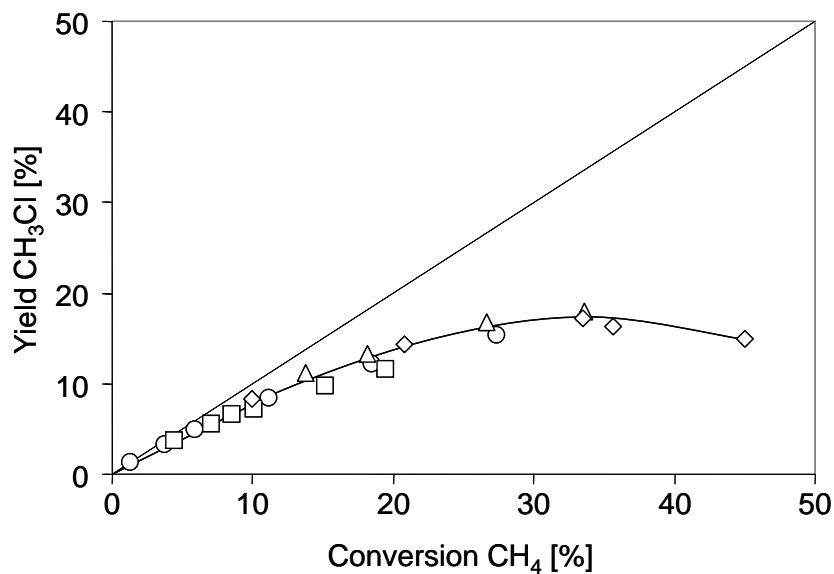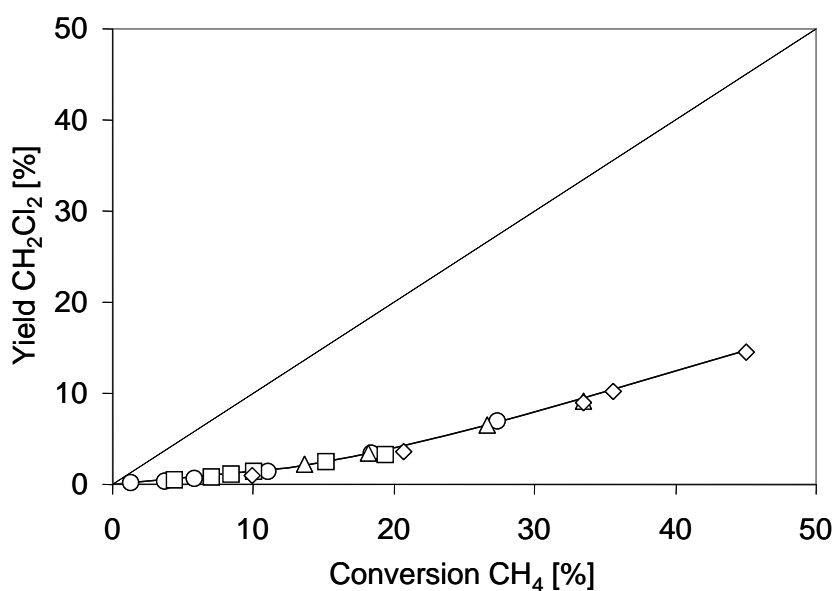

Figure 4.10: Dependence of CH_2Cl_2 yield on CH_4 conversion in the temperature range between 450°C and 550°C at a constant space velocity (CH_4:HCl:O_2:He:N_2 = 2:2:1:1:4:1); □ S1 (NH_4OH) △ S2 (TEAOH), ◇ S3 (TPAOH), ○ S4 (TBAOH), ⎯ 100% selectivity line

4.4   Discussion

The specific surface area and the pore size in precipitated chlorides depend in a complex way on the used bases and the drying methods employed. Compared with NH_4OH, organic bases led to a significantly higher specific surface area. This can be attributed on the one hand to the higher base strength, leading to a higher concentration of primary nuclei during the precipitation. It could also be speculated that the organic rest induces locally some sort of templating, such as the pore building action during the formation of zeolite gel precursors [13, 14]. The fact that TEAOH led to the highest specific surface area points to the fact that latter influence is less important than the more rapid nucleation step. However there is also indication of pore collapse during calcination of $La(OH)_2Cl$ to $LaOCl$ (see Figure 4.11).
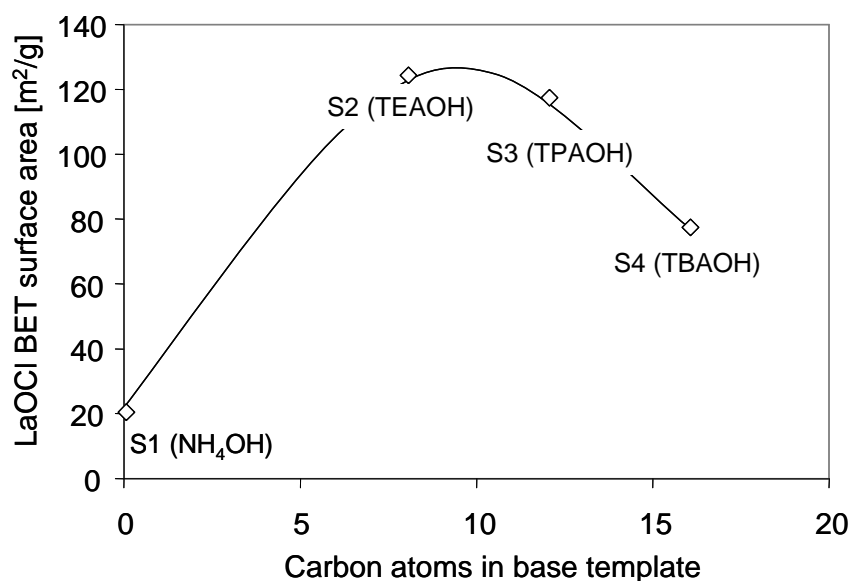
Figure 4.11: Influence of the number of carbon atoms in the base template on LaOCl BET surface area

The composition of the surface obtained from the EDX analysis indicates a non-stoichiometric composition of the lattice for the organic precipitated samples. In general, a higher La/Cl ratio is observed on the samples precipitated with organic bases. In contrast, the NH_4OH precipitated sample shows a nearly ideal La/Cl ratio of 1.0. The deviation from the La/Cl ratio of 1.0 is attributed to traces of carbonates in the sample presumably on the catalyst

surface. The higher La/Cl ratio of the LaOCl samples precipitated with organic bases stems form the higher lanthanum carbonate content. Marsal *et al.* reported the excellent CO_2 absorption properties of LaOCl samples at low temperature and humid conditions [8, 15]. Thus, surface lanthanum carbonate can be generated by CO_2 adsorption from air. It should be pointed out that bulk carbonate can be formed in the organic precipitated samples by the adsorption of CO_2 which is a product of the decomposition of the amines occurring during the calcination treatment of the precipitated $La(OH)_2Cl$.

The variations in the BET surface area and the mesoporous structure influences also the chlorination behavior of the samples. Temperature programmed chlorination is used to monitor the chlorination ability of LaOCl to $LaCl_3$ (equ. 4.11).

$$LaOCl + 2HCl \rightleftharpoons LaCl_3 + H_2O \qquad\qquad (4.11)$$

Simultaneously lanthanum dioxocarbonate which is present in the sample is also chlorinated with 6 mol HCl (equ. 4.13). Lanthanum dioxocarbonate is generated by the decomposition of lanthanum carbonate during the activation treatment in helium (equ. 4.12).

$$La_2(CO_3)_3 \xrightarrow{\Delta T} La_2O_2CO_3 + 2CO_2 \qquad\qquad (4.12)$$

$$La_2O_2CO_3 + 6HCl \rightarrow 2LaCl_3 + CO_2 + 3H_2O \qquad\qquad (4.13)$$
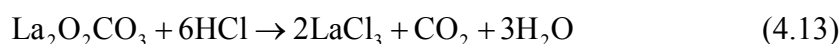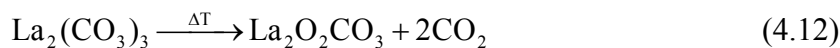
Therefore, the HCl uptake is correlated with the carbonate content of the samples. Figure 4.12 clearly shows the linear correlation between the HCl uptake and the carbon content of the sample, which represents the carbonate content. Lanthanum carbonate has an maximum chlorination temperature of 440°C and the LaOCl samples are commonly chlorinated at 400°C. Thus, the lanthanum carbonate chlorination is slower compared to the LaOCl chlorination. However, a 10 h chlorination treatment is sufficient to chlorinate all present carbonates, because after such chlorination no remaining carbonate was found by CHN analysis.

The HCl uptake is not only influenced by the carbonate content of the sample, but also by the BET area of the LaOCl precursor as well. The S1 (NH_4OH) catalyst which has the lowest BET surface area of all samples possesses also the lowest HCl uptake. The mesoporous structure of the organic precipitated samples facilitates the chlorination because HCl can easily penetrate the bulk of LaOCl via the pore structure. The S1 (NH_4OH) sample is

chlorinated only via the outer surface and bulk chlorination takes place by oxygen diffusion to the surface. This explains also the higher optimum chlorination temperature of S1 (NH$_4$OH). Furthermore the S1 (NH$_4$OH) catalyst has an almost ideal LaOCl structure, which is more difficult to chlorinate compared to the disordered LaOCl structure of the organic precipitated samples.
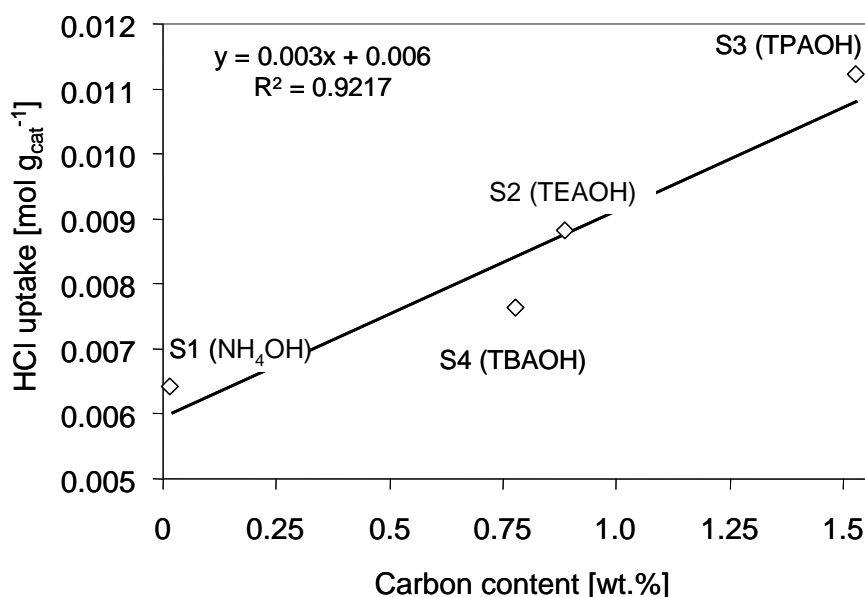

Figure 4.12: Influence of the carbon content in the catalyst precursor on the HCl uptake

The reactant conversion of S1 (NH$_4$OH) and S3 (TPAOH), showed that at low reaction temperature the methane, oxygen and hydrogen chloride conversion is equal. This indicates the stoichiometric conversion of methane and oxygen to methyl chloride and that the catalyst surface is regenerated with HCl according to equation 4.1. Methyl chloride is formed as a primary product over LaCl$_3$-based catalysts [2, 16]. Methyl chloride can either desorb from the surface or parts of the formed methyl chloride species can be retained on the surface. This leads to a catalytic pathway that favors the reaction of the strongly bound (partially chlorinated) methyl species with hydroxy groups formed during the initial step or with oxygen present in the sample. In addition to this pathway the re-adsorption of methyl chloride and additional chlorination or oxidation of the re-adsorbed species to CO can takes place. The more pronounced increase of the oxygen conversion with increasing reaction temperature is Figure 4.7a and Figure 4.8a is, thus, attributed on the one hand to the further chlorination of methyl chloride to methylene chloride, which consumes the double amount of hydrogen

chloride and oxygen compared to the methyl chloride formation while the methane conversion is not affected. On the other hand oxygen is also consumed due to the further oxidation of the chlorinated products to CO, while during the catalytic destruction of chlorinated products to CO hydrogen chloride is released [2, 17-19]. Thus, the increase of hydrogen chloride conversion parallels with the methane conversion even though higher chlorinated products are formed.

The presence of the same active site in all samples is confirmed by the same correlation of methyl chloride selectivity with methane conversion, which is observed to lie almost along the same line for all samples. Thus, it is concluded that only the active sites concentration must be different, as at the same reaction conditions higher methane conversions can be reached with the organic precipitated catalysts.

Also the porosity and morphology change by chlorination as shown by the N_2 physisorption results and SEM photographs of the chlorinated samples. The high BET surface area of the organic precipitated samples cannot be preserved during chlorination. In this process LaOCl samples are transformed to $LaCl_3$ and the structural information of the precursor is lost.

However, a direct relation exists between the specific surface area after chlorination and the CH_4 conversion as shown in Figure 4.13. This trend clearly supports the conclusion that the oxyhydrochlorination of methane is a surface catalyzed reaction.
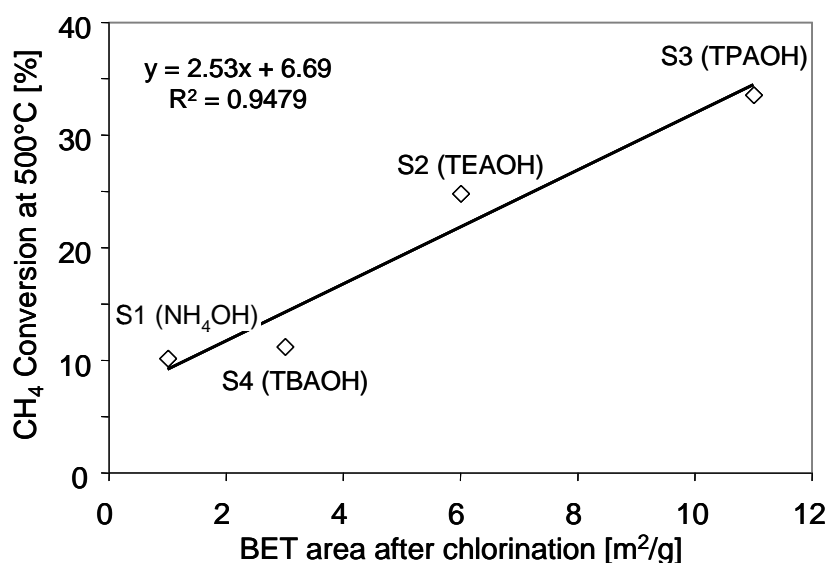

Figure 4.13: Correlation of methane conversion at 500°C with the BET surface area after chlorination

It is interesting to note, however, that a direct correlation between the specific surface area of LaOCl and the specific surface area of the chlorinated catalyst does not exist. While the S3 (TPAOH) precursor does not have the highest BET surface area, it shows the highest BET area after chlorination. The S3 (TPAOH) sample is characterized by the highest carbonate content of all prepared samples. As the LaOCl phase is faster chlorinated than lanthanum dioxocarbonate, the latter acts like a structural promoter and stabilizes the porous structure.

In the final step lanthanum dioxocarbonate is then fully chlorinated, but the already converted LaCl$_3$ suffices to stabilize the pore structure better. This connection is shown in Figure 4.14. The BET surface area after chlorination is influenced by the carbon content in the catalyst precursor.

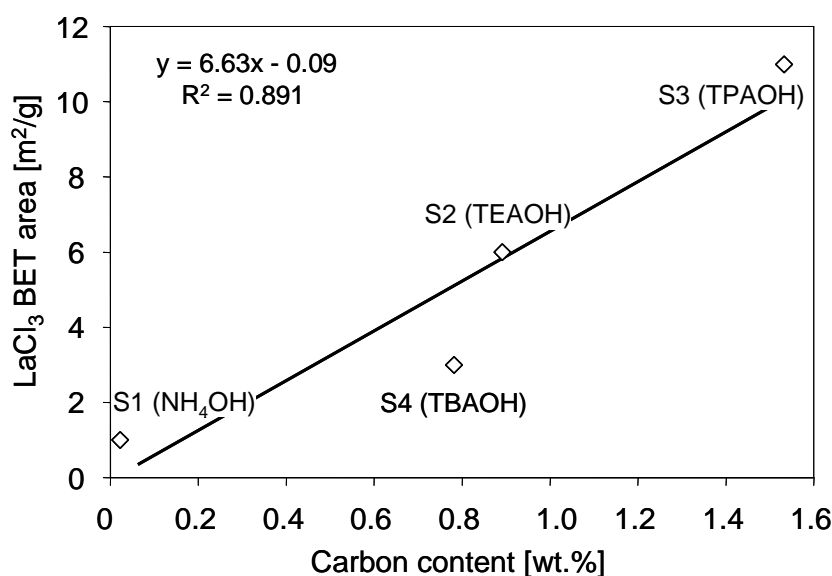**Figure 4.14**: Influence of the carbon content of the catalyst precursor on the LaCl$_3$ BET surface area

4.5   Conclusion

Samples of LaOCl with high specific surface area can be prepared, using the organic bases as precipitating agents. During the chlorination treatment the specific surface area drastically decreases. The decrease of the specific surface area is influenced by the carbonate

content of the catalysts. The chlorination of lanthanum dioxocarbonate proceeds more slowly than LaOCl, and thus lanthanum dioxocarbonate acts like a structural promoter during chlorination, stabilizing the BET surface area. Eventually the lanthanum dioxocarbonate is also fully chlorinated. The methane conversion shows a linear correlation with the specific surface area after chlorination, indicating that all site generated have identical catalytic properties. The LaOCl specific surface area and the carbon content influence also the chlorination behavior of the catalyst and results in a lower optimum temperature for the HCl uptake. High surface area samples have a higher HCl uptake because HCl can easily penetrate LaOCl through the pores.

4.6   Acknowledgment

4.7   References

1.   Schweizer, A.E., Jones, M.E., and Hickman, D.A., *Oxidative halogenation of C1 hydrocarbons to halogenated C1 hydrocarbons and integrated processes related thereto*, in *US 6452058 B1*. 2002, Dow Global Technologies Inc. (Midland, MI).

2.   Peringer, E., Podkolzin, S.G., Jones, M.E., Olindo, R., and Lercher, J.A., Top. Catal., **2006,** 38(1-3), 211-220.

3.   Podkolzin, S.G., Stangland, E.E., Jones, M.E., Peringer, E., and Lercher, J.A., J. Am. Chem. Soc., **2007,** 129, 2569-2576.

4.   Hölsä, J. and Niinisto, L., Thermochim. Acta, **1980,** 37(2), 155-160.

5.   Hölsä, J., Lahtinen, M., Lastusaari, M., Valkonen, J., and Viljanen, J., J. Solid State Chem., **2002,** 165(1), 48-55.

6.   Lee, J., Zhang, Q., and Saito, F., J. Solid State Chem., **2001,** 160(2), 469-473.

7.   Podkolzin, S.G., Manoilova, O.V., and Weckhuysen, B.M., J. Phys. Chem. B, **2005,** 109(23), 11634-11642.

8.   Marsal, A., Dezanneau, G., Cornet, A., and Morante, J.R., Sens. Actuators, B, **2003,** 95, 266-270.

9.   Dezanneau, G., Sin, A., Roussel, H., Vincent, H., and Audier, M., Solid State Commun., **2002,** 121(2-3), 133-137.

10.   Klevtsov, P.V., C. R. l'Academie. Sci., Ser. III, **1968,** 266(6), 385.

11.   Horvath, G. and Kawazoe, K., J. Chem. Eng. Jpn., **1983,** 16(6), 470-475.

12.   Sing, K.S.W., Everett, D.H., Haul, R.A.W., Moscou, L., Pierotti, R.A., Rouquerol, J., and Siemieniewska, T., Pure Appl. Chem., **1985,** 57(4), 603-619.

13.   Elanany, M., Su, B.L., and Vercauteren, D.P., Journal Of Molecular Catalysis A-Chemical, **2007,** 270(1-2), 295-301.

14.   Fouad, O.A., Mohamed, R.M., Hassan, M.S., and Ibrahim, I.A., Catal. Today, **2006,** 116(1), 82-87.

15.   Marsal, A., Rossinyol, E., Bimbela, F., Tellez, C., Coronas, J., Cornet, A., and Morante, J.R., Sens. Actuators, B, **2005,** 109, 38-43.

16.   Peringer, E., Salzinger, M., Hutt, M., and Lercher, J.A., ready for submission to J. Catal., **2008**.

17.   Van der Avert, P. and Weckhuysen, B.M., Angew. Chem. Int. Ed., **2002,** 41(24), 4730-4732.

18.   Van der Avert, P. and Weckhuysen, B.M., Phys. Chem. Chem. Phys., **2004,** 6(22), 5256-5262.

19.   Van der Heijden, A.W.A.M., Garcia Ramos, M., and Weckhuysen, B.M., Chem. Eur. J., **2007,** 109(1-2), 97-101.

Chapter 5

Modified lanthanum catalysts for oxidative chlorination of CH$_4$

Abstract

Mixtures of LaOCl and LaCl$_3$ are promising catalysts for oxidative chlorination of methane to methyl chloride. The influence of metal dopants such as Mg, Ni, Co, and Ce, which form stable chlorides under anticipated reaction conditions, was explored with respect to physicochemical and catalytic properties. The presence of markedly redox-active dopants such as cobalt and cerium leads to a higher rate of methane conversion. However, the formed methyl chloride is strongly adsorbed and directly oxidized to CO leading to low methyl chloride selectivity. The modification with nickel leads to high methyl chloride selectivity, but also to a less active catalyst. MgCl$_2$ leads to a decrease in activity while the typical selectivities of the parent LaOCl are retained.

5 Modified lanthanum catalysts for oxidative chlorination of CH$_4$

5.1 Introduction

The direct functionalization of methane is very challenging due to its tetrahedral geometry and the strong C-H bonds (439 kJ mol^{-1}) [1, 2]. In consequence, thermodynamic boundaries dictate that substituting hydrogen in methane for another element requires coupling to a strong exothermic (oxidative) reaction. As the resulting products are chemically more reactive than methane, over-oxidation, or over-functionalization of methane are frequent problems encountered.

A promising approach is the selective catalytic methane conversion to methyl chloride *via* oxidative chlorination (equ. 5.1), since methyl chloride is an important reactant in a number of chemical processes, such as in the production of silicon [3] or methanol [4]. Potentially, methyl chloride could also be used as the basis of the synthesis of higher hydrocarbons, whereby the HCl set free in the process can then be reused for the oxidative chlorination [4-6].

$$CH_4 + HCl + 0.5\,O_2 \rightarrow CH_3Cl + H_2O \qquad \Delta G^0 = \text{-141kJ/mol} \qquad (5.1)$$
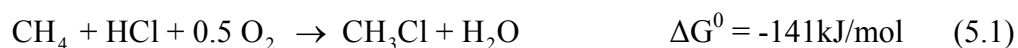
Recent reports [7, 8] showed that LaCl$_3$ is a promising stable catalyst for the conversion of methane to methyl chloride by oxidative chlorination using oxygen and HCl. It is superior to the well-established copper based catalysts [9-12], which are unstable and volatile under reaction conditions. These also catalyze the formation of chlorine *via* the Deacon reaction, initiating radical gas phase chlorination with low selectivity towards methyl chloride.

LaCl$_3$ catalyzes the reaction without a change in the oxidation state of lanthanum through a surface catalyzed reaction with a transient hypochlorite species as active site [7]. The hypochlorite species is formed on the chloride surface by reaction with oxygen from the gas phase. Methane exchanges hydrogen for positively charged chlorine atom of the transiently formed hypochlorite carbonium ion like transition state. This leads to a chlorine atom vacancy. Hydrogen chloride is regenerating the surface via substituting the OH-group formed in the exchange with Cl$^-$ generating water. Selectivities for methyl chloride above

90% can be obtained between 300 and 360°C at low conversions. As the conversion increases, the selectivity to CH_2Cl_2 increases, with $CHCl_3$ and CCl_4 being notably absent in the product mix.

It should be noted that the active catalyst $LaCl_3$ is in equilibrium with $LaOCl$ (equ. 5.2). Under reaction conditions, the surface is partially de-chlorinated.

$$LaCl_3 + H_2O \rightleftharpoons LaOCl + 2HCl \qquad\qquad \Delta G^0 = 79 \text{ kJ/mol} \qquad (5.2)$$

Especially above 500 °C, $LaCl_3$ releases HCl in the presence of water and is partially transformed to $LaOCl$. Oxidative chlorination can also be understood as a dynamic transformation between $LaCl_3$ and $LaOCl$. Chlorine is provided to the reaction in a Mars van Krevelen type mechanism [8]. Without HCl present in the gas phase, $LaCl_3$ transforms gradually into $LaOCl$.

In the preceding chapter, the rate of methane conversion has been positively correlated to the specific surface area [13]. This indicates that the same acid site density exists on the active materials studied. The question arises now, if the reactivity of the active sites (involving La^{3+}) can be modified by other metal cations. To probe this, $LaOCl$ catalysts were modified with metal chloride salts such as $MgCl_2$, $NiCl_2$, $CoCl_2$, and $CeCl_3$, which show a melting point higher than 550°C. The impact of $CeCl_3$ is particularly interesting; it is a lanthanide metal, but contrary to La it can change its formal oxidation state. The so prepared catalysts are characterized and tested for the synthesis of chloromethane from methane, HCl, and oxygen.

5.2 Experimental

5.2.1 Catalyst preparation

The $LaCl_3$ catalysts were prepared *in situ* in an HCl flow from $LaOCl$ precursors. The $LaOCl$ precursor was prepared by precipitation at room temperature using ammonium hydroxide (20% NH_4OH, Merck) and a solution of lanthanum(III)chloride heptahydrate (99%, Merck) in ethanol. After drop-wise addition of the base to the solution, the suspension was stirred for 1 h to facilitate complete precipitation. The precipitate obtained by centrifugation was washed twice with an excess of ethanol to remove the residual base.

Finally, the gel was freeze dried and calcined for 8 h at 550°C in synthetic air, using an increment of 5°C min^{-1} and a flow of 200 ml min^{-1}.

LaOCl was impregnated by incipient wetness impregnation with an aqueous solution of nickel dichloride hexahydrate (Merck, 98%), cobalt dichloride hexahydrate (Riedel de Haën, 99%), magnesium dichloride hexahydrate (Sigma-Aldrich, 99.995%) or cerium trichloride heptahydrate (Sigma-Aldrich, 99.9%), respectively. In each case, LaOCl was loaded with 5 mol% of the metal chloride. Due to the low solubility of cerium chloride, only one third of the calculated amount was dissolved in distilled water and the impregnation was repeated three times until the desired cerium content was reached. The materials were freeze dried over night before and after impregnation.

LaOCl was initially activated in He flow (40 ml min^{-1}) at 550°C for 1 h using an increment of 10°C min^{-1}. Subsequently, the material was converted to LaCl$_3$ *in situ* by reacting with HCl (20 vol. % HCl in He, total flow 50 ml min^{-1}) at 400°C for 14 h. The samples are named Me/LaOCl independent of their state of chlorination indicating the precursor material.

5.2.2 Physicochemical characterization

The crystallographic structure of the LaOCl precursors and resulting LaCl$_3$ catalysts was determined by XRD with a Philips X'Pert Pro System (CuK$_{\alpha 1}$-radiation) at 45 kV / 40 mA. The measurements were performed with a step scan of 0.017° min^{-1} from 10° to 60° 2θ. The morphology and particle size of the LaOCl precursor was examined by scanning electron microscopy using a *JEOL* 500 SEM-microscope (accelerating voltage 25 kV). Before recording the SEM images, the sample was outgassed for two days at room temperature and sputtered with gold.

BET surface area and pore volume were determined by nitrogen adsorption at 77.4 K using a PMI automated BET Sorptometer. The mesopore size distribution was obtained from the desorption branch of the isotherm using the Barret–Joyner–Halenda (BJH) method, the micropore volume was obtained from the desorption branch of the isotherm using the Horvath–Kawazoe (HK) method [14]. Prior to measurement, the LaOCl samples were outgassed in vacuum (10^{-3} Pa) at 250°C for 2 h.

5.2.3   Thermogravimetry

The thermal stability of the materials was investigated by thermogravimetric methods in a modified *Setaram TG-DSC 111* system. The samples were pressed into thin wafers and subsequently broken into small platelets. Approximately 17 mg of these platelets were charged into the quartz sample holder of the balance. The samples were heated in vacuum ($1 \cdot 10^{-6}$ bar) with a temperature increment of 5 °C min^{-1} to 750°C. Changes in weight were observed and the gases evolved were analyzed with a *Balzers* quadrupole mass spectrometer.

In order to understand the correlation between the product distribution and the catalytic activity of the prepared catalysts, the oxygen uptake was investigated by using TG/DSC. Approximately 50 mg of each catalyst, pressed and sieved, filled in the quartz sample holder and activated for 1h at 550°C in vacuum. After activation, the sample was cooled down to 100°C and oxygen (500 mbar) was introduced in the system and kept at 100°C for 0.5 h. Then, the temperature was increased up to 350°C with a temperature increment of 5°C min^{-1} and hold at 350°C for 0.5 h for oxygen adsorption. After the absorption period, the system is again cooled down to 100°C with a rate of 5°C min^{-1} and hold at 100°C for 1h in O_2 atmosphere. The oxygen uptake was determined by the weight increase of the sample.

5.2.4   Catalytic tests

The *in situ* prepared $LaCl_3$ sample was tested in methane oxidative chlorination using a fixed-bed quartz tubular reactor filled initially with 500 mg of LaOCl precursor (0.3 - 0.6 mm size fraction). The temperature of the reactor oven was controlled by a thermocouple placed above the catalyst bed. The gas flows (CH_4, O_2, HCl, N_2, He) were adjusted using mass flow controllers. Helium was used as a diluent, and nitrogen as an internal standard. The reactor outlet was analyzed online by a Siemens Maxum Edition II gas chromatograph. After analysis, the gases were passed through a NaOH scrubber to remove unreacted HCl. The lines of the setup were coated with glass lining and heated to 150°C to prevent water condensation and corrosion. CH_4 (purity 4.5) and O_2 (4.5) were provided from Messer Griesheim and HCl (2.8), N_2 (5.0) and He (4.6) by Air Liquid. All gases were used without further purification.

The dependence of the product distribution on methane conversion was evaluated by varying the space velocity, changing the total flow from 5 to 25 ml min^{-1} using a stoichiometric ratio of reactants (CH_4:HCl:O_2:He:N_2 = 2:2:1:4:1) at 475°C. Before starting the

analysis, the catalyst was stabilized for 8h at 475°C. Each space velocity was maintained for 1.5 h to ensure stable operating conditions.

The onset temperature and dependence of the product distribution on temperature was probed with temperature programmed reaction (TPR) by heating the catalyst from 200°C to 650°C with an increment of 1°C min^{-1} and feeding reactants at a stoichiometric ratio (CH$_4$:HCl:O$_2$:He:N$_2$ = 2:2:1:4:1) with a total flow of 10 ml min^{-1}.

The apparent activation energy was determined by varying the reaction temperatures between 400 and 500°C in 25°C increments and by adjusting the total flow rate to maintain the conversion below 10 %, so that a differential reactor model could be used in data analysis. In order to keep the catalyst in its chlorinated form, the tests were performed with an HCl excess (CH$_4$:HCl:N$_2$:O$_2$ = 2:6:1:1) and the catalyst was regenerated after each temperature step for 1h with 80 vol. % HCl in He.

The ability of the catalyst to accept chlorine was studied with temperature programmed chlorination experiments. A mixture of He:HCl (4:1; 50 ml min^{-1}) was passed over the sample while increasing the temperature from room temperature to 650°C with 3°C min^{-1}. The HCl uptake was monitored by GC analysis.

5.2.5   In situ Raman measurements

In situ Raman measurements were performed with an industrial LaOCl catalyst provided by The Dow Chemical Company in a tubular fix-bed quartz reactor system. The activation, chlorination and reaction conditions were similar to the catalytic test. In situ Raman spectra were collected at ambient conditions through a hole in the oven with a Holoprobe Kaiser Optical spectrometer equipped with a holographic notch filter, CCD camera and 532 nm laser. The Raman spectra were collected at different reaction temperatures with an exposure time of 1 sec and 50 accumulations.

5.3   Results

5.3.1   Chemical composition, morphology and structural aspects

The results of the N$_2$ physisorption and concentration of the dopant metal in the fresh and used catalysts are summarized in Table 5.1. After the catalytic tests at 475°C for 15h, the

concentration of dopant metals decreased in all cases. The most significant loss of dopant was observed for Mg/LaOCl and Ni/LaOCl. The loss of dopants was also observed visually by the migration of the yellow color of nickel and the blue color of cobalt downstream of the catalyst bed. The loss in metal is attributed to the significant vapor pressures of these metal chloride salts and the facilitation of the surface migration of the chlorides by the abundance of HCl in the gas phase. In this context it should be noted that magnesium and nickel chloride have a vapor pressure of $1.1 \cdot 10^{-4}$ and $3.1 \cdot 10^{-5}$ mbar at 475°C, respectively [15].

The parent LaOCl had the highest BET surface area of 17 m^2 g^{-1}. The surface areas and the pore volumes were lower after impregnation with metal salts (9-13 m^2 g^{-1}). The N_2 physisorption for the samples after 14h chlorination at 400°C showed that the BET surface area was further decreased, e.g., to 7 m^2/g and 8 m^2/g for Mg/LaOCl and Ce/LaOCl, respectively. The decrease in specific surface area is attributed to the partial collapse of the pore structure during the chlorination of LaOCl to $LaCl_3$.

Table 5.1: N_2 physisorption and AAS results of the fresh catalysts and dopant loss after reaction at 475°C

Sample	BET area [m^2/g]	Pore volume [cm^3/g]	Dopant content [Me mol%]	Dopant content [Me wt.%]	Dopant loss [%]
LaOCl	17	0.060	-	-	-
Mg/LaOCl	13	0.053	4.4	0.56	38
Co/LaOCl	13	0.056	4.7	1.45	8
Ni/LaOCl	9	0.045	5.0	1.53	24
Ce/LaOCl	9	0.030	5.1	3.72	14

The morphology of the samples as prepared was inhomogeneous, with a wide distribution of particles with irregular shape and diameters between 2.5 and 20 μm. The particles were characterized by a fragmented surface and were composed of agglomerated nano-particles (see Figure 5.1a). The morphology of the impregnated samples was hardly changed and showed the same agglomerated nano-particles like the parent LaOCl, as shown in Figure 5.1b for Ce/LaOCl. The similar shape also indicates that the added salts are deposited in the pore structure as expected from incipient wetness impregnation and the modification procedure does not lead to pronounced particle agglomeration.
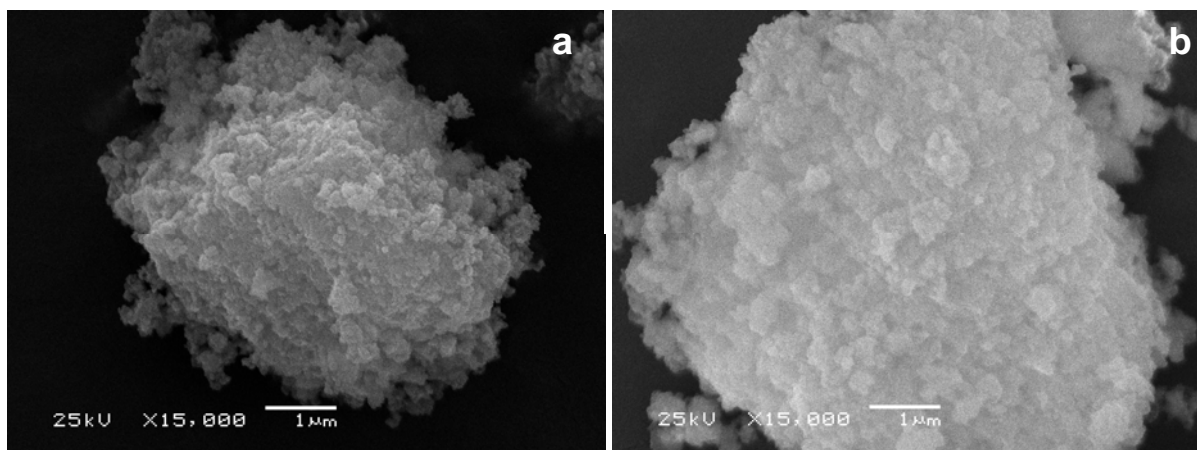
Figure 5.1 a+b: SEM photographs of a) parent LaOCl and b) Ce/LaOCl

5.3.2   Thermogravimetry

The thermal stability of the synthesized catalysts was investigated by thermogravimetry. For the parent LaOCl the main desorbing compounds were water ($m/z = 18$) and HCl ($m/z = 36$). Desorption of water was observed in the temperature range 60-425°C (see Figure 5.2). A maximum was found at 275°C and a smaller peak at 125°C. At 285°C hydrogen chloride ($m/z = 36$) began to evolve. It showed a maximum at 360°C and decayed in a long tail until the end of the measurement.
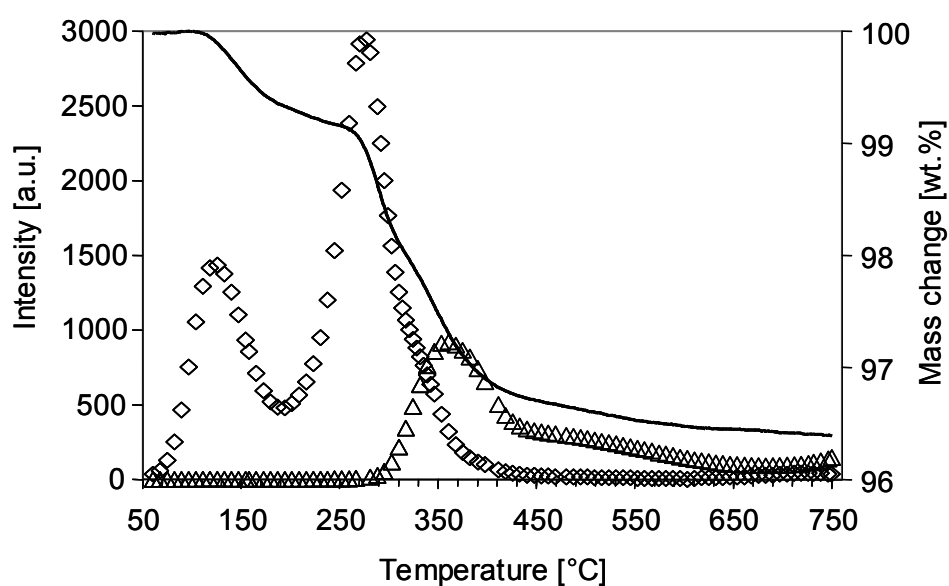

Figure 5.2: TGA profile of LaOCl in the temperature range of 50 to 750°C ($\diamond$ $H_2O = m/z$ 18, $\triangle$ HCl $= m/z$ 36)

The HCl evolution is attributed to the partial hydrolysis of LaOCl to La_2O_3. Besides HCl also Cl_2 release (m/z = 70) and CO_2 (m/z = 44) were observed. The formation of carbon dioxide indicated the decomposition of residual lanthanum carbonate on the surface. However, the weight loss due to the Cl_2 and CO_2 liberation was negligible compared to the weight loss by water and HCl evolution.The total weight loss of the parent LaOCl in the whole temperature range was 3.6 wt.%. The thermogravimetric results of all samples are summarized in Table 5.2. The release of water and hydrogen chloride of Ni/LaOCl was only slightly higher compared to the parent LaOCl. The other impregnated samples released around the double amount of water and HCl compared to the parent LaOCl. Co/LaOCl desorbed even the triple amount of water. For all catalysts, around 75% of the total HCl evolution occurred below the generally applied activation temperature of 550°C.

Table 5.2: Thermogravimetric results in the temperature range from 50°C to 750°C for activation in vacuum (10^{-7} mbar)

Sample	H$_2$O release [wt.%]	HCl release [wt.%]	Total weight loss * [wt.%]
LaOCl	1.7	1.2	3.6
Mg/LaOCl	3.5	2.3	9.8
Co/LaOCl	5.1	2.6	8.7
Ni/LaOCl	1.9	1.4	5.6
Ce/LaOCl	3.3	2.6	7.3

*Besides H$_2$O and HCl, the total weight loss also includes the release of Cl$_2$, CO$_2$ and metal compounds.

During the activation in vacuum at 10^{-7} mbar evolution of the metal salts were also observed by mass spectrometry in the temperature range 300°C to 450°C. This is attributed to the significant vapor pressures of some metal chloride salts. At 350°C magnesium chloride and nickel chloride have vapor pressures of $3.0 \cdot 10^{-5}$ mbar and $2.3 \cdot 10^{-6}$ mbar, respectively [15]. This explains also the remarkably higher total weight loss of the metal impregnated catalyst compared to the parent LaOCl. The difference between the total weight loss and the loss due to water and hydrogen chloride release showed the same trend like the dopant loss after reaction (see Table 5.1).

The ability of the catalysts to bind and activate oxygen on their surface was investigated by thermogravimetry. Depending on the type of the metal dopant, the concentration of oxygen uptake by the catalyst varied (Table 5.3). The parent LaOCl adsorbed $1.49 \cdot 10^{-3}$ mmol O_2 g_{cat}^{-1}. It is interesting to note that Co/LaOCl had a significantly higher uptake, whereas the Mg modified showed only around half of the oxygen uptake of the parent LaOCl.

Table 5.3: Oxygen uptake per catalyst

Sample	O_2 uptake [mmol g_{cat}^{-1}]	relative to LaOCl
LaOCl	$1.49 \cdot 10^{-3}$	1.00
Mg/LaOCl	$8.43 \cdot 10^{-4}$	0.57
Co/LaOCl	$2.45 \cdot 10^{-3}$	1.65
Ni/LaOCl	$1.45 \cdot 10^{-3}$	0.98
Ce/LaOCl	$1.79 \cdot 10^{-3}$	1.20

5.3.3 Catalytic conversion of methane

5.3.3.1 Activity and selectivity

After chlorination of the catalysts at 400°C, which converts LaOCl into $LaCl_3$ the more catalytically active form, the catalytic performance in oxidative chlorination of methane was tested at 475°C varying the weight hourly space velocity (WHSV). Figure 5.3 shows the linear correlation of methane conversion at 475°C with the inverse WHSV for all studied catalysts. With increasing the 1/WHSV, methane conversion of the parent LaOCl increased as expected from 3% to 12% as the inverse WHSV is directly proportional to the residence time. The effect of Co and Ce dopants on the conversion of methane was very pronounced. By adding these metals salts the methane conversion was almost tripled approaching around 30% methane conversion at an inverse WHSV of 2.06 h. In contrast, the impregnation with nickel and magnesium chloride caused a decrease of the methane conversion at the same 1/WHSV compared to the parent LaOCl.
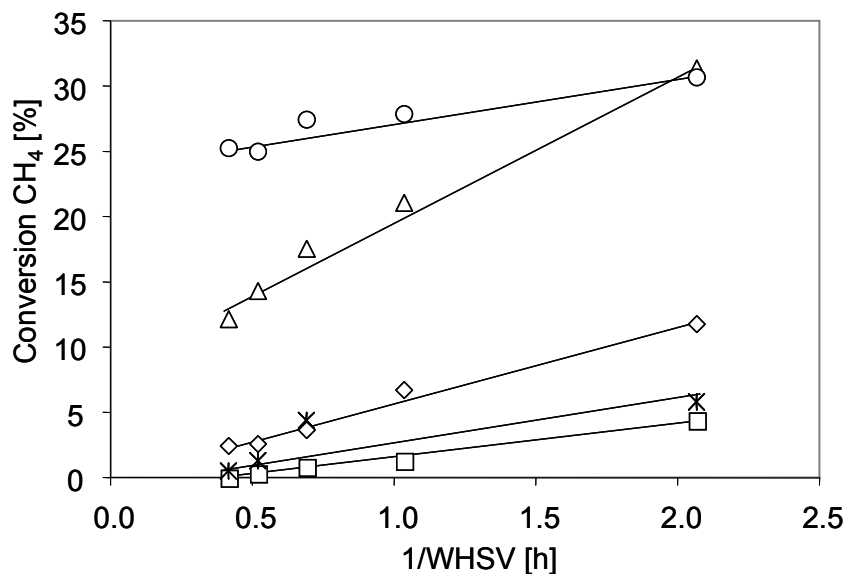
Figure 5.3: Conversion of methane as a function of inverse weight hourly space velocities (WHSV) at 475°C with stoichiometric flow $CH_4:HCl:O_2:He:N_2 = 2:2:1:4:1$ ($\diamond$ LaOCl, $*$ Mg/LaOCl, $\circ$ Co/LaOCl, $\square$ Ni/LaOCl, $\triangle$ Ce/LaOCl)

The methane conversion is neither influenced by the BET surface area of the catalyst precursor nor from the BET surface area of the chlorinated catalyst. Mg/LaOCl and Ce/LaOCl showed under the same WHSV a totally different methane conversion even though they have around the same BET surface area before and after chlorination (see Table 5.1).

The dependence of the product yields on methane conversion of the parent LaOCl is shown in Figure 5.4. Methyl chloride was always the main product and was formed with the highest selectivity and thus the highest product yield. The dotted line illustrates the yield for 100% selectivity. The initial yield of methyl chloride (dashed line) showed already at low methane conversion a deviation from the 100% selectivity line.

The main by-product formed was carbon monoxide. It is important to note that the selectivity to methyl chloride is lower and the initial oxidation of methane to CO is significantly higher than in the material reported in refs. [7, 8] We speculate at present that the materials prepared here, retain on their surface a part of the formed methyl chloride species. This leads to a catalytic pathway that favors the reaction of the (partially chlorinated) methyl species with the hydroxy groups formed during the initial steps or with oxygen present in the sample. Thus, the deviation of the initial methyl chloride yield from the 100% selectivity line is attributed to the direct oxidation of adsorbed methyl chloride to carbon monoxide. It is important to note that in addition to this pathway the readsorption of methyl chloride,

additional chlorination, and oxidation of the readsorbed species may takes place, which causes a further decrease of the methyl chloride selectivity and increase of the CO and methylene chloride selectivity at higher methane conversion, respectively.
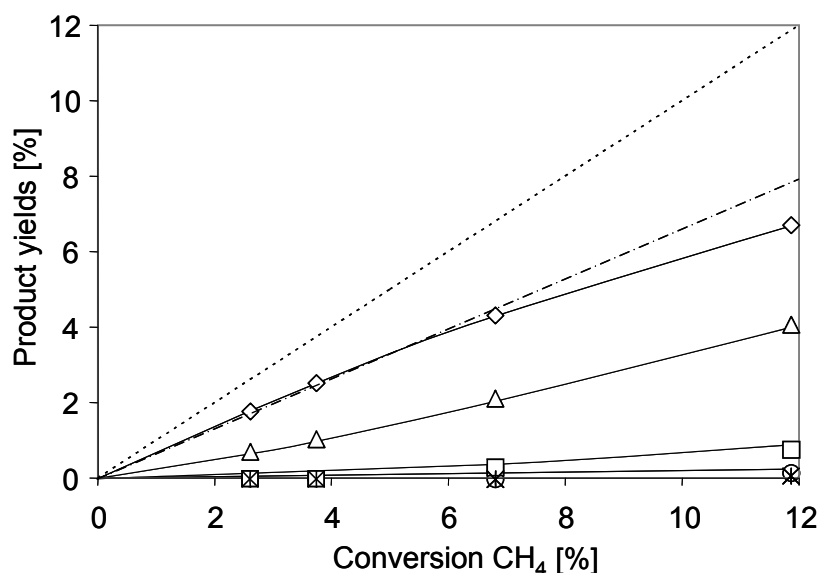

Figure 5.4: Product yields as a function of conversion over LaOCl at 475°C with stoichiometric flow $CH_4:HCl:O_2:He:N_2 = 2:2:1:4:1$ ($\diamond$ CH_3Cl, $\square$ CH_2Cl_2, $\bigcirc$ $CHCl_3$, $\triangle$ CO, $\ast CO_2$, $--\cdot$ initial CH_3Cl yield, $\cdots$ 100% selectivity line)

The deviation of the methyl chloride yield to the initial yield became stronger at higher methane conversion due to the increasing methylene chloride yield. This indicates that that the (undesired) formation of CH_2Cl_2 proceeds *via* a consecutive reaction by the further chlorination of methyl chloride. Higher chloromethanes, as $CHCl_3$ (maximum yield 0.2%) and CCl_4, were only detected in trace amounts. The deep oxidation product CO_2 was hardly detected even at higher conversions.

The most significant effect of doping was achieved with the cerium modified catalyst. The activity of this catalyst was higher than that of the other materials (Figure 5.5). However, the selectivity and thus the yield to methyl chloride over Ce/LaOCl was relatively low. In the observed conversion range (up to 31%), carbon monoxide was the main product (CO yield up to 19%) followed by methyl chloride, methylene chloride and carbon dioxide. Chloroform was formed in very low concentration with a maximum yield of 2%. However, the yield was remarkably higher compared to the parent LaOCl catalyst.
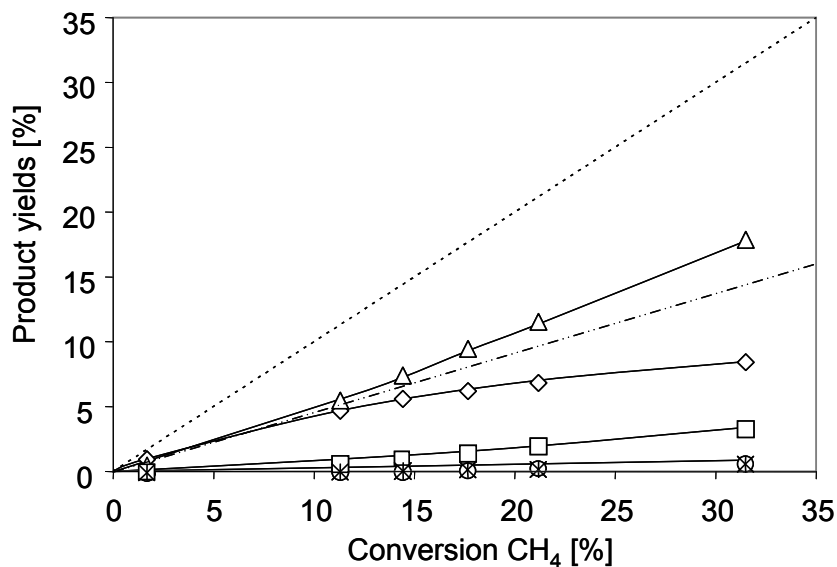
Figure 5.5: Product yields as a function of methane conversion over Ce/LaOCl at 475°C with stoichiometric flow $CH_4:HCl:O_2:He:N_2 = 2:2:1:4:1$ ($\diamond$ CH_3Cl, $\square$ CH_2Cl_2, $\bigcirc$ $CHCl_3$, $\triangle$ CO, $\ast$ CO_2, $^{---}$ initial CO yield, $^{......}$100% selectivity line)

Tetrachloromethane was formed only in negligible amounts. The formation of CO by the preferred reaction of strongly bound (partly chlorinated) surface species with hydroxy groups and oxygen is more pronounced over Ce/LaOCl compared to LaOCl. The positive deviation of the CO yield to the initial yield is attributed to the formation of higher chlorinated methane which is more reactive towards further oxidation to carbon monoxide and HCl.

Co/LaOCl exhibited also a high methane conversion ranging up to 31% with even higher yield up to 24% towards CO (results not shown). Over this catalyst the methyl chloride yield reached a maximum of 4.3% at 27.5% methane conversion. The Co/LaOCl catalysts showed the highest yield towards $CHCl_3$ and CCl_4 of all catalysts with a maximum of 3% for chloroform and 0.4% for tetrachloromethane.

Ni/LaOCl and Mg/LaOCl were less reactive than the parent LaOCl. These catalysts reached a maximum methane conversion of around 5% under the present reaction conditions. Over Ni/LaOCl methyl chloride was the main product and was very selectively formed and approached a methyl chloride yield of 4% (Figure 5.6). The yield towards methylene chloride was relatively low, while the CO yield reached 0.6%. Carbon dioxide, chloroform and tetrachloromethane were never observed. In contrast to the other studied catalysts, the initial methyl chloride selectivity is close to the 100% selectivity line. Mg/LaOCl showed a higher

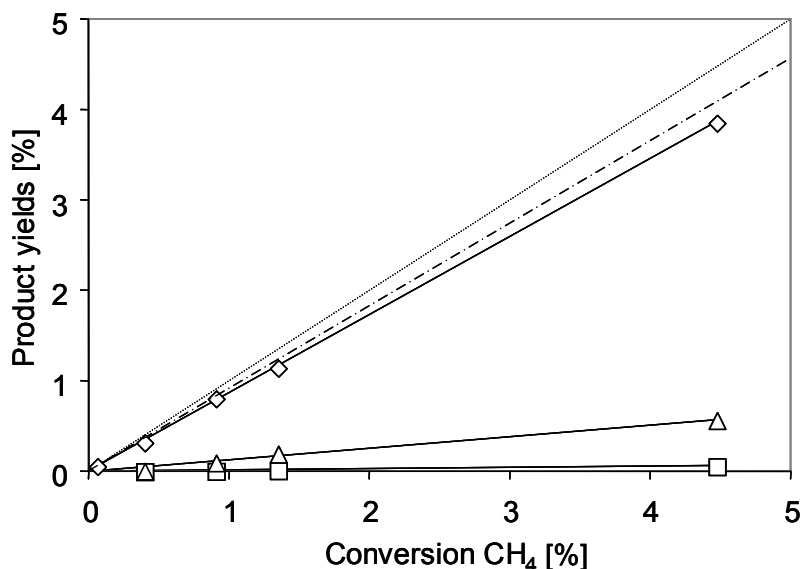selectivity towards carbon monoxide compared to Ni/LaOCl. Chloroform and tetrachloromethane were not formed.

Figure 5.6: Product yield as a function of methane conversion over Ni/LaOCl at 475°C with stoichiometric flow CH_4:HCl:O_2:He:N_2 = 2:2:1:4:1 ($\diamond$ CH_3Cl, $\square$ CH_2Cl_2, $\bigcirc$ $CHCl_3$, $\triangle$ CO, ✳CO_2, $-\cdot-$ initial CH_3Cl yield ⋯⋯ 100% selectivity line)

The correlation of methane conversion and CH_3Cl selectivity at 475°C for all catalysts is depicted in Figure 5.7. The comparison of the methyl chloride selectivity at around 5% methane conversion showed that Ni/LaOCl was the most selective catalyst. The Ni/LaOCl catalyst reached 86% selectivity towards methyl chloride whereas Mg/LaOCl and the parent LaOCl reached only 65% and 70% methyl chloride selectivity, respectively. In contrast, Ce/LaOCl and Co/LaOCl exhibited at 5% methane conversion only a methyl chloride selectivity of 53% and 43%, respectively.

In order to increase the reactivity of Ni/LaOCl the reaction temperature was increased to 580°C and runs were conducted at WHSV ranging from 0.48 to 2.91 h^{-1} (filled squares in Figure 5.7). In fact, at this temperature methane conversions between 6.6% and 23.6% were obtained which are close to the conversions obtained with Ce/LaOCl. In contrast to Ce/LaOCl methyl chloride was the main product for Ni/LaOCl at these conversions. The selectivity towards methyl chloride was in the range between 79% and 62%. Carbon monoxide was

formed but with low selectivity not surpassing 20%. Chloroform and carbon dioxide were formed in negligible amounts.
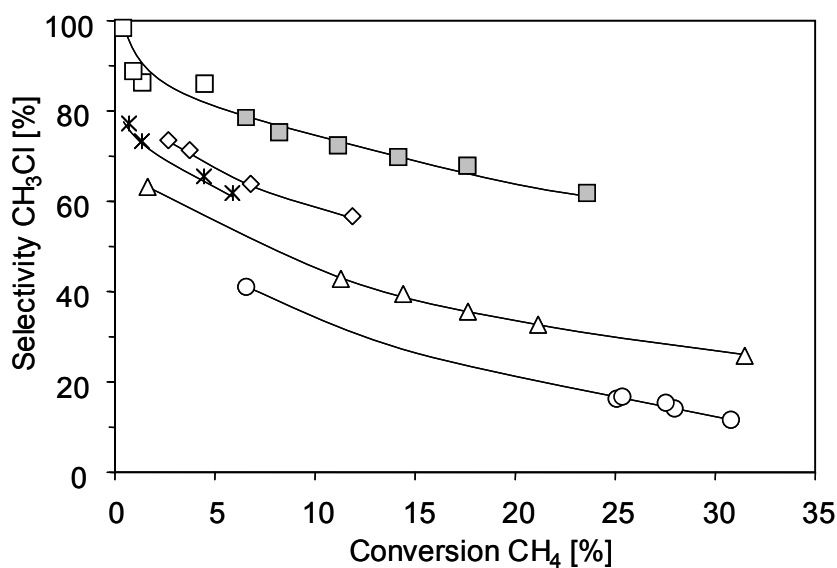

Figure 5.7: CH_3Cl selectivity vs. CH_4 conversion at 475°C with stoichiometric flow CH_4:HCl:O_2:He:N_2 = 2:2:1:4:1 ($\diamond$ LaOCl, ✶ Mg/LaOCl, ○ Co/LaOCl, △ Ce/LaOCl, □ Ni/LaOCl; ▣ Ni/LaOCl at 580°C)

5.3.3.2 Determination of the apparent activation energy

The apparent activation energy for conversion of methane, in the temperature range between 400°C and 550°C, was determined at 122 kJ mol^{-1} for the parent LaOCl. The apparent activation energies of all catalysts are listed in Table 5.4.

Table 5.4: Apparent activation energies of the studied catalysts

Sample	E_a [kJ mol^{-1}]
LaOCl	122±7
Mg/LaOCl	130±8
Co/LaOCl	91±5
Ni/LaOCl	162±32
Ce/LaOCl	99±11

Co/LaOCl and Ce/LaOCl have a significantly lower apparent activation energy compared to the parent LaOCl, while the apparent activation energy of Mg/LaOCl was slightly increased. Ni/LaOCl showed a high apparent activation energy of 162 kJ mol^{-1}.

5.3.3.3 Temperature programmed reaction (TPR)

In order to explore the reactivity of the catalysts as a function of temperature, a temperature programmed reaction (TPR) was performed with the chlorinated catalysts. While such an experiment cannot account for deactivation or transient modifications of the catalyst, it probes the general reaction sequence and thus is therefore useful to explore the trends in reactivity including the thermal onset of the reaction and the thermal stability with respect to the dechlorination of the catalyst. The temperature dependence of the reactant conversions and the product yields over the parent LaOCl are provided in Figure 5.8a and b, respectively.

The temperature dependence of the reactant conversion and product yields can be classified into three areas. At low temperatures (370°C to 425°C) the methane conversion was low and methyl chloride was formed as a primary product with high selectivity. With the increase of methane conversion, also the oxygen conversion started to increase. However, the hydrogen chloride conversion was still zero and started to increase at higher temperatures. At higher methane conversion (425°C to 550°C) the hydrogen chloride conversion was almost equal to the methane conversion implying that the catalyst surface was regenerated with hydrogen chloride. At temperatures between 425°C and 550°C carbon monoxide is formed and increased with the same trend like methyl chloride. This indicates that methyl chloride did not totally desorb from the surface but was directly further oxidized to carbon monoxide. Also methylene chloride was formed and the increase of the methyl chloride yield with temperature was reduced as a result thereof. The oxygen conversion was in this temperature range much higher than the methane conversion due to the oxygen consumption for oxidation of the chlorinated products to carbon monoxide. From 525°C on, the surface started to dechlorinate to LaOCl according to the equilibrium between LaCl$_3$ and LaOCl (equ. 5.2). The restructuring of the catalyst surface was accompanied with the abrupt increase in carbon monoxide yield and also a slight increase of the yield of higher chlorinated products. At temperatures above 545°C, also the bulk of the catalyst started to dechlorinate to LaOCl which was characterized first by the decrease of the HCl consumption during the temperature programmed reaction, which eventually turns into an HCl outlet concentration that is higher

than the inlet concentration. Using the chlorine mass balance, we exclude that this HCl evolution was the result of HCl excess initially adsorbed on the sample.
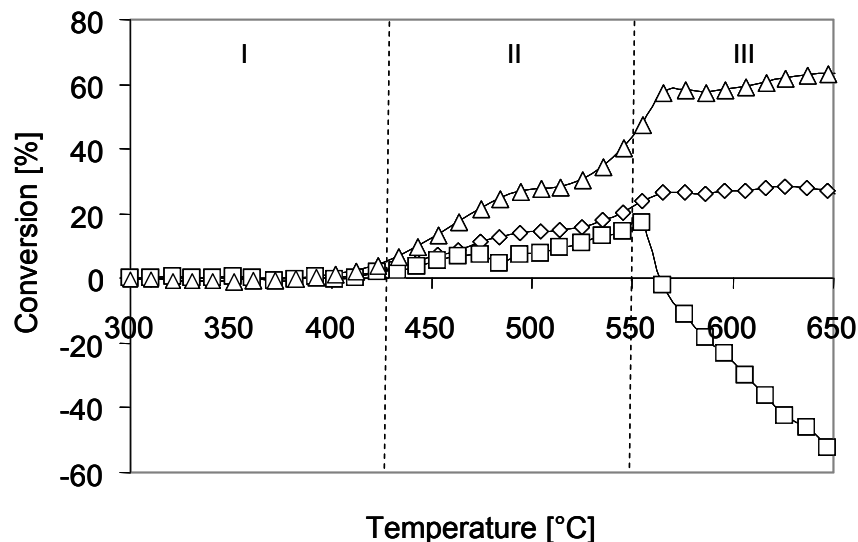

Figure 5.8a: Profile of the reactant conversion during temperature programmed reaction (1°C min^{-1}) over the parent LaOCl with stoichiometric flow $CH_4:HCl:O_2:He:N_2$ = 2:2:1:4:1 ($\diamond$ CH_4, $\square$ HCl, $\triangle$ O_2)

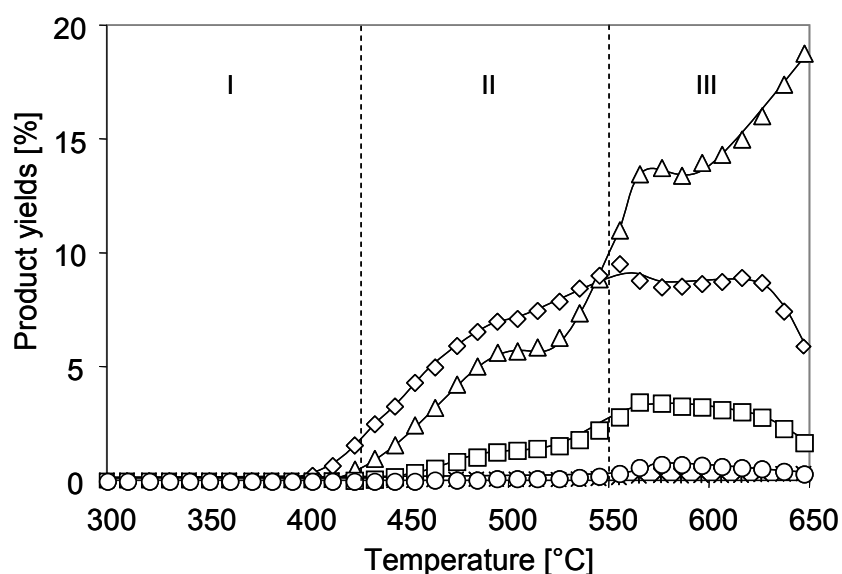**Figure 5.7b:** Profile of the product yields during temperature programmed reaction (1°C min^{-1}) over the parent LaOCl with stoichiometric flow $CH_4:HCl:O_2:He:N_2$ = 2:2:1:4:1 ($\diamond$ CH_3Cl, $\square$ CH_2Cl_2, $\circ$ $CHCl_3$, $\triangle$ CO, $\ast$ CO_2)

The methane conversion remained from the start of dechlorination on constant, whereas the oxygen conversion slightly increased. When chlorine has been almost depleted from the surface (T > 615°C), the CO yield increased further due to further oxidation of chlorinated products on a chlorine leaner surface. As a result thereof, the rate of formation of chloride and methylene chloride decreased. The TPR profiles of Ce/LaOCl are shown in Figure 5.9a and Figure 5.9b, respectively. Methyl chloride was detected from 366°C on and thus also the methane and oxygen conversion started to increase. With a short delay also the HCl conversion started to increase. Methyl chloride was the only product formed till 390°C. At this temperature carbon monoxide also appeared. Higher chlorinated products such as methylene chloride and chloroform were formed from 450°C on. Above 450°C, the readsorption of methyl chloride became favored which resulted in a constant formation of methyl chloride but an increase of the formation rate of methylene chloride and carbon monoxide. The oxygen conversion increased in a more pronounced way than methane conversion which is due to the high formation of carbon monoxide. The dechlorination of the catalyst started at 540°C. From this temperature on, the methane and oxygen consumption remains almost constant like for the parent LaOCl catalysts, indicating that the temperature effect on the reaction rate must be compensated by an increasingly lower concentration of active sites. At 620°C the HCl release stopped and the HCl conversion showed a reversion to positive values. The yield of carbon monoxide showed a steep increase until 650°C at the expense of the chlorinated products especially of CH_2Cl_2 and $CHCl_3$
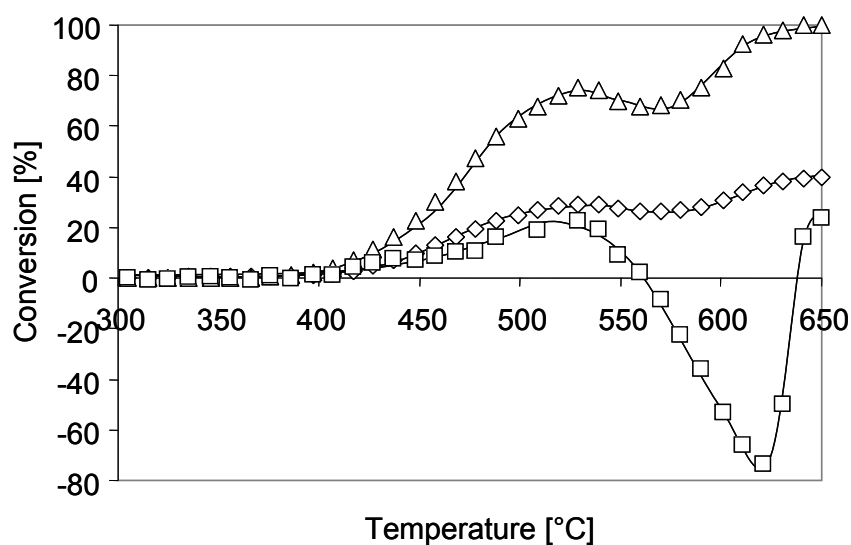

Figure 5.9a: Profile of the reactant conversion during temperature programmed reaction (1°C min^{-1}) over Ce/LaOCl with stoichiometric flow $CH_4:HCl:O_2:He:N_2 = 2:2:1:4:1$ ($\diamond$ CH_4, $\square$ HCl, $\triangle$ O_2)
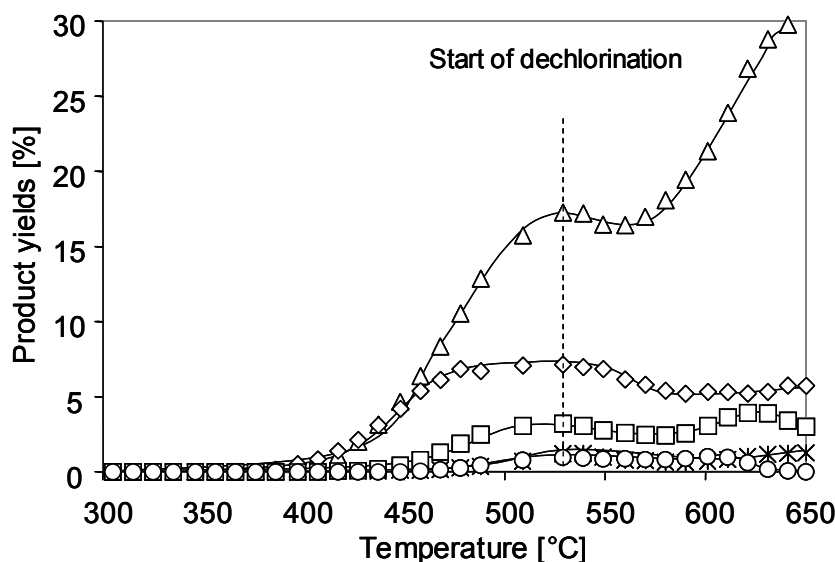
Figure 5.8b: Profile of the product yields during temperature programmed reaction (1°C min$^-$^{1}) over Ce/LaOCl with stoichiometric flow CH_4:HCl:O_2:He:N_2 = 2:2:1:4:1 ($\diamond$ CH_3Cl, $\square$ CH_2Cl_2, O $CHCl_3$, $\triangle$ CO, $\ast$ CO_2)

       The TPR profiles of Co/LaOCl (not shown here) showed the same trends as Ce/LaOCl. However, over Co/LaOCl a higher yield of carbon monoxide was observed, which showed a very steep increase with temperature. The methyl chloride yield is lower compared to Ce/LaOCl. The start of dechlorination of Co/LaOCl was observed at 530°C.

       The TPR profile of Ni/LaOCl are shown in Figure 5.10a and Figure 5.10b. The start of methane and oxygen conversion over Ni/LaOCl was shifted to higher temperatures compared to the parent LaOCl by 25°C. However, methyl chloride is the only formed product until 500°C and the CH_3Cl yield was steadily increasing till 650°C (Figure 5.10b). Above 500°C methylene chloride and carbon monoxide were formed. Also chloroform formation was observed. In contrast to the other modified catalysts, methyl chloride was always the main product and the carbon monoxide yield was even at higher temperatures much lower than the methylene chloride yield. The dechlorination of Ni/LaOCl started at 585°C. In contrast to the parent LaOCl and Ce/LaOCl, the methane conversion continued to increase further even after the start of dechlorination until 640°C. Also the product yields seemed unaffected from the dechlorination.
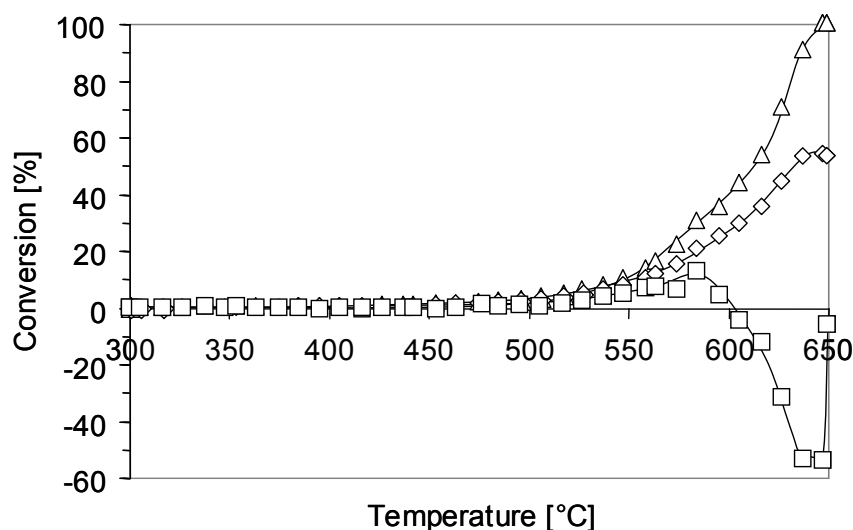
Figure 5.10a: Profile of the reactant conversion during temperature programmed reaction (1°C min^{-1}) over Ni/LaOCl with stoichiometric flow $CH_4:HCl:O_2:He:N_2$ = 2:2:1:4:1 ($\diamond$ CH_4, $\square$ HCl, $\triangle$ O_2)
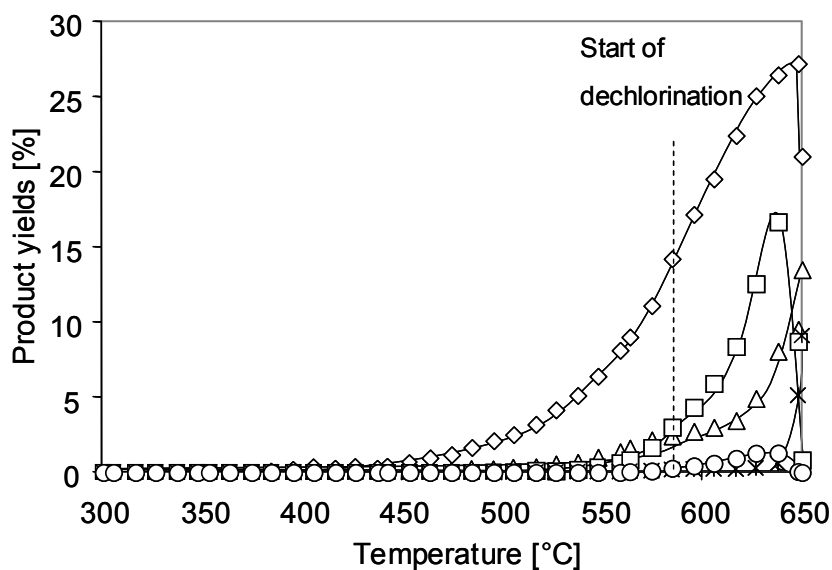
Figure 5.10b: Profile of the product yields during temperature programmed reaction (1°C min^{-1}) over Ni/LaOCl with stoichiometric flow $CH_4:HCl:O_2:He:N_2$ = 2:2:1:4:1 ($\diamond$ CH_3Cl, $\square$ CH_2Cl_2, $\circ$ $CHCl_3$, $\triangle$ CO, $\ast$ CO_2)

Mg/LaOCl is the least active catalyst. The methane and oxygen conversion never exceeded 10% in the whole temperature range. The methyl chloride yield did not exceed 2%. Furthermore the catalyst showed no dechlorination of the surface (results not shown).

The consumption and evolution of HCl during the temperature programmed reaction for the parent LaOCl and the doped catalysts is shown in Figure 5.11.

Figure 5.11: Profile of HCl consumption / evolution during temperature programmed reaction (1°C min^{-1}) with 20 vol. % HCl in the feed. ($\diamond$ LaOCl, ✳ Mg/LaOCl, ○ Co/LaOCl, □ Ni/LaOCl, △ Ce/LaOCl)
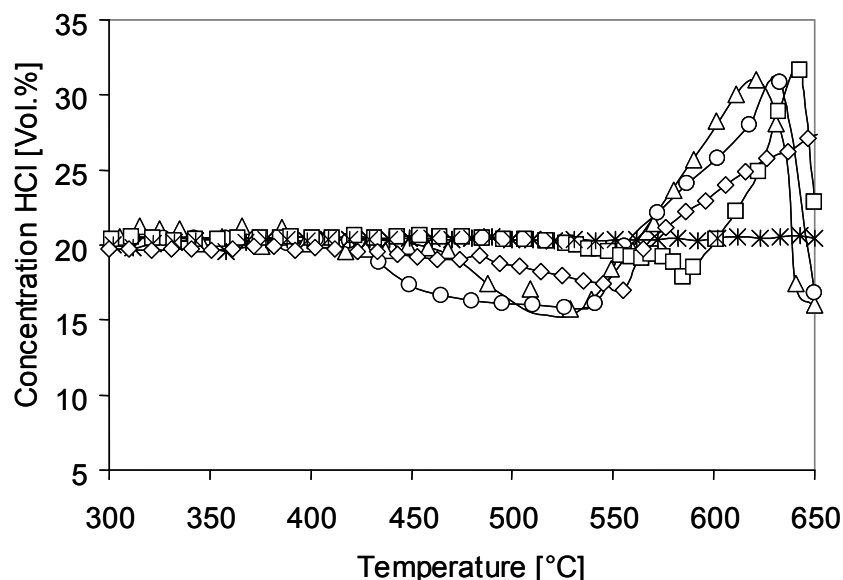
LaCl$_3$ is in equilibrium with LaOCl. The equilibrium is shifted towards LaOCl in the presence of water and at high temperatures, while HCl is released (equ. 5.2). Fully chlorinated LaCl$_3$ which was heated in a helium flow to 650°C (rate 3°C min^{-1}) did not show a release of HCl and thus no dechlorination due to the absence of water. The parent LaOCl catalyst started to dechlorinate at 545°C, Co/LaOCl and Ce/LaOCl already at 530°C and 540°C, respectively. In contrast, Ni/LaOCl started to dechlorinate at 585°C, while Mg/LaOCl did not show a consumption or release of HCl. Even at high temperatures, the HCl concentration in the effluent stream did not increase. Mg/LaOCl showed during the temperature programmed reaction a very low methane conversion and thus the amount of water was not sufficient to shift the equilibrium towards LaOCl.

The total amount of HCl release was calculated by integrating the area of the HCl profile that lies above the inlet concentration baseline of HCl. The parent LaOCl showed an HCl release of 7.6·10^{-5} mol. This did not correspond to a fully transformation of lanthanum chloride to lanthanum oxychloride. The bulk of the catalyst seems to remain unchanged. The highest HCl

release was detected for Co/LaOCl, followed by Ce/LaOCl, whereas Ni/LaOCl showed a less release of HCl. It should be noted, that the HCl release of the metal chloride doped samples cannot only originate from the metal chloride used for impregnation, as the detected amount was much higher. The start of dechlorination and the total amount of released HCl is summarized in Table 5.5. The observed trend in the HCl release corresponds to the trend in the activity for oxidative chlorination.

Table 5.5: Start of dechlorination and HCl release during temperature programmed reaction (1°C min^{-1})

Sample	Start of dechlorination [°C]	HCl release [mmol g^{-1}]	relative to LaOCl
LaOCl	545	0.15	1.0
Mg/LaOCl	-	-	-
Co/LaOCl	530	0.25	1.6
Ni/LaOCl	585	0.13	0.9
Ce/LaOCl	540	0.24	1.6

The yield of the desired product methyl chloride reached over all catalysts a certain level and was then almost constant over the whole temperature range (Figure 5.12).
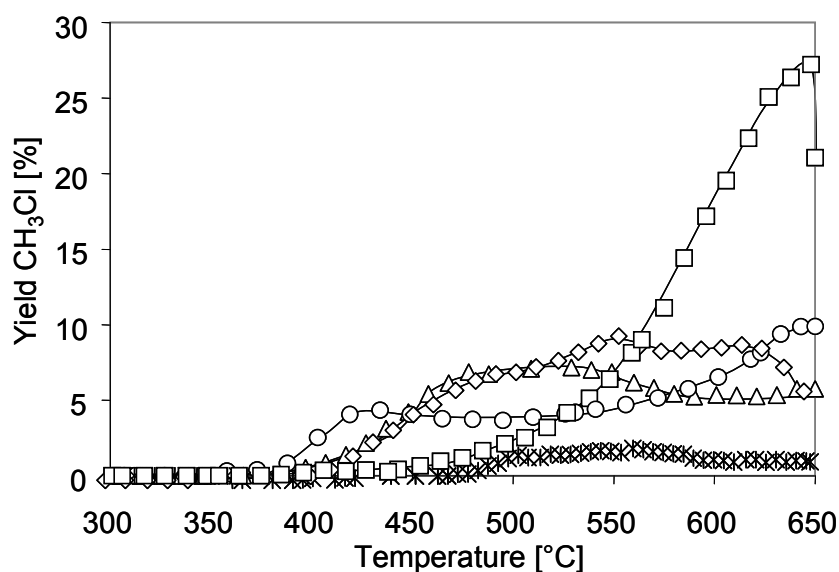

Figure 5.12: Methyl chloride yield during temperature programmed reaction (1°C min^{-1}) with stoichiometric flow CH$_4$:HCl:O$_2$:He:N$_2$ = 2:2:1:4:1; ($\diamond$ LaOCl, ✸ Mg/LaOCl, ○ Co/LaOCl, □ Ni/LaOCl, △ Ce/LaOCl)

Whereas the Ni/LaOCl showed a lower yield of methyl chloride up to 500°C, beyond this temperature a dramatic increase of the methyl chloride yield with a maximum at 650°C was observed, even though the catalyst has already started to dechlorinate.

5.3.4   XRD- Analysis

The crystal structures of the samples were investigated by X-ray diffraction. The X-ray diffractograms showed that the impregnation method did not influence the LaOCl crystal structure (Figure 5.13). The diffraction pattern for tetragonal LaOCl was present in all samples with same intensity ratios and width compared to the parent LaOCl catalyst (JCPDS file 88-0064) [16].
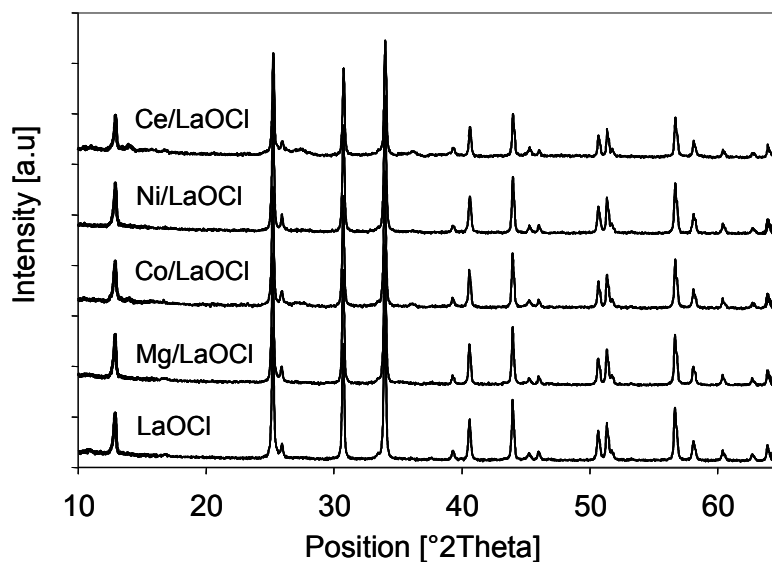
Figure 5.13: XRD diffractograms of the parent LaOCl precursor and the metal modified
catalysts

After chlorination at 400°C for 14h, the chlorinated particles were grinded and XRD measurements were performed. The parent LaOCl sample was fully transformed into $LaCl_3$. However, e.g. for Ni/LaOCl the transformation was not completed as shown in Figure 5.14. The pattern after chlorination (Figure 5.14b) showed both $LaCl_3$ and LaOCl phase. The semi-quantitative analysis of the XRD pattern after chlorination gave a $LaCl_3$:LaOCl ratio of 3:1. Thus, the bulk of the particles were not fully chlorinated. This was in line with the results of

the temperature programmed chlorination, where Ni/LaOCl showed the lowest HCl uptake of all studied catalysts (results not shown).
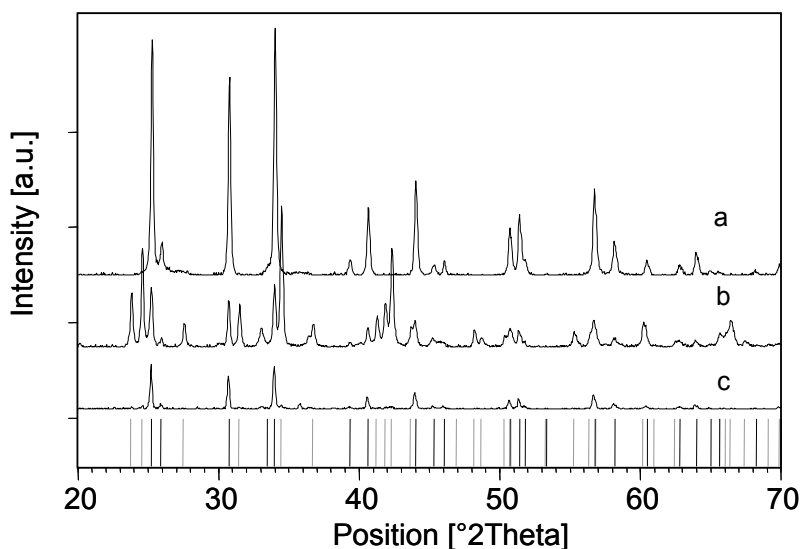
Figure 5.14: XRD analysis of Ni/LaOCl a) after calcination, b) after chlorination for 14h at 400°C, c) after temperature programmed reaction (⎯ calculated pattern for LaOCl JCPDS-file 73-2063, ⎯ calculated pattern for LaCl₃ JCPDS-file 73-0479)

The position of the calculated diffraction lines for LaOCl and LaCl$_3$ are shown in Figure 5.14 as lines of arbitrary heights. As expected during the temperature programmed reaction the equilibrium shifted under reaction conditions towards LaOCl and thus only the LaOCl phase was observed by XRD with the used catalyst (Figure 5.14c).

5.3.5   In situ Raman measurements

The transformation of LaCl$_3$ to LaOCl on the surface under reaction conditions using stoichiometric flow of CH$_4$:HCl:O$_2$ = 2:2:1 at different temperatures were also investigated by *in situ* Raman spectroscopy (Figure 5.15). At the start of the measurements, bands of LaOCl were present. Due to the cut off of the notch Raman filter, only the bands at 330 and 430 cm^{-1} are visible which are associated with the motion of the oxygen atoms [8]. After chlorination at

400°C, the LaOCl bands disappeared, indicating the chlorination of the catalyst to LaCl₃. The Raman bands of LaCl₃ are all below 219 cm^{-1} and were thus not visible [17].
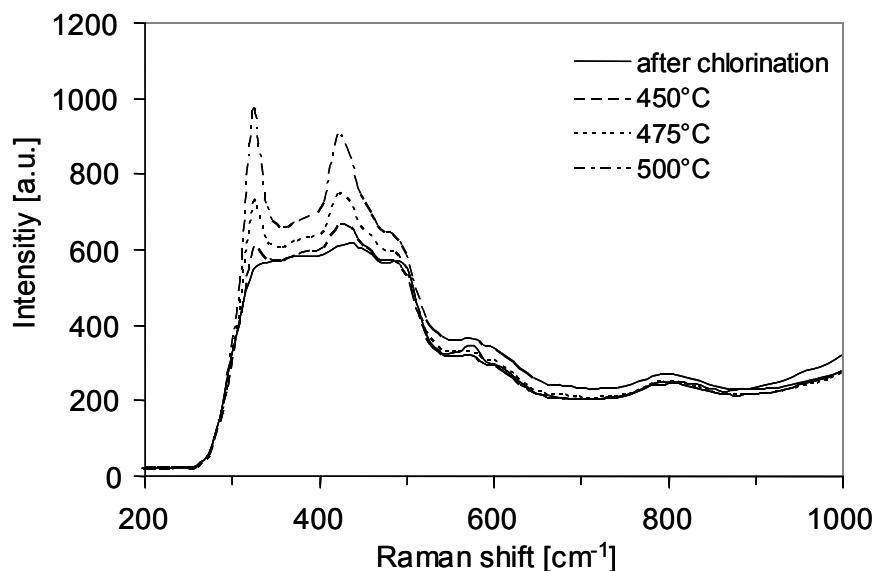
Figure 5.15: In situ Raman spectra of pure LaOCl (industrial sample) after chlorination and during reaction and at different temperatures with stoichiometric flow $CH_4:HCl:O_2:He = 2:2:1:5$ (532nm laser)

Under oxidative chlorination conditions at 450°C weak bands of LaOCl were observed indicating that partial dechlorination of the surface under reaction conditions. The LaOCl bands gained in intensity with increasing the reaction temperature to 500°C suggesting a shift of the equilibrium from LaCl₃ towards LaOCl.

5.4 Discussion

The impregnation of LaOCl with metal chloride salts influences the physicochemical properties and the catalytic performance for oxidative chlorination of methane. The thermostability of the chloride is reduced by impregnation, as indicated by the more pronounced HCl release of Mg/LaOCl, Co/LaOCl and Ce/LaOCl during activation in vacuum. The pronounced release of HCl from these samples parallels with their higher water content compared to the parent LaOCl. Around 75% of HCl liberation is below the applied activation temperature of 550°C. Thus, during thermal activation, part of LaOCl is hydrolyzed

and chlorine defect sites or even minor amounts of La_2O_3 are likely generated. It is speculated that these defects are the initial sites of chlorine uptake during chlorination of the thermally activated LaOCl.

The modification of LaOCl with cobalt and cerium has a high influence on the activity in oxidative chlorination of methane. The methane conversion is at the same reaction conditions for Co/LaOCl and Ce/LaOCl three times higher compared to the parent LaOCl sample, whereas the methane conversion of Mg/LaOCl and Ni/LaOCl is lowered (Figure 5.3). In a preceding study, the influence of the specific surface area of the chlorinated catalysts was studied. It has been shown that the rate of methane conversion linearly correlates with the specific surface area of $LaCl_3$ [13]. However, in the case of the modified catalysts this effect offers no explanation for the different activity of Ce/LaOCl and Mg/LaOCl. The methane conversion of Ce/LaOCl is much higher than the conversion of Mg/LaOCl, even though these samples have almost the same specific surface area of 8 and 7 m^2/g. Thus, it seems that the chemical effect of the modification with different dopants is the predominant.

Chemisorption of molecular oxygen on the activated and chlorinated materials is critical for the formation of the transient active species on LaOCl or $LaCl_3$, i.e., $Cl^{\delta+}$ in an OCl^- anion as shown conclusively by DFT calculations [7]. Under steady state conditions, the adsorption of oxygen can, therefore, not cause the formation of stable OCl^-, but transient species could cause a synproportionation of Cl^- and Cl^+ to Cl_2. This could desorb or remain at the catalyst surface. Thus, oxygen adsorption capacity conceptually is a descriptor of one aspect of catalytic activity. As one notes, the ability to adsorb oxygen decreases in the sequence Co/LaOCl > Ce/LaOCl > LaOCl ~ Ni/LaOCl > Mg/LaOCl. The sequence is identical with the ranking of activities of the materials. The increased oxygen uptake of Ce/LaOCl and Co/LaOCl points to the enhanced formation of hypochlorite as the active site and thus to a higher rate of methane conversion. Furthermore, with a higher concentration of the hypochlorite species on the surface, also a higher chlorination is possible. Over Ce/LaOCl and Co/LaOCl the yield of chloroform is indeed higher than over the parent LaOCl catalyst. However, it is still negligible.

Methyl chloride is formed as the primary product over all catalyst, followed by carbon monoxide. The activity measurements show that the CH_3Cl yield and CO yield strongly differs for the different catalysts. Especially the Ni containing sample showed a decreased activity in activation of methane but demonstrates a superior selectivity to the desired product methyl chloride compared to the other catalysts. However, the apparent activation energy for methane activation is increased by the nickel impregnation and thus higher reaction

temperatures are necessary to obtain methane conversions at comparable levels. Even at this temperature the selectivity towards methyl chloride retained at quite high levels. In contrast, over Co/LaOCl and Ce/LaOCl carbon monoxide is the main product. We speculate that over these catalysts the formed (partially chlorinated) methyl species are more strongly bound to the surface than e.g. over Ni/LaOCl. Thus this strongly bound surface species undergoes without desorbing a direct reaction with either hydroxyl groups or oxygen atoms present on the surface, leading to the formation of CO and HCl. By the modification with magnesium or nickel salts the ability to retain the chlorinated fragments is either hindered or these unselective sites are blocked by the metal dopant.

For the desorbed methyl chloride also the possibility of re-adsorption exists and thus either a further chlorination or the oxidation of the reabsorbed species takes place. This is indicated by the simultaneous decrease of the methyl chloride selectivity and the increase of CO and methylene chloride selectivity with increasing methane conversion. The tendency for oxidation increases with the chlorine content of the adsorbed species [18]. Thus the high CO selectivity of Co/LaOCl and Ce/LaOCl is attributed on the one hand to the strong adsorption of the (partially chlorinated) methyl species over these catalysts and the further oxidation to CO. Furthermore, Co/LaOCl and Ce/LaOCl show an enhanced adsorption of oxygen und it is therefore speculated that these catalysts have a higher concentration of OCl$^-$ species on the surface and thus provide an enhanced chlorination ability. As a result also the formation of higher chlorinated products is feasible which are more easily oxidized to CO.

The temperature programmed reaction gives an insight to the reaction mechanism and an explanation for the catalytic performance. The evolution of HCl conversion shows an interesting characteristic. While methane and oxygen conversion start with the methyl chloride formation, the HCl conversion is still zero, indicating that the surface chlorine atoms are used as a chlorine source. These results confirm that the role of HCl in the gas phase is limited to regenerate the surface via addition of Cl$^-$ and the formation of water [8]. However, as shown with *in situ* Raman measurements, the catalyst surface is not fully regenerated and LaOCl bands with small intensity are already visible at 450°C. Thus a partial dechlorinated surface is assumed to be the state of the catalyst under reaction conditions. At a certain temperature, the HCl profile shows a reverse to negative HCl conversions. At this point, the rate for methane chlorination (equ. 5.1) is equal to the rate of dechlorination of the catalyst surface (equ. 5.2). At higher temperatures the rate of dechlorination is then higher than the rate for chlorination of the catalyst and the catalyst surface fully dechlorinates to LaOCl. In consequence, the methane conversion remains constant even though the temperature is

steadily increasing. The temperature effect on the reaction rate is thus compensated by the lower concentration of active sites due to dechlorination of the surface. The HCl conversion shows again a reversal back to positive HCl conversion, when the dechlorination is completed.

The start temperature of dechlorination is affected by the impregnation with different metal salts and directly correlates with the activity at 475°C. The most active catalysts, Co/LaOCl and Ce/LaOCl, start to dechlorinate at much lower temperatures than the parent LaOCl. This effect can be explained due to the amount of water which is necessary to shift the equilibrium towards LaOCl. The more active catalysts Co/LaOCl and Ce/LaOCl are able to supply the required amount of water in order to shift the equilibrium towards LaOCl at a lower reaction temperature than Ni/LaOCl, which results in a lower start temperature for dechlorination. When the transformation of LaCl$_3$ to LaOCl is completed, the selectivity towards CO increases, whereas the selectivity towards chlorinated products decreases. This is attributed to the increased activity of LaOCl in catalytic destruction of chlorinated products as shown by the studies of Weckhuysen and coworkers [18-21]. Therefore the selectivity of methylene chloride decreases more drastically than the selectivity of methyl chloride. Ni/LaOCl showed a totally different HCl-TPR profile. The maximum HCl conversion reached only 12% and the start of dechlorination is shifted to higher temperatures due to the low activity. Even though the start temperature is higher compared to the parent LaOCl and the release of HCl is lower compared to the parent LaOCl, the dechlorination seems to be completed at 640°C. Thus it is conclude that Ni/LaOCl is in a less chlorinated state, which results in a lower concentration of active sites and thus a decreased activity. The low chlorination degree of Ni/LaOCl is confirmed by the XRD analysis after chlorination (see Figure 5.14) and also by the low HCl uptake during temperature programmed chlorination.

In contrast to the other studied catalysts, the methane conversion and also the rate of methyl chloride formation increase further, even after the dechlorination start. Moreover, the Ni/LaOCl is the most selective catalyst regarding the methyl chloride formation. In order to reach a sufficient high methane conversion, high reaction temperatures are necessary. However, even at increased reaction temperatures (higher conversions) the methyl chloride selectivity is still high. It is thus concluded, that the low activity but high selectivity towards methyl chloride is caused by the low concentration of active sites and thus an isolation of the active sites. Therefore, Ni/LaOCl favors only the first step of chlorination of methane to methyl chloride. Furthermore, the formed methyl species is weakly bound on the surface and the desorption of methyl chloride is more favored than the direct oxidation to carbon

monoxide like for Co/LaOCl. The further increase of methane conversion after the start of dechlorination is attributed to the increased activation energy of Ni/LaOCl. Thus, the temperature effect on the reaction rate is more pronounced for Ni/LaOCl than for the other catalysts. The rate for dechlorination of the catalyst is considered to be similar for all catalysts because for the same parent LaOCl material was used for all catalysts. Thus, over Ni/LaOCl the methane conversion is still increasing even though the dechlorination of the catalyst surface has already started.

5.5   Conclusion

LaCl$_3$ is a unique catalyst for functionalization of methane as methyl chloride in an oxychlorination reaction. The addition of various metal dopants to LaCl$_3$ has different effects on the activity in oxidative chlorination. The modification with cobalt and cerium chloride causes a remarkable increase of methane conversion due to the enhanced oxygen adsorption capacity and thus a higher concentration of the active site OCl$^-$. However, the formed (partially chlorinated) methyl species is strongly adsorbed on the surface and further oxidized to CO, which results in a low selectivity to methyl chloride. On the other hand, the impregnation with nickel and magnesium chloride salt yield to a reduced activity of LaOCl for methane activation. Especially, Ni/LaOCl demonstrates superior methyl chloride selectivity. However, the apparent activation energy is high leading to low catalyst activity. The high methyl chloride selectivity is affiliated with low chlorination degree of the surface and thus due to the low concentration of active sites which are highly isolated. By modification with Ni the ability to retain the chlorinated fragments is reduced and/or the unselective sites are blocked by the metal dopant. Modification with the redox inactive magnesium in contrast leads to a strong decrease in activity, while retaining the typical selectivities of the parent LaOCl.

5.6   Acknowledgment

5.7   References

1.   Golden, D.M. and Benson, S.W., Chem. Rev., **1969,** 69(1), 125-134.

2.   Crabtree, R.H., Chem. Rev., **1995,** 95(7), 2599-2599.

3.   Bablin, J.M., Lewis, L.N., Bui, P., and Gardner, M., Ind. Eng. Chem. Res., **2003,** 42(15), 3532-3543.

4.   Periana, R.A., Mironov, O., Taube, D., Bhalla, G., and Jones, C.J., Science, **2003,** 301(5634), 814-818.

5.   Noronha, L.A., Souza-Aguiar, E.F., and Mota, C.J.A., Catal. Today, **2005,** 101(1), 9-13.

6.   Sun, Y., Campbell, S.M., Lunsford, J.H., Lewis, G.E., Palke, D., and Tau, L.M., J. Catal., **1993,** 143(1), 32-44.

7.   Peringer, E., Podkolzin, S.G., Jones, M.E., Olindo, R., and Lercher, J.A., Top. Catal., **2006,** 38(1-3), 211-220.

8.   Podkolzin, S.G., Stangland, E.E., Jones, M.E., Peringer, E., and Lercher, J.A., J. Am. Chem. Soc., **2007,** 129, 2569-2576.

9.   Garcia, C.L. and Resasco, D.E., Appl. Catal., **1989,** 46(2), 251-267.

10.   Kenney, C.N., Cat. Rev. - Sci. Eng., **1975,** 11(2), 197-224.

11.   Rouco, A.J., J. Catal., **1995,** 157(2), 380-387.

12.   Wattimena, F. and Sachtler, W.M.H., Stud. Surf. Sci. Catal., **1982,** 7, 816-827.

13.   Peringer, E., Tejuja, C., Salzinger, M., A.A. Lemonidou and Lercher, J.A., ready for submission to Appl. Catal., **2008**.

14.   Horvath, G. and Kawazoe, K., J. Chem. Eng. Jpn., **1983,** 16(6), 470-475.

15.   Weast, R.C., *Handbook of Chemistry and Physics*. 56 ed. 1975-1976, Cleveland: CRC Press Inc.

16.   Hölsä, J., Lastusaari, M., and Valkonen, J., J. Alloys Compd., **1997,** 262, 299.

17.   Weckhuysen, B.M., Rosynek, M.P., and Lunsford, J.H., Phys. Chem. Chem. Phys., **1999,** 1(13), 3157-3162.

18.   Van der Avert, P. and Weckhuysen, B.M., Phys. Chem. Chem. Phys., **2004,** 6(22), 5256-5262.

19.   Van der Heijden, A.W.A.M., Garcia Ramos, M., and Weckhuysen, B.M., Chem. Eur. J., **2007,** 109(1-2), 97-101.

20.   Van der Heijden, A.W.A.M., Bellière, V., Alonso, L.E., Daturi, M., Manoilova, O.V., and Weckhuysen, B.M., J. Phys. Chem. B, **2005,** 109, 23993-24001.

21.   Van der Avert, P. and Weckhuysen, B.M., Angew. Chem. Int. Ed., **2002,** 41(24), 4730-4732.

Chapter 6

Summary

6.1   Summary

Methane is not widely used as a feedstock by the chemical industry because selective activation is difficult due to the tetrahedral symmetry of the molecule, with all four C-H bonds being equally very strong (439 kJ mol^{-1}), which results in an overall low reactivity. However, the need to utilize methane efficiently as an alternative chemical feedstock is becoming more urgent due to diminishing proven oil reserves and the increasing consumption of crude oil. Conversion of methane currently requires the production of synthesis gas, a mixture of carbon monoxide and hydrogen, through steam reforming, partial oxidation or a combination thereof. Methane conversion through synthesis gas is capital and energy intensive, yet this route remains the only commercially viable technology for converting methane into chemicals. It is expected to remain the dominant technology in the industrial conversion of natural gas to chemical products. However, 30-60% of the natural gas reserves are classified as stranded, meaning gas reservoirs which are too small or in remote areas and cannot be used locally or efficiently transported to market due to a lack of infrastructure. A promising approach to utilize methane of small reservoirs or at remote locations is the oxychlorination of methane with hydrogen chloride and oxygen to methyl chloride and water. Methyl chloride is an important reactant in a number of chemical processes, such as in the production of silicon or methanol. Potentially, methyl chloride could also be used as the basis of synthesis of higher hydrocarbons, whereby the HCl set free in the process can then be reused for the oxidative chlorination. LaCl$_3$, generated by chlorination of LaOCl, has been shown to be an active, selective and stable catalyst for oxidative chlorination of methane to methyl chloride.

The main objective of this thesis was the investigation of the catalytic chemistry of LaCl$_3$ in oxidative chlorination of methane by combining activity measurements with characterization of LaCl$_3$ catalyst and the catalyst precursor LaOCl. In chapter 3, consolidated experimental information and density-functional theory (DFT) calculations are used to propose a mechanism for this intriguing new catalyst for oxidative chlorination. Methyl chloride is formed as a primary product and can be further chlorinated in sequential steps to higher chlorinated products. Methylene chloride and carbon monoxide are the main side products at higher methane conversion levels. Only trace amounts of carbon dioxide and chloroform were observed and tetrachloromethane was never observed. Flow and pulse experiments indicate that the presence of hydrogen chloride is not required for activity, and its role appears to be limited to maintaining the

extent of catalyst chlorination. In contrast, the presence of gas-phase oxygen is essential for the catalytic activity. The reaction is proposed to proceed without a change in the formal oxidation state of the metal cation *via* transient surface OCl^- species, which is formed by dissociative adsorption of oxygen and the change of the formal oxidation state of Cl changing from -1 to +1. A hydrogen atom in methane is proposed to be substituted by Cl^+ of OCl^- via a carbonium ion transition state. A reaction mechanism without a change of the oxidation state is unique, because it was generally accepted that the active catalyst site has to be based on a reducible metal. Furthermore the incorporation of a positive charged chlorine atom presents a selectivity advantage since the incorporation of Cl atoms into methane makes the carbon progressively more electropositive and the electrophilic reaction with $Cl^{\delta+}$ becomes progressively less favorable. Although it is a surface catalyzed reaction, the available kinetic information indicates that catalysts based on pure $LaCl_3$ do not provide a selectivity advantage compared to gas-phase chlorination regarding the further chlorination of methyl chloride. However, it combines activity in oxidative chlorination and the limited formation of higher chlorinated products like $CHCl_3$ and CCl_4 due to catalytic destruction of higher chlorinated hydrocarbons once these are formed. Depending on the gas-phase composition and the reaction temperature, the catalytic surface can dynamically transform by changing its stoichiometry from $LaCl_3$ to $LaOCl$. At high temperatures, catalytic surface spontaneously dechlorinates and the surface or even the bulk can be converted to $LaOCl$. Carbon monoxide is proposed to form as a side product from chlorinated products by catalytic destruction over partially dechlorinated $LaCl_3$ or $LaOCl$. A partially dechlorinated surface is the status of a catalyst under reaction conditions, as shown by *in situ* Raman measurements.

Chapter 4 focuses on the synthesis of the catalyst precursor $LaOCl$. $LaOCl$ is prepared by precipitation of $La(OH)_2Cl$, which is further calcined to $LaOCl$. $LaCl_3$ is *in situ* generated by chlorination of $LaOCl$. Besides ammonium hydroxide also the organic bases tetraethylammonium hydroxide (TEAOH), tetrapropylammonium hydroxide (TPAOH) and tetrabutylammonium hydroxide (TBAOH) were used, in order to obtain high BET surface area samples. This organic bases act as precipitating agents and as template at the same time. The influence of the used base on morphology and composition of the sample before and after chlorination was investigated. Furthermore, the catalytic performance of the prepared samples in oxyhydrochlorination was studied. By using these organic bases the BET surface area of $LaOCl$ can be strongly increased, e.g. from 21 m^2/g to 125 m^2/g with TEAOH. However, after chlorination the BET surface areas

decreased drastically. The decrease of the BET surface area is influenced by the carbonate content and the initial LaOCl BET surface area. The chlorination of lanthanum dioxocarbonate proceeds more slowly than the chlorination of LaOCl, and thus lanthanum dioxocarbonate acts like a structural promoter during chlorination stabilizing the specific surface area. Finally the dioxocarbonate itself is chlorinated. A correlation between the specific surface area after chlorination and the rate of methane conversion exists. This is a clear indication for a surface catalyzed reaction. However, the methyl chloride selectivity is a function of the methane conversion and decreases with increasing methane conversion. The LaOCl specific surface area and the carbon content influence the chlorination behavior of the catalyst and results in a lower optimum temperature for the HCl uptake. High surface samples have a higher HCl uptake because HCl can deeply penetrate LaOCl through the pores.

The influence of metal dopants on the oxychlorination activity of $LaCl_3$ was investigated in Chapter 5. The catalyst precursor LaOCl was impregnated by incipient wetness impregnation with metal chloride salts such as $MgCl_2$, $NiCl_2$, $CoCl_2$, and $CeCl_3$. The so prepared catalysts are characterized and tested for the synthesis of chloromethane from methane, HCl and oxygen. Kinetic measurements at 475°C showed that methane conversion is remarkably increased over the cerium and cobalt modified catalysts. The enhanced activity of these catalysts is related to an enhanced oxygen adsorption capacity and thus a higher concentration of the active site OCl^-. However, over Co/LaOCl and Ce/LaOCl the formed (partially chlorinated) methyl species is strongly adsorbed on the surface and further oxidized to CO, which results in a low selectivity to methyl chloride. On the other hand, the activity of LaOCl for methane activation is reduced by the impregnation with nickel magnesium chloride salt. Especially, the Ni/LaOCl catalyst demonstrates a superior methyl chloride selectivity. However, the apparent activation energy was increased and thus higher reaction temperatures are necessary to obtain sufficient methane conversions. The high methyl chloride selectivity is thought to be a result of a low chlorination degree of the surface and thus due to the low number of active sites which are highly isolated. Furthermore, the ability to retain the chlorinated fragments is either hindered or the unselective sites are blocked by the metal dopant. The modification with $MgCl_2$ leads to a strong decrease in activity while the typical selectivities of the parent LaOCl are retained

6.2   Zusammenfassung

Methan wird derzeit nur wenig als Rohstoff in der chemischen Industrie genutzt, da die selektive Aktivierung wegen der tetraedrischen Symmetrie mit vier gleich starken C-H Bindungen und der daraus folgenden geringen Reaktivität, schwierig ist. Die Notwendigkeit Methan als einen alternativen Rohstoff zu nutzen wird jedoch aufgrund abnehmender Erdölvorkommen und des steigenden Bedarfes an Rohöl immer zwingender. Derzeit erfodert die Umsetzung von Methan die Produktion von Synthesegas, einer Mischung von Kohlenmonoxid und Wasserstoff, durch Dampfreformierung, Partialoxidation oder eine Kombination beider Reaktionen. Obwohl diese Art der Methanumsetzung sehr kapital- und energieintensiv ist, bleibt es doch die einzig großtechnisch zugängliche Technologie für die Umsetzung von Methan zu Chemikalien. Es wird erwartet, dass dies die dominierede Technologie im industriellen Bereich bleiben wird. Allerdings sind 30-60% der Erdgasreserven derzeit für eine wirtschafltliche Förderung nicht zugänglich, da die Reserven entweder zu klein oder zu abgelegen sind und vor Ort nicht verbraucht werden können oder ein effizienter Transport wegen fehlender Infrastruktur nicht möglich sind. Ein vielversprechender Ansatz um Methan in abgelegenen Gegenden zu nutzen, ist die Oxychlorierung von Methan mit Chlorwasserstoff und Sauerstoff zu Methylchlorid und Wasser. Methylchlorid ist ein wichtiger Reaktionspartner in zahlreichen chemischen Prozessen, wie etwa in der Herstellung von Silikon oder Methanol. Methylchlorid kann aber auch als Basis zur Synthese höherer Kohlenwasserstoffe genutzt werden. Der dabei freigesetzte Chlorwasserstoff kann wieder für die oxidative Chlorierung eingesetzt werden. $LaCl_3$, das durch die Chlorierung von LaOCl erzeugt wird, hat sich als aktiver, selektiver and stabiler Katalysator für die oxidative Chlorierung von Methan zu Methylchlorid erwiesen.

Die Hauptzielsetzung dieser Doktorarbeit war die Untersuchung der katalytischen Aktivität von $LaCl_3$ in der oxidativen Chlorierung von Methan durch Kombination von Aktvitätsmessungen mit der Charakterisierung von $LaCl_3$ und der Katalysatorvorstufe LaOCl. Um einen Reaktionsmechanismus für die Oxychlorierung für diesen faszinierenden Katalysator vorzuschlagen, wurden auf konsolidierte experimentelle Informationen und auf Berechnungen nach der Dichtefunktionaltheorie (DFT) zurückgegriffen. Methylchlorid wird als Primärprodukt gebildet, kann aber in Folgereaktionen zu höher chlorierten Produkten weiterchloriert werden. Bei hohen Methanumsätzen sind Methylenchlorid und Kohlenmonoxid die überwiegenden Nebenprodukte. Kohlendioxid und Tetrachlormethan werden nur in Spuren beobachtet.

Kontinuierliche und Puls-Experimente zeigen, dass die Anwesenheit von Chlorwasserstoff für die Aktivität nicht erforderlich ist. Seine Rolle scheint auf die Chlorierung der Katalysatoroberfläche beschränkt zu sein. Im Gegensatz dazu ist Sauerstoff in der Gasphase essenziell für die katalytische Aktiviät. Es wird angenommen, dass die Reaktion ohne Änderung der formalen Oxidationsstufe des Metallkations über eine transiente OCl$^-$ Oberflächenspezies abläuft. Diese Spezies wird durch dissoziative Adsorption von Sauerstoff und der formalen Oxidation des Chloratoms von -1 zu +1 gebildet. Ein Wasserstoffatom im Methan wird durch ein Cl$^+$ aus OCl$^-$ über einen Carboniumion-Übergangszustand substituiert. Dieser Reaktionmechanismus ohne eine Änderung des Oxidationszustandes ist einzigartig, da es bisher allgemein akzeptiert war, dass das katalytisch aktive Zentrum auf einem reduzierbaren Metall basieren muss. Darüber hinaus stellt die Eingliederung eines positiv geladenen Chloratoms einen Selektivitätsvorteil dar, da die Eingliederung eines Chloratoms in Methan das Kohlenstoffatom stufenweise elektronegativer macht, und damit eine elektrophile Reaktion mit Cl$^{\delta+}$ zunehmend weniger begünstigt wird. Obwohl es sich um eine Oberflächen-katalysierte Reaktion handelt, zeigen die vorhandenen kinetischen Informationen, dass LaCl$_3$ keinen Selektivitätsvorteil gegenüber der Gasphasenchlorierung bezüglich der Weiterchlorierung zu Methylenchlorid bietet. Jedoch verbindet LaCl$_3$ eine Aktivität für Oxychlorierung und zugleich eine eingeschränkte Bildung von höher chlorierten Produkten wie CHCl$_3$ und CCl$_4$ durch katalytischen Abbau von höher chlorierten Kohlenwasserstoffen. Abhängig von der Gasphasenzusammensetzung und der Reaktionstemperatur kann sich die katalytische Oberfläche durch die Veränderung der Stöchiometrie von LaCl$_3$ zu LaOCl dynamisch umwandeln. Bei hohen Temperaturen und in Anwesenheit von Wasser wird das Gleichgewicht zwischen LaCl$_3$ und LaOCl zu Gunsten von LaOCl verschoben und die Oberfläche dechloriert oder sogar der gesammte Katalysator zu LaOCl umgewandelt. Unter Reaktionsbedingungen ist die Oberfläche des Katalysators teilweise dechloriert wie mit *in situ* Raman-Messungen gezeigt wurde.

Kapitel 4 beschäftigt sich mit der Synthese der Katalysatorvorstufe LaOCl. LaOCl wird durch Ausfällen von La(OH)$_2$Cl, das weiter zu LaOCl kalziniert wird, hergestellt. LaCl$_3$ wird *in situ* durch Chlorierung von LaOCl erzeugt. Neben Ammoniumhydroxid wurden auch organische Basen wie Tetraethylammoniumhydroxid (TEAOH), Tetrapropylammoniumhydroxid (TPAOH) und Tetrabutylammoniumhydroxid (TBAOH) verwendet, um Proben mit hohen BET Oberflächen zu erhalten. Diese dienen sowohl als Fällungsreagenz als auch als Templat während des Aufällens. Der Einfluß der verwendeten Base auf die Morphologie und die

Zusammensetzung der Probe vor und nach der Chlorierung wurde untersucht. Zudem wurde die katalytische Aktivität der präparierten Proben in der Oxychlorierung ausgewertet. Mit den organischen Basen konnte die BET Oberfläche stark erhöht werden, z.B. mit TEAOH von 21 m^2/g auf 125 m^2/g. Jedoch war nach der Chlorierung die Oberfläche stark reduziert. Die Abnahme der Oberfläche hängt vom Carbonatgehalt und der anfänglichen LaOCl BET Oberfläche ab. Die Chlorierung von Lanthandioxocarbonat verläuft langsamer als die Chlorierung von LaOCl. Lanthandioxocarbonat wirkt daher wie ein struktureller Promoter während der Chlorierung und stabilisiert somit die spezifische Oberfläche. Zum Schluß wird Lanthandioxocarbonate selbst chloriert. Es besteht ein Zusammenhang zwischen der spezifischen Oberfläche nach der Chlorierung und dem Methanumsatz. Dies ist ein klarer Hinweis für eine Oberflächen-katalysierte Reaktion. Allerdings ist die Methylchloridselektivität eine Funktion des Methanumsatzes und sinkt deswegen mit steigendem Methanumsatz. Die spezifische Oberfläche von LaOCl und der Kohlenstoffgehalt beeinflussen auch das Chlorierungsverhalten des Katalysators und ergeben eine niedrigere optimale Temperatur für die HCl-Aufnahme. Proben mit einer hohen BET Oberfläche besitzen eine höhere HCl-Aufnahme, da HCl über die Poren tiefer in LaOCl eindringen kann.

Der Einfluß von Metallen auf die Oxychlorierungsaktivität von LaCl$_3$ wurde in Kapitel 5 untersucht. Die Katalysatorvorstufe LaOCl wurde mit Metallchloridsalzen wie MgCl$_2$, NiCl$_2$, CoCl$_2$ and CeCl$_3$ impregniert. Die so hergestellten Katalysatoren wurden für die Synthese von Chlormethanen aus Methan, Chlorwasserstoff und Sauerstoff untersucht. Kinetische Messungen bei 475°C zeigen, dass der Methanumsatz für die mit Cobalt und Cer modifizierten Katalysatoren bemerkenswert erhöht ist. Die erhöhte Aktivität dieser Katalysatoren wird der verbesserten Adsorptionskapazität von Sauerstoff zugeschrieben und der damit verbundenen erhöhten Konzentration an aktiven Zentren auf der Oberfläche. Allerdings ist die gebildete (teilweise chlorierte) Methylspezies bei Co/LaOCl und Ce/LaOCl stärker auf der Oberfläche adsorbiert und wird daher direkt zu Kohlenmonoxid oxidiert. Daraus resultiert eine geringere Selektivität für Methylchlorid. Durch die Impregnierung mit Nickel und Magnesium wird die Aktivität von LaOCl für die Aktivierung von Methan reduziert. Besonders Ni/LaOCl zeigt eine überdurchschnittliche Methylchloridselektivität. Jedoch ist die scheinbare Aktivierungsenergie erhöht und daher sind höhere Reaktionstemperaturen nötig, um ausreichende Methanumsätze zu erreichen. Die hohe Methylchloridselektivität wird auf auf den geringen Chlorierungsgrad der

Oberfläche und der daraus resultierenden geringeren Anzahl an aktiven Zentren, die stark isoliert sind, zurückgeführt.

7 Curriculum Vitae

Elvira Theresia Peringer was born on November, 30th of 1978 in Mallersdorf-Pfaffenberg, Germany. She attended the Gymnasium der Ursulinen in Straubing from 1989 to 1998 from which she graduated with the general qualification for university entrance (Abitur). She started immediately studying chemistry at the Technischen Universität München in November 1998. During her studies she was supported by the Hanns-Seidel-Foundation. In 2003 Elvira Peringer joined Prof. Johannes A. Lercher's group (Chair for technical chemistry II) at the Technischen Universität München for her Diploma Thesis entitled "New materials for the adsorption of SO_2 in oxygen rich atmosphere". After graduation as "Diplom-Chemiker" (master degree) in February 2004 she started to work as a PhD student in Prof. Johannes A. Lercher's group. Her work was focused on the oxidative chlorination of methane over $LaCl_3$-ased catalysts.

8 List of Publications

1. E. Peringer, S.G. Podkolzin, M.E. Jones, R. Olindo, and J.A Lercher, Top. Catal., **2006,** 38(1-3), 211-220.

2. S.G. Podkolzin, E.E. Stangland, M.E. Jones, E. Peringer, A.A. Lemonidou and J.A. Lercher, J. Am. Chem. Soc., **2007,** 129, 2569-2576.

3. E. Peringer, C. Tejuja, M. Salzinger, A.A. Lemonidou and J.A. Lercher, submitted to Appl. Catal., **2008**.

4. E. Peringer, M. Salzinger, M. Hutt, A.A. Lemonidou and J.A. Lercher, ready for submission to J. Catal., **2008**.

9 Oral and poster presentation

1. DGMK/SCI-Conference "Oxidation and functionalization: Classical and alternative routes and sources" 12. – 14. Oktober in Milan, Italy
    E. Peringer, B. Tope, O. Manoilova, J.A. Lercher, oral presentation.

2. XXXIX. Jahrestreffen Deutscher Katalytiker, 15. - 17. March 2006 in Weimar;
    E. Peringer, R. Olindo, J.A. Lercher, oral presentation.

3. XXXX. Jahrestreffen Deutscher Katalytiker, 14. - 16. March 2007 in Weimar
    E. Peringer, S.G. Podkolzin, M.E. Jones, Olindo, J.A. Lercher, poster presentation.